Report No. CDOT-2013-15
Final Report

EVALUATION OF SEISMIC TESTING FOR QUALITY ASSURANCE OF LIME-STABILIZED SOIL

Michael A. Mooney
Richard G. Bearce

August 2013

COLORADO DEPARTMENT OF TRANSPORTATION
DTD APPLIED RESEARCH AND INNOVATION BRANCH

The contents of this report reflect the views of the author(s), who is(are) responsible for the facts and accuracy of the data presented herein. The contents do not necessarily reflect the official views of the Colorado Department of Transportation or the Federal Highway Administration. This report does not constitute a standard, specification, or regulation.

Technical Report Documentation Page

1. Report No.	2. Government Accession No.	3. Recipient's Catalog No.
CDOT-2013-15		

4. Title and Subtitle	5. Report Date
EVALUATION OF SEISMIC TESTING FOR QUALITY ASSURANCE OF LIME-STABILIZED SOIL	August 2013
	6. Performing Organization Code
7. Author(s)	8. Performing Organization Report No.
Michael A. Mooney, Ph.D., P.E.; Richard G. Bearce, M.S.	CDOT-2013-15
9. Performing Organization Name and Address	10. Work Unit No. (TRAIS)
Colorado School of Mines 1500 Illinois St. Golden, CO 80401	11. Contract or Grant No. 80.30
12. Sponsoring Agency Name and Address	13. Type of Report and Period Covered
Colorado Department of Transportation - Research 4201 E. Arkansas Ave. Denver, CO 80222	Final
	14. Sponsoring Agency Code

15. Supplementary Notes

Prepared in cooperation with the US Department of Transportation, Federal Highway Administration

16. Abstract

This study sought to determine the technical feasibility of using seismic techniques to measure the laboratory and field seismic modulus of lime-stabilized soils (LSS), and to compare/correlate test results from bench-top (free-free resonance) seismic testing on LSS cylinders to in-situ (surface seismic) testing performed on field-constructed LSS. In addition, this research sought to develop a pilot specification for quality assurance of LSS using seismic test methods. The growth of modulus was found to vary as a non-linear function of both temperature and curing time. Differences in modulus growth between free-free resonance (LSS cylinders) and surface wave (field-constructed LSS) data can be attributed to construction-related issues, and are not the result of testing equipment/practice. The study supports the recommendations of the CDOT specification for LSS (Section 307) in that grading should be performed immediately after construction as grading conducted on later days (i.e., days 4-8) resulted in significant seismic modulus loss on field-constructed LSS.

Implementation

This study recommends the use of seismic testing for QA of LSS via the pilot specification developed in Chapter 5 of this report. The specification allows for the use of either cylinder or surface wave testing to determine the seismic modulus of field-constructed LSS. It is written in a manner that allows CDOT personnel to implement the proposed approach.

17. Keywords	18. Distribution Statement
LSS, free-free resonance (FFR), surface wave seismic testing, cylinder seismic testing, seismic modulus, maturity index, QA	This document is available on CDOT's website http://www.coloradodot.info/programs/research/pdfs

19. Security Classif. (of this report)	20. Security Classif. (of this page)	21. No. of Pages	22. Price
Unclassified	Unclassified	108	

Evaluation of Seismic Testing for Quality Assurance of Lime-Stabilized Soil

by
Principal Investigators
Michael A. Mooney, Ph.D., P.E., Professor
Richard G. Bearce, M.S., Ph.D. Candidate

Report No. CDOT-2013-15

Prepared by
Colorado School of Mines
Department of Civil and Environmental Engineering
1500 Illinois Street
Golden, Colorado 80401

Sponsored by the
Colorado Department of Transportation
DTD Applied Research and Innovation Branch
4201 E. Arkansas Ave.
Denver, CO 80222

ACKNOWLEDGEMENTS

The authors wish to thank the CDOT-DTD Applied Research and Innovation Branch for funding this study and Roberto DeDios and Rich Griffin for overseeing the project on behalf of CDOT.

We wish to thank the project panel members - C.K. Su, Gary DeWitt, Alan Hotchkiss, Aziz Khan, Shamshad Hussain, Matt McMechen, Scott Roalofs, Michael Stanford, and Jim Noll (Kumar & Associates).

We would particularly like to acknowledge Derek Garben (ARS, Inc.) for his assistance in locating test sites. In addition, we would like to acknowledge David Glater (CTL Thompson, Inc.), and Darin Duran (J.A. Cesare and Associates, Inc.) for their assistance in obtaining geotechnical test information for test sites.

EXECUTIVE SUMMARY

This report presents the findings from CDOT Study 80.30 entitled "Evaluation of Seismic Testing for Quality Assurance of Lime-Stabilized Soil." The objectives of this study were to determine the technical feasibility of using seismic techniques to measure the laboratory and field seismic modulus of lime-stabilized soils (LSS), and to compare/correlate test results from bench-top (free-free resonance) seismic testing on LSS cylinders to in-situ (surface seismic) testing performed on field-constructed LSS. In addition, this research sought to develop a pilot specification for quality assurance of LSS using seismic test methods.

Lime stabilization of roadway subgrade soils is widely used to reduce soil plasticity, mitigate heave, and increase subgrade stiffness and strength. LSS performance requires careful construction, and the relatively involved construction process requires diligent quality control (QC) and quality assurance (QA). The need to assess design related parameters such as elastic modulus and 28-day unconfined compressive strength of LSS during QC/QA conflicts with more rapid pavement construction schedules. Strength and modulus growth in LSS stem from pozzolanic reactions that are a function of both time and temperature. These reactions continue over months, but construction schedules often desire evaluation of acceptance after days. For this reason, an important part of this project was to explore and develop a maturity index for LSS (i.e., a function that accurately predicts LSS modulus growth as a function of both curing temperature and curing time).

A thorough literature review investigated the technical feasibility of using free-free resonance and surface wave testing to determine the seismic modulus of LSS. In addition, a review of commercially available seismic test equipment is presented to inform future seismic LSS testing.

A combined laboratory (cylinder) and field (cylinder and surface wave) testing program was conducted at three LSS construction sites in the Denver metropolitan area. For the cylinder approach, field-mixed LSS was gathered on the day of final remix/compaction and reconstituted into 8 in height by 4 in diameter cylinders. These cylinders were cured at varying temperature regimes including normal ($23^{o}C/73^{o}F$), accelerated ($41^{o}C/105^{o}F$), and decelerated ($8^{o}C/46^{o}F$). Cylinders were also cured at the LSS field site to mimic the temperature regime experienced by the field-constructed LSS. For the surface wave approach, seismic surface wave testing was

performed at several locations on the field-constructed LSS to determine seismic modulus. To assist in the development of a maturity index for LSS, ambient (air) and soil temperatures were monitored in the laboratory and field using temperature probes. The experimental results (from both cylinder and surface wave testing) suggest that LSS experiences modulus growth over 28+ days but cannot be characterized as a function of curing day alone. Instead, a maturity index for LSS modulus growth must also consider curing temperature. Based on the experimental results, the authors have developed a LSS maturity index that characterizes modulus growth as a function of both curing time and curing temperature, and proposed a pilot specification for QA of LSS via seismic testing and maturity index-based acceptance criteria.

The following conclusions are drawn from the results of this study, and subsequent recommendations are made for CDOT practice:

1. Temperature has a significant impact on LSS modulus growth with curing time. The growth of modulus was found to vary as a non-linear function of both temperature and curing time. This function was inferred from the fitting of constant and variable curing temperature free-free resonance data, and is a seismic modulus maturity index for LSS.
2. The LSS maturity index is a function of soil temperature, not ambient (air) temperature. Both LSS and air temperature were monitored during field construction, and a correlation between the two is obtained. This correlation can simplify the implementation of the LSS maturity index pilot specification as only air temperature needs to be obtained.
3. Differences in modulus growth between free-free resonance (cylinders) and surface wave (field-constructed LSS) data can be attributed to construction-related issues, and are not the result of testing equipment/practice. To this end, the study supports the recommendations of the CDOT specification for LSS (Section 307) in that grading should be performed immediately after construction. Grading conducted on later days (i.e., days 4-8) resulted in significant seismic modulus loss on field-constructed LSS.
4. The study supports the use of both cylinder and surface wave seismic testing for the QA of LSS. As the goal of LSS QA should be to evaluate the actual field-constructed LSS, either method is valid so long as appropriate LSS field construction procedure is followed.
5. The study recommends the use the seismic LSS maturity index developed herein. Results suggest that significant differences in LSS seismic modulus behavior occur due to curing

temperature variation. For this reason, acceptance via seismic QA on field-constructed LSS must consider curing temperature.

6. A pilot specification for QA of LSS via seismic testing is developed in Chapter 5. This specification allows for the use of either cylinder or surface wave testing to determine the seismic modulus of field-constructed LSS. Experimental results are statistically adjusted based on % confidence criteria, and acceptance/rejection is verified via the field curing temperature and the LSS maturity index.

7. In the event that simultaneous acceptance via unconfined compressive strength (UCS) testing is desired, a correlation between seismic modulus and UCS is recommended. Attempts to core field-constructed LSS for UCS testing were not successful, and this approach is not recommended.

Implementation

The study supports the use of both cylinder and surface wave seismic testing for the QA of LSS. In addition, the study recommends the use the seismic LSS maturity index developed herein. Results suggest that significant differences in LSS seismic modulus behavior occur due to curing temperature variation. For this reason, acceptance via seismic QA on field-constructed LSS must consider curing temperature. A pilot specification for QA of LSS via seismic testing is presented herein. This specification allows for the use of either free-free resonance or surface wave testing to determine the seismic modulus of field-constructed LSS. Experimental results are statistically adjusted based on % confidence criteria, and acceptance/rejection is verified via the field curing temperature and the LSS maturity index. In the event that simultaneous acceptance via unconfined compressive strength (UCS) testing is desired, a correlation between seismic modulus and UCS is recommended. Attempts to core field-constructed LSS for UCS testing were not successful, and this approach is not recommended.

TABLE OF CONTENTS

CHAPTER 1: INTRODUCTION 1
1.1 Overview and Objectives 1
1.2 Summary of Report 2

CHAPTER 2: LITERATURE REVIEW 3
2.1 Laboratory Characterization of Seismic Modulus via Free-Free Resonance 3
2.2 Field Characterization of Seismic Modulus via Surface Wave Analysis 3
2.3 Discussion of Commercially Available Surface Wave Test Equipment 5

CHAPTER 3: TEST PROGRAM 9
3.1 Test Site Summary 9
3.2 Laboratory Test Program 13
3.2.1 Specimen Preparation and Storage 13
3.2.2 Free-Free Resonance Testing 15
3.3 Field Test Program 16
3.3.1 Principles of Surface Wave Testing 16
3.3.2 Experimental Setup and Interpretation of Surface Wave Data 21
3.3.3 Considerations for Testing on Field LSS 23

CHAPTER 4: RESULTS 26
4.1 Temperature Raw Data 26
4.2 Free-Free Resonance 29
4.3 Surface Wave Test Results 35
4.4 Development of a Maturity Index for LSS 39
4.5 Comparison of FFR and Surface Wave Data Using LSS Maturity Index 51
4.6 Conclusions 56

CHAPTER 5: PILOT SPECIFICATION 58

REFERENCES 74

APPENDIX A: TABULAR SEISMIC MODULUS DATA (FFR) A-1

APPENDIX B: TABULAR SEISMIC MODULUS DATA (SURFACE WAVE) B-1

APPENDIX C: SPECTRAL ANALYSIS OF SURFACE WAVES PROCEDURE C-1

APPENDIX D: SEISMIC MODULUS – TEMPERATURE CORRELATION PLOTS D-1

APPENDIX E: TEMPERATURE INTERPRETATION E-1

LIST OF FIGURES

Figure 2.1: (a) Diagram of a typical SASW setup (from (Kim et al. (2001)), (b) a typical wrapped phase difference, and (c) phase velocity (from (Ryden & Lowe, 2004)).
Figure 2.2: (a) Diagram of typical MASW setup (from (Park *et al*., 1997)) and (b) a raw data file from MASW testing (from (Ryden *et al.*, 2004)).
Figure 2.3: (a) SeisNDT experimental setup for free-free resonance and (b) surface wave testing.
Figure 2.4: (a) Sensor array for the Dirt Seismic Property Analyzer (D-SPA), and (b) full D-SPA setup (Nazarian et al., 2006).
Figure 2.5: (a) Components of the Olson Engineering SASW-S, and (b) the SASW-S in use.
Figure 2.6: The Continuous Surface Wave System (CSWS) by GDP Instruments.
Figure 3.1: Field test site locations in the Denver Metro Area (image modified from Google Earth).
Figure 3.2: Truth Christian Academy Field Site (image modified from Google Earth).
Figure 3.3: Candelas Field Site (image modified from Google Earth).
Figure 3.4: Solterra Field Site (image modified from Google Earth).
Figure 3.5: (a) Application of quicklime slurry, (b) application of cement, (c) soil/stabilizer mixing, and (d) final compaction.
Figure 3.6: (a) FFR cylinder preparation and (b) example specimen.
Figure 3.7: (a) FFR field cylinder storage trench uncovered and (b) covered.
Figure 3.8: (a) Cylinder, accelerometer, and impact orientation for FFR longitudinal excitation with (b) corresponding windowed time history, and (c) frequency spectrum with selected resonant frequencies.
Figure 3.9: Particle motion for propagating P waves , S waves , and Rayleigh waves (modified from Ryden (2004)).
Figure 3.10: (a) Source and receiver configuration for simple surface wave testing, (b) waveform identification for example record 1, and (c) waveform identification for example record 2.
Figure 3.11: SeisNDT experimental surface wave test setup.
Figure 3.12: (a) Surface wave testing setup utilized in this research, (b) raw time domain data from one of these tests, and (c) magnified raw time domain data for easier identification of waveforms.
Figure 3.13: (a) Illustration of field condition variability - significant post-compaction grading, and (b) surface cracking. Note the reference ruler in these images is 10 cm in length.
Figure 4.1: TinyTag 2.0 Temperature sensory and in-situ soil probe used for temperature measurement.
Figure 4.2: Ambient, trench, and field-constructed LSS temperature history for TCA 2011.
Figure 4.3: Ambient, trench, and field-constructed LSS temperature history for TCA 2012.
Figure 4.4: Ambient, trench, and field-constructed LSS temperature history for Candelas.
Figure 4.5: Ambient, trench, and field-constructed LSS temperature history for Solterra.
Figure 4.6: Correlation between ambient and LSS soil temperature.
Figure 4.7: (a) Seismic Young's modulus vs. curing time for TCA 2011 – Zone 1, (b) curing temperature regime for field cylinders, and (c) range/mean for the data in (a).
Figure 4.8: (a) Seismic Young's modulus vs. curing time and (b) range/mean of data for TCA 2011 – Zone 2.

Figure 4.9: (a) Seismic Young's modulus vs. curing time for Candelas– Zone 1, (b) curing temperature regime for field cylinders, and (c) range/mean for the data in (a).
Figure 4.10: (a) Seismic Young's modulus vs. curing time for Candelas – Zone 2, (b) curing temperature regime for field cylinders, and (c) range/mean for the data in (a).
Figure 4.11: (a) Seismic Young's modulus vs. curing time for Solterra, (b) curing temperature regime for field cylinders, and (c) range/mean for the data in (a).
Figure 4.12: Seismic Young's modulus (Surface Wave vs. FFR) for Candelas.
Figure 4.13: Seismic Young's modulus (Surface Wave vs. FFR) for Solterra.
Figure 4.14: Seismic Young's modulus (Surface Wave vs. FFR) for TCA 2011 – Zone 1.
Figure 4.15: Seismic Young's modulus (Surface Wave vs. FFR) for TCA 2011 – Zone 2.
Figure 4.16: (a) Seismic Young's modulus (Surface Wave) for TCA 2012 – Zone 3 compared to FFR from TCA 2011 (Zone 2), and (b) corresponding field temperature curing regimes.
Figure 4.17: Seismic Young's modulus vs. curing time and maturity index for TCA 2011 – Zone 1.
Figure 4.18: Seismic Young's modulus vs. curing time and maturity index for Candelas.
Figure 4.19: Seismic Young's modulus vs. curing time and maturity index for Solterra.
Figure 4.20: Correlation between E_0 and $\bar{T}_t$ for days 3, 7, 14, and 28.
Figure 4.21: η_t as a function of curing day (t) with best fit equation.
Figure 4.22: β as a function of curing day (t).
Figure 4.23: Plots of (a) η_t, (b) $e^{\beta \bar{T}_t}$, and (c) the family of curves generated by multiplying the two together.
Figure 4.24: Averaged E_0 data sets at constant curing temperatures compared to E_{Pred} (4^oC intervals) generated using Equation 4.4.
Figure 4.25: Individual FFR data sets compared to E_{Pred} from the maturity index for (a) $\bar{T}_t$= 8^oC, (b) $\bar{T}_t$ = 23^oC, and (c) $\bar{T}_t$= 41^oC.
Figure 4.26: (a) Development of E_{Pred} expressed through maturity curves, and (b) $\bar{T}_t$ used to obtain the results in part (a).
Figure 4.27: E_0 compared to E_{Pred} for the $\bar{T}_t$ regime shown in Figure 4.26b.
Figure 4.28: (a) Experimental surface wave and FFR results compared to E_{Pred} for respective curing regimes, and (b) corresponding $\bar{T}_t$ data for TCA 2011.
Figure 4.29: (a) Experimental surface wave and FFR results compared to E_{Pred} for respective curing regimes, and (b) corresponding $\bar{T}_t$ data for TCA 2012.
Figure 4.30: (a) Experimental surface wave and FFR results compared to E_{Pred} for respective curing regimes, and (b) corresponding $\bar{T}_t$ data for Candelas.
Figure 4.31: (a) Experimental surface wave and FFR results compared to E_{Pred} for respective curing regimes, and (b) corresponding $\bar{T}_t$ data for Solterra.
Figure 5.1: (a) FFR cylinder preparation and (b) example cylinder.
Figure 5.2: (a) FFR field cylinder storage trench uncovered and (b) covered.
Figure 5.3: Free-free resonance testing with longitudinal excitation.
Figure 5.4: (a) instrumented hammer used as source impact, (b) accelerometer with no spike for greased coupling, and (c) accelerometer with ground spike for direct coupling.
Figure 5.5: (a) Source and receiver configuration for simple surface wave testing, (b) waveform identification for example record 1, and (c) waveform identification for example record 2.
Figure 5.6: LSS acceptance intervals assuming normally distributed data.
Figure 5.7: Flow chart for LSS QA specification.
Figure 5.8: Synthetic data LSS site with 3 mixed sections and ten surface wave tests per section.

Figure 5.9: Visual representation of unaveraged E_0 data, E_{Tar}, and various acceptance levels for Section 1.
Figure 5.10: Visual representation of unaveraged E_0 data, E_{Tar}, and various acceptance levels for Section 2.
Figure 5.10: Visual representation of unaveraged E_0 data, E_{Tar}, and various acceptance levels for Section 3.
Figure C1: Raw time history data with labeled wave velocities (a), dispersion curve resulting from the raw data in (a) with wave velocities identified (b), and thickness frequency identification from layer interface reflection (c).
Figure D1: Correlation between E_0 and curing temperature (day 1).
Figure D2: Correlation between E_0 and curing temperature (day 2).
Figure D3: Correlation between E_0 and curing temperature (day 3).
Figure D4: Correlation between E_0 and curing temperature (day 4).
Figure D5: Correlation between E_0 and curing temperature (day 5).
Figure D6: Correlation between E_0 and curing temperature (day 6).
Figure D7: Correlation between E_0 and curing temperature (day 7).
Figure D8: Correlation between E_0 and curing temperature (day 8).
Figure D9: Correlation between E_0 and curing temperature (day 9).
Figure D10: Correlation between E_0 and curing temperature (day 10).
Figure D11: Correlation between E_0 and curing temperature (day 11).
Figure D12: Correlation between E_0 and curing temperature (day 12).
Figure D13: Correlation between E_0 and curing temperature (day 13).
Figure D14: Correlation between E_0 and curing temperature (day 14).
Figure D15: Correlation between E_0 and curing temperature (day 16).
Figure D16: Correlation between E_0 and curing temperature (day 18).
Figure D17: Correlation between E_0 and curing temperature (day 20).
Figure D18: Correlation between E_0 and curing temperature (day 22).
Figure D19: Correlation between E_0 and curing temperature (day 24).
Figure D20: Correlation between E_0 and curing temperature (day 26).
Figure D21: Correlation between E_0 and curing temperature (day 28).
Figure E1: (a) Various interpretations of $\bar{T}_t$ used for experimental data fitting, and (b) resulting E_{Pred} from $\bar{T}_t$ (t) in part a.

LIST OF TABLES

Table 3.1: Summary of soil properties and lime/cement mix designs for all sites tested in this study.
Table 3.2: Summary of FFR and surface wave testing program for all sites.
Table 5.1: Synthetic surface wave E_0 data from section 1-3 on days 3, 5, and 7.
Table 5.2: $\boldsymbol{\mu}$ and $\boldsymbol{\sigma}$ for each data set presented in Table 5.1.
Table 5.3: Average daily ambient temperature, average daily soil temperature, and cumulative average temperature for synthetic data example.
Table 5.4: Evaluation of acceptance criteria for synthetic LSS data set.
Table A1: Seismic modulus values obtained via FFR for Solterra (days 1-10).
Table A2: Seismic modulus values obtained via FFR for Solterra (days 11-28).
Table A3: Seismic modulus values obtained via FFR for TCA 2011-Zone 1 (days 1-10).
Table A4: Seismic modulus values obtained via FFR for TCA 2011-Zone 1 (days 11-28).
Table A5: Seismic modulus values obtained via FFR TCA 2011-Zone 2 (days 1-10).
Table A6: Seismic modulus values obtained via FFR TCA 2011-Zone 2 (days 11-28).
Table A7: Seismic modulus values obtained via FFR Candelas – Zone 1 (days 1-10).
Table A8: Seismic modulus values obtained via FFR Candelas-Zone 1 (days 11-28).
Table A9: Seismic modulus values obtained via FFR Candelas – Zone 2 (days 1-10).
Table A10: Seismic modulus values obtained via FFR Candelas – Zone 2 (days 11-28).
Table B1: Seismic modulus values obtained via surface wave testing for TCA 2011 – Zone 1.
Table B2: Seismic modulus values obtained via surface wave testing for TCA 2011 – Zone 2.
Table B3: Seismic modulus values obtained via surface wave testing for TCA 2012.
Table B4: Seismic modulus values obtained via surface wave testing for Solterra.
Table B5: Seismic modulus values obtained via surface wave testing for Candelas.

CHAPTER 1: INTRODUCTION

1.1 Overview and Objectives

In the AASHTO Mechanistic-Empirical Pavement Design Guide (MEPDG) procedure, the critical design parameter required for subgrade, subbase, base and stabilized layers is the elastic (resilient) modulus. In CDOT design practice, the resilient modulus (M_R) of the material is estimated via correlation to unconfined compressive strength (UCS). During quality assurance (QA) process, the M_R is also estimated from correlation to UCS. For stabilized soils, the correlation to M_R is based upon UCS of samples that have undergone accelerated curing (41^{o}C/105 ^{o}F) for 5 to 7 days. There are a number of limitations to this QA approach:

- This lab-based assessment is not a true evaluation of the field-constructed product. While the soil does come from the construction site, specimens are prepared in the lab using standard Proctor energy (and not actual field compaction energy). This creates a structure that is different from the field-compacted soil. It has been demonstrated that field compaction and lab compaction can be significantly different.
- The estimation of field-constructed M_R comes from a correlation to UCS that may not be representative for all soils. The test does not directly measure M_R.
- The M_R - UCS correlation equation is based on 28-day normally cured samples; however, the M_R is determined via correlation by using UCS results from accelerated cure (e.g., 5 days at 41^{o}C/105 ^{o}F) samples to expedite construction. This introduces additional uncertainty because 5-day accelerated curing is only an approximation of 28-day normal temperature curing. As documented in Report No. CDOT-2010-1, there is no unique 41^{o}C/105 ^{o}F curing duration that mimics 28-day normal curing for all soils. Therefore, 5-day 41^{o}C/105 ^{o}F curing will overestimate or underestimate strength and stiffness, depending on soil type.

Ideally, a QA approach should directly measure the design parameter (i.e., modulus) of the field-constructed material. The technique should allow for testing after 3, 4 or 5 days to expedite construction. The seismic technique enables the direct measurement of modulus in the lab and in the field. Seismic waves propagate through the soil at a speed that is proportional to Young's modulus and shear modulus. The design modulus may be determined in the laboratory

for the given stabilized soil using a free-free resonant (FFR) test and can be verified directly in the field with a surface seismic method.

This report presents the results of seismic testing conducted on three construction sites in the Denver metropolitan area. These results, in addition to measured temperature data, are used to develop a seismic modulus maturity index for LSS. Using this LSS maturity index, a pilot specification for QA of LSS with seismic testing is developed.

1.2 Summary of Report

Chapter 1 explains the objectives of the study and how they were achieved. Chapter 2 presents a detailed review of literature on seismic testing and its applicability to LSS QA. Field test site summaries and laboratory/field data is presented in Chapter 3. This data is used to develop a seismic modulus maturity index and form conclusions in Chapter 4. In Chapter 5, a pilot specification for seismic QA of LSS is developed.

CHAPTER 2: LITERATURE REVIEW

2.1 Laboratory Characterization of Seismic Modulus via Free-Free Resonance

Free-free resonant column (FFR) testing has been utilized to estimate low strain (i.e., $1x10^{-6}$), or seismic modulus of reconstituted soil cylinders by several researchers (Nazarian *et al.* 2002, Ryden *et al.* 2006). FFR testing was performed on lime and cement stabilized soils by Åhnberg and Holmen (2008) and Ryden *et al.* (2006). FFR testing is attractive for QA/QC of LSS because it is non-destructive (i.e., modulus growth from one specimen can be measured over time because cylinders are not destroyed during testing). This technique requires the preparation and testing of reconstituted soil cylinders.

Toohey and Mooney (2012) performed FFR testing on LSS cylinders of three different lime-soils mix designs. Their results indicate that LSS seismic modulus growth for a given day can be predicted using a power-law statistical model relationship, the day 1 seismic modulus, and the current curing day. Furthermore, the authors showed that seismic Young's modulus was well correlated to unconfined compressive strength measurements (i.e., $R^2 = 0.89$). These results demonstrate the value of FFR as a predictive tool for LSS QA, but results from this research were based on lab-cured (i.e., constant temperature) cylinders only. Because LSS maturity is time and temperature dependent, the implementation of a power-law function to predict LSS seismic modulus growth at variable temperatures (i.e., field conditions) may be over simplified. Ideally, LSS seismic modulus growth would be predicted a maturity index function that incorporates both time and temperature dependence (e.g., the concrete maturity index).

2.2 Field Characterization of Seismic Modulus via Surface Wave Analysis

Because laboratory (benchtop) and field (surface wave) seismic modulus are directly related (Nazarian *et al.*, 2002, Ryden *et al.*, 2006), it logically follows that QA of field-constructed LSS should be performed on the field-constructed surface. Several approaches to material characterization via surface wave analysis have been developed and widely utilized for soil and pavement evaluation. Surface wave testing estimates material modulus by performing either time domain analysis or frequency domain (spectral) analysis on measured surface wave data. While material wave velocity can be determined with time domain analysis, most studies in literature utilize spectral analysis because it also allows for the estimation of layer thickness. This section discusses literature that has utilized surface wave analysis for soil testing

applications with limited procedural discussion. A detailed discussion of surface wave testing procedure is presented in Chapter 3.

Since its development (Heisey, 1982), spectral analysis of surface waves (SASW) has been used to non-destructively estimate modulus in pavement and soil systems. To conduct SASW testing, two ground sensors (accelerometers or geophones) are placed on the soil surface, an impulse load is applied at the source (a distance *D* from one of the geophones), and the resulting surface waves are measured (Kim *et al.*, 2001) (Figure 2.1). Further advances to the method (Nazarian, 1984 and Stokoe *et al.*,1994) have resulted in the SASW method becoming a common modern method for soil evaluation (Ryden & Park, 2006).

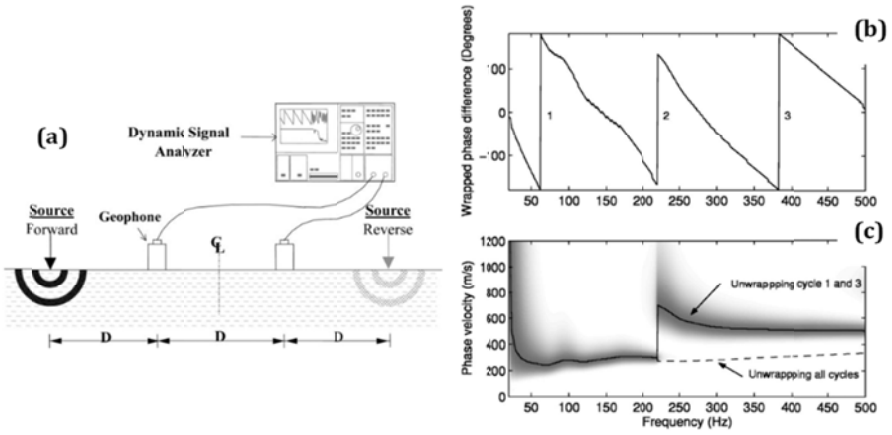

Figure 2.1: (a) Diagram of a typical SASW setup (from Kim *et al.*, 2001), (b) a typical wrapped phase difference, and (c) phase velocity (from (Ryden & Lowe, 2004)).

Multichannel Analysis of Surface Waves (MASW) is similar to SASW, but utilizes multiple simultaneous measurements to estimate soil properties (Figure 2.2). Instead of just two geophones, MASW utilizes an entire series of geophones to capture wave response at all desired depths (Park *et al.* 1997). MASW data also contain information about higher order wave propagation modes because of the method's richer spatial data sampling. Ryden *et al.* (2004) describe the multichannel approach as, "a pattern recognition method that can delineate the complexity of seismic characteristics through the coherency measurement in velocity and attenuation of different types of seismic waves (e.g., multi-modal surface waves, various types of body waves, and a wide variety of ambient noise)" (Ryden *et al.* 2004). To this end, the MASW method is often used to evaluate multi-layer soil/pavement systems.

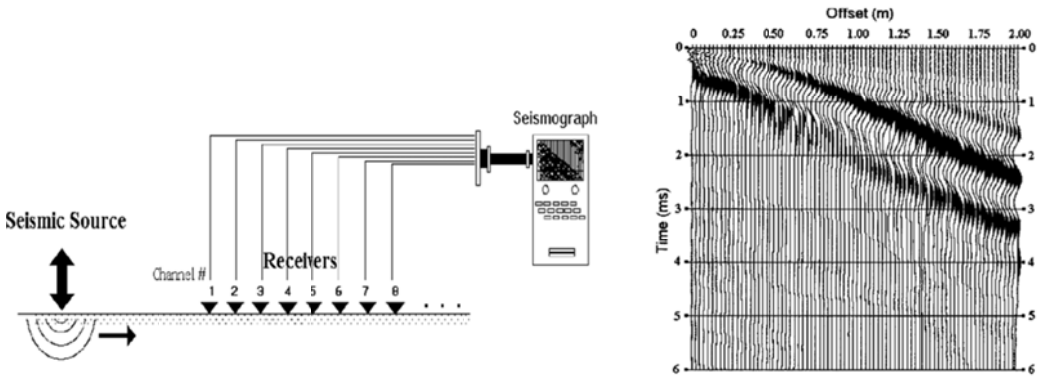

Figure 2.2: (a) Diagram of typical MASW setup (from Park *et al.*, 1997) and (b) a raw data file from MASW testing (from Ryden *et al.*, 2001).

2.3 Discussion of Commercially Available Surface Wave Test Equipment

Seismic data for this project (both FFR and surface wave) were acquired with the SeisNDT system (Figure 2.3) developed by Dr. Nils Ryden. This system is advantageous in that it can be used for both resonant column and surface wave seismic testing. To conduct surface wave tests with this device, a methodology known as multiple source one receiver (MSOR) is used. A procedural discussion of this method is presented in Chapter 3. While methodically valid, MSOR is significantly less efficient than single source methods (e.g., D-SPA) when a large number of evaluation locations are desired. Furthermore, these systems are built by Dr. Ryden, and future commercial availability of this setup is unknown. For this reason, several other commercially available surface wave test setups are discussed in this section.

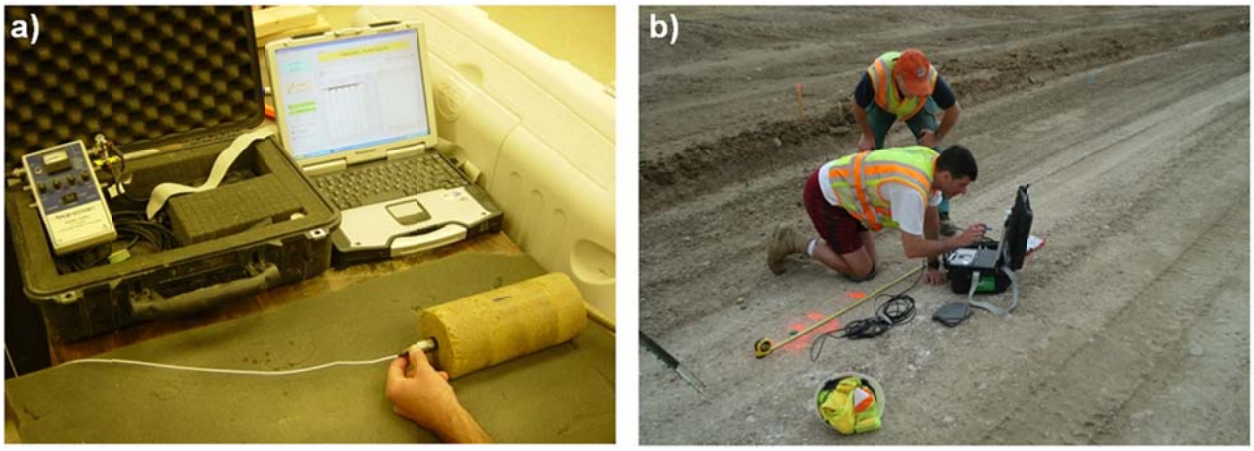

Figure 2.3: (a) SeisNDT experimental setup for free-free resonance and (b) surface wave testing.

One commercially available surface wave testing device is the Dirt Seismic Property Analyzer (D-SPA), developed by Dr. Soheil Nazarian (Figure 2.4). This device is designed for rapid testing and can estimate seismic modulus within a few seconds in the field. For data collection, the operator starts the test sequence with a software trigger, and all acquisition and processing is handled by the computer. This system could be used for time domain analysis, but the program automatically converts into the frequency domain for dispersion curve analysis. The resulting dispersion curve can be used estimate both layer modulus and thickness. This device is considerably more efficient and user-friendly than the SeisNDT setup.

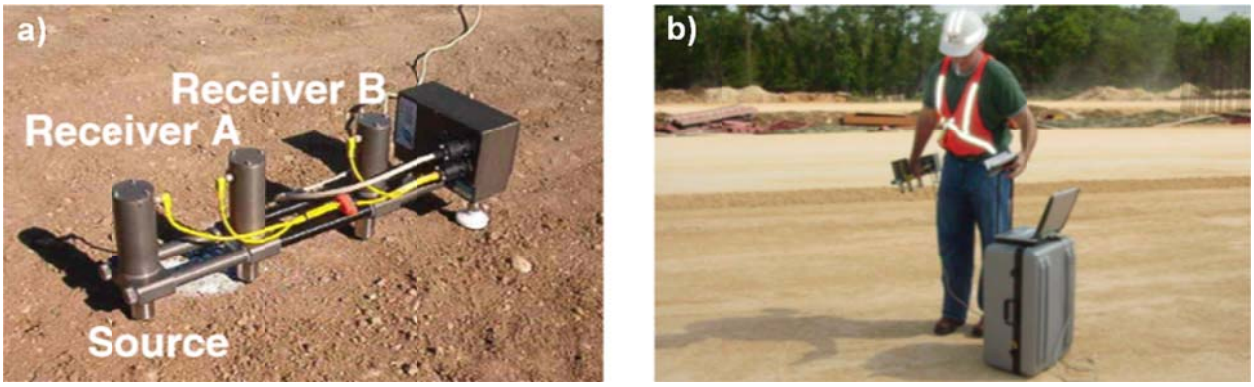

Figure 2.4: (a) Sensor array for the Dirt Seismic Property Analyzer (D-SPA), and (b) full D-SPA setup (Nazarian et al., 2006).

The Olson Engineering SASW system is a commercially available surface wave test setup that is suitable for evaluation of structural, soil and pavement systems (Figure 2.5). This system is available in three models that are designed for different applications. The base model, the SASW-S, is capable of evaluation to depths of 0.8m (2.6 ft), which is sufficient for testing of most field-constructed LSS layers. This system is also user-friendly, integrating with a computer and in-house software from Olson Engineering.

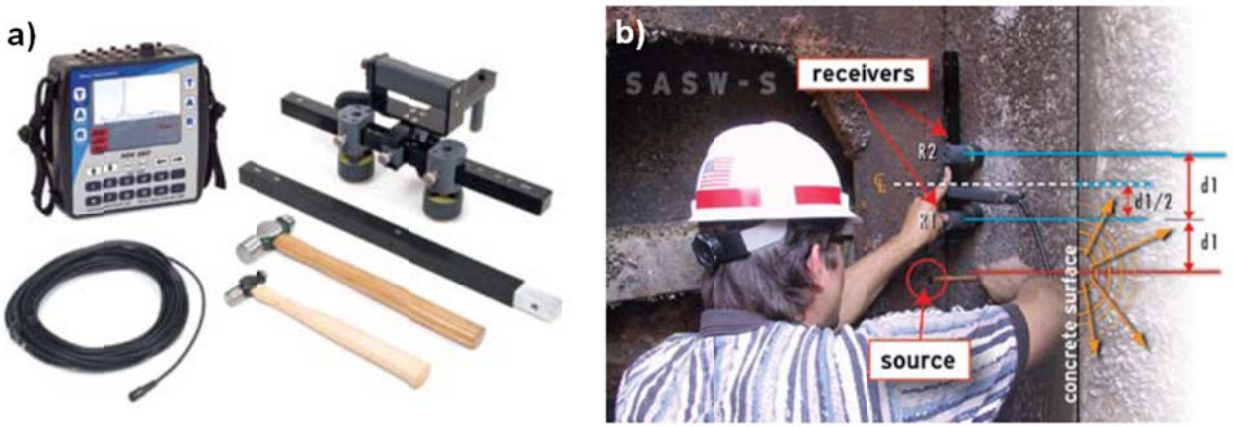

Figure 2.5: (a) Components of the Olson Engineering SASW-S, and (b) the SASW-S in use.

The Olson Engineering Multiple Impact Surface Waves (MISW) is similar to the SASW-S, and is also a suitable system for soil/pavement system surface wave testing. This system uses a testing procedure similar to the MSOR method used by SeisNDT. The MISW is user-friendly, and automatically processes raw data via Olson Engineering software and a Freedom PC. The MISW-SL is the most basic model, and is well suited for top layer modulus measurement. The MISW-ML is the more advanced version of this setup, and is capable of estimating modulus in the top two layers (via theoretical modeling). Note that because of the MSOR approach, testing with this system is more time consuming than with the DSPA.

Another commercially available surface wave test setup is the Continuous Surface Wave System (CSWS) by GDP Instruments (Figure 2.6). This system can evaluate clays to a depth of 30 ft, but has a sufficient data acquisition rate for evaluation of shallower layers (e.g., LSS). The source input for this system can be a continuous vibration source or a single impact source for SASW. In addition, the frequency of input vibration can be adjusted to evaluate a range of depths. This system offers user-friendly MS Windows-based interface with automated data acquisition and both time domain and spectral processing. The downside to this system is that it can take up to 45 minutes to generate one modulus profile, making it considerably less efficient than the D-SPA.

Figure 2.6: The Continuous Surface Wave System (CSWS) by GDP Instruments.

CHAPTER 3: TEST PROGRAM

3.1 Test Site Summary

There were no CDOT LSS projects constructed within the Denver metropolitan area during this study period. Therefore, experimental efforts including seismic testing of LSS were conducted at three housing development sites, namely Truth Christian Academy (Lakewood), Solterra (Lakewood), and Candelas (Arvada) (Figure 3.1). Soil properties, site construction details, and lime/cement mix designs are summarized in Table 3.1. Both free-free resonance testing of reconstituted LSS cylinders and surface wave testing of field-constructed LSS were performed at all three sites. Individual site maps with test locations are shown for Truth Christian Academy (TCA), Candelas, and Solterra in Figures 3.2, 3.3, and 3.4, respectively. Lime stabilization at all three sites was conducted by ARS, Inc. Each site was treated (application + mixing) with hydrated quicklime (in accordance with mix design specifications) and allowed to mellow for 2-4 days (Figure 3.5a). On the day of compaction, TCA and Candelas soils were treated with dry cement powder (Figure 3.5b), remixed at optimum moisture content (Figure 3.5c), and compacted (Figure 3.5d). Solterra soil was not cement treated; compaction was performed after final remixing and moisture conditioning of lime-treated, mellowed soil. A summary of the laboratory and field testing program is presented in Table 3.2.

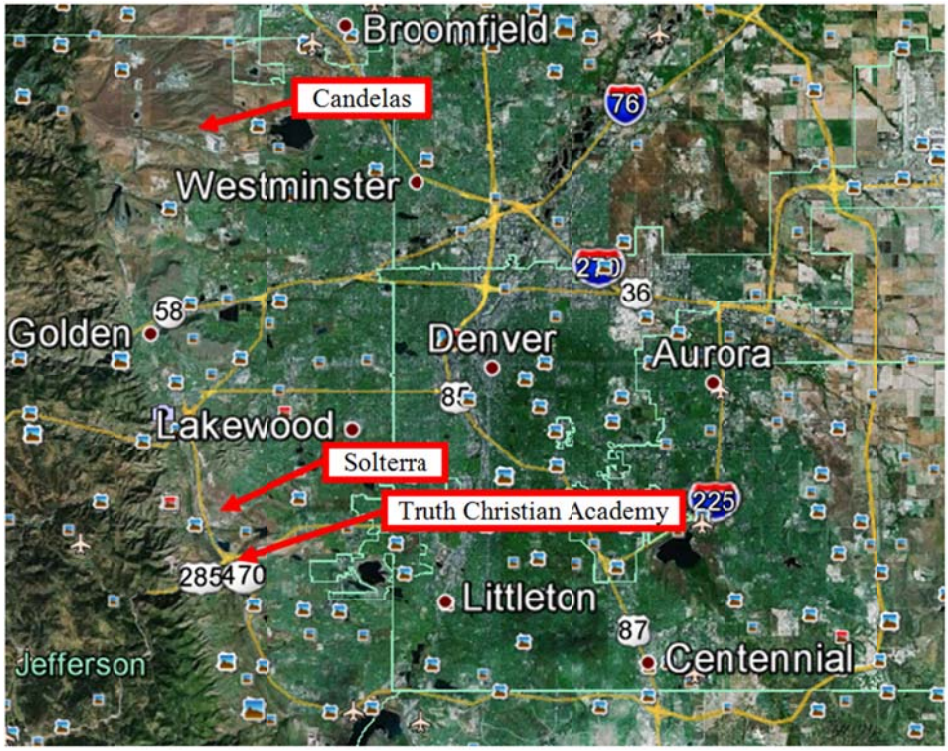

Figure 3.1: Field test site locations in the Denver Metro Area (image modified from Google Earth).

Table 3.1: Summary of soil properties and lime/cement mix designs for all sites tested in this study.

Site	Construction Date	AASHTO Classification	LL	PL	PI	Lime Content (%)	Cement Content (%)
TCA	8/23/2011 [a] 3/25/2012	A-7-6	55	19	36	5	3.0
Candelas	8/22/2012	A-7-6	53	23	30	4.0	2.0
Solterra	11/7/2012	A-7-6	51	19	32	5.0	0.0

[a] TCA Zones 1 and 2 were constructed on 8/23/11. TCA Zone 3 was constructed on 3/25/12.

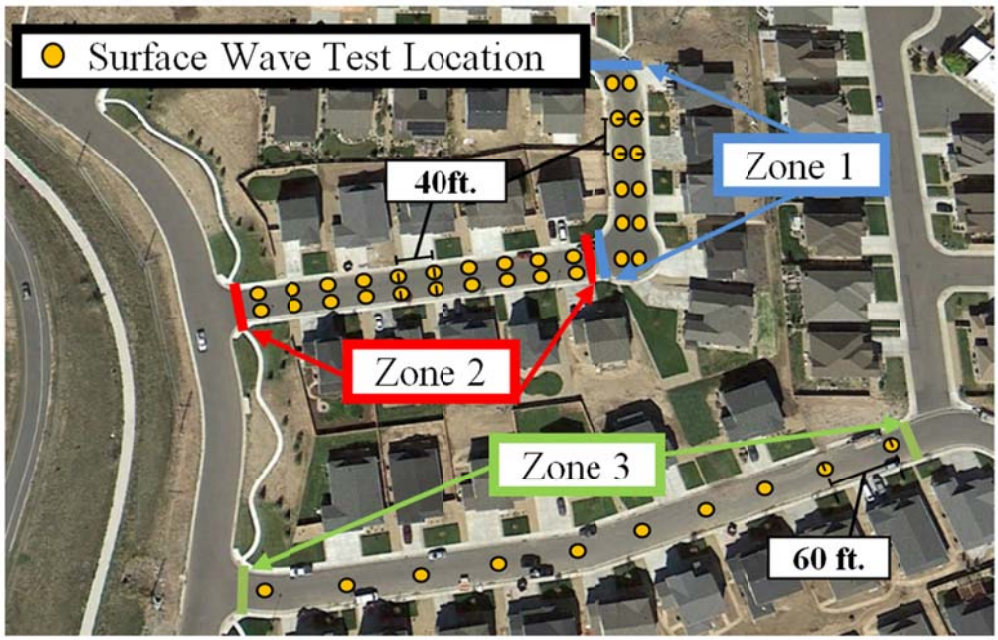

Figure 3.2: Truth Christian Academy Field Site (image modified from Google Earth).

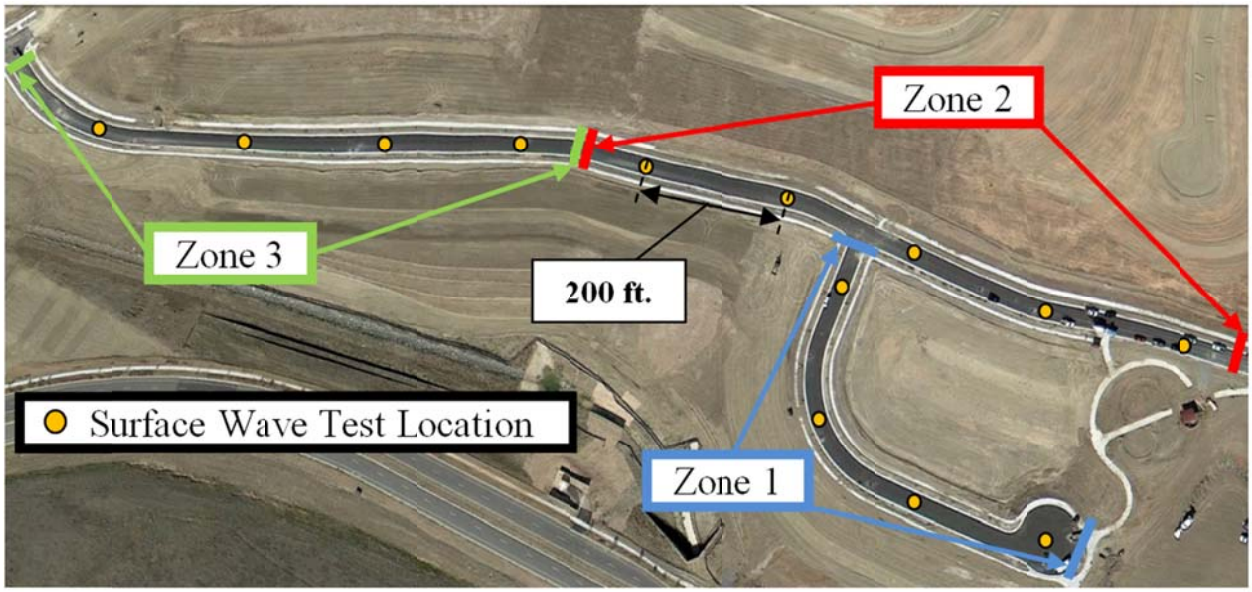

Figure 3.3: Candelas Field Site (image modified from Google Earth).

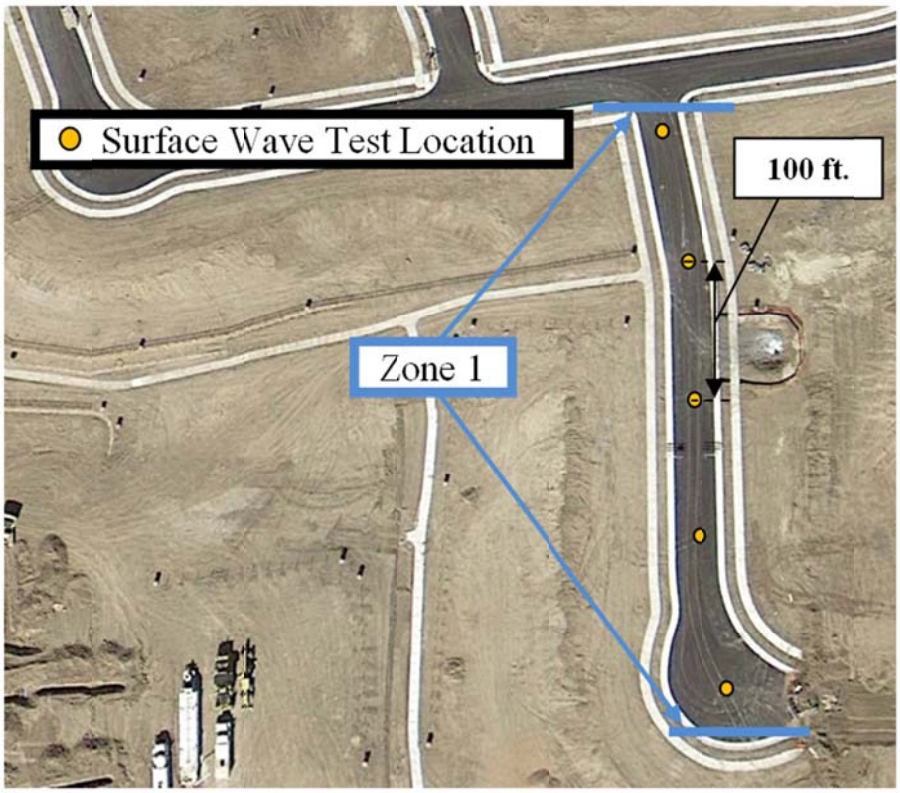

Figure 3.4: Solterra Field Site (image modified from Google Earth).

Table 3.2: Summary of FFR and surface wave testing program for all sites.

Site	Zone	FFR Cylinders (#)				Surface Wave Test Locations (#)	Zone Length (ft)	Test Location Spacing (ft)	Array Length (m) [a]
		8°C	23°C	Field	41°C				
TCA	1	0	5	5	0	12	200	40	1
	2	0	5	0	0	20	340	40	1
	3	5	5	5	5	10	560	60	3
Candelas	1	0	5	5	0	4	650	200	3
	2	5	5	5	5	5	1000	200	3
	3	0	5	0	0	4	1000	200	3
Solterra	1	5	5	5	5	5	400	100	3

[a] Because SeisNDT inputs and exported results are in SI units, information pertaining to FFR and surface wave testing remains in SI units.

Figure 3.5: (a) Application of quicklime slurry, (b) application of cement, (c) soil/stabilizer mixing, and (d) final compaction.

3.2 Laboratory Test Program

3.2.1 Specimen Preparation and Storage

On the day of final field remix and compaction of an LSS section, the mixed LSS was gathered (prior to final compaction) for cylinder preparation. At each soil gather location (1 per mixed section), enough loose LSS was gathered to prepare 5 cylinders per curing regime. Cylinder number and curing regime for each site are summarized in Table 3.2, and further discussion of temperature curing regime significance is presented in Section 4.1. Specimens were reconstituted with a 4 in diameter by 8 in tall cylindrical soil compaction mold, using four hand-tamped 2 in (compacted) layers of predefined soil mass (Figure 3.6). This process mimics the specimen preparation technique used for resilient modulus testing (AASHTO T294), and is also

the technique used by Toohey and Mooney (2012). Immediately after preparation, the reconstituted LSS cylinders were sealed in plastic bags. Some cylinders were returned to the laboratory for curing, while others were placed in a soil trench on site to simulate field curing (Figure 3.7). This trench was approximately 6 in deep, 10 in tall, and long enough to accommodate the desired number of cylinders to be cured in the field. The cylinders were placed in the trench and covered with loose soil, mounded to a height approximately 5 in above the ground surface (Figure 3.7b). A temperature probe was placed in the soil trench to record the in-situ curing temperature. Further discussion of temperature measurement is discussed in section Chapter 4.

Figure 3.6: (a) FFR cylinder preparation and (b) example specimen.

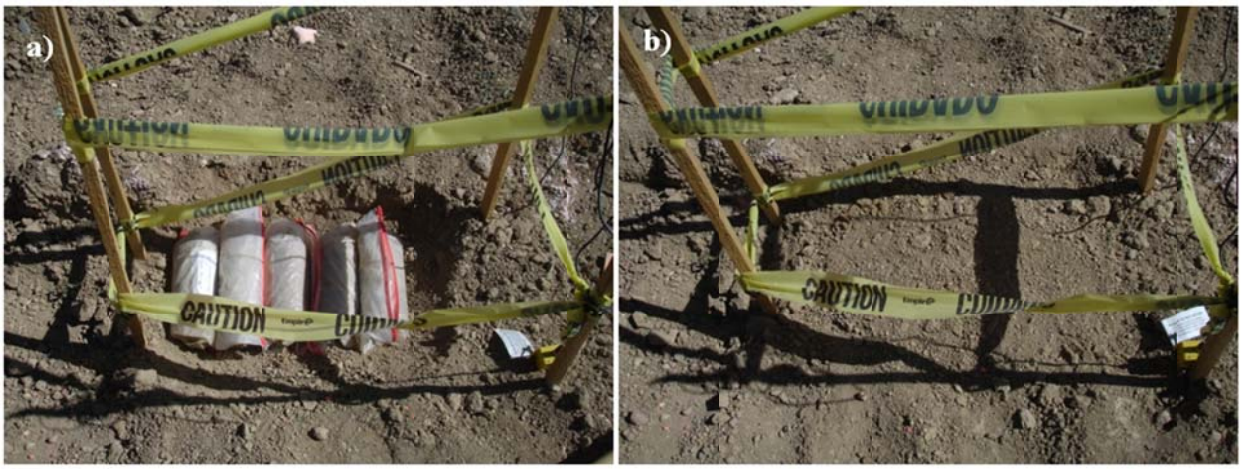

Figure 3.7: (a) FFR field cylinder storage trench uncovered and (b) covered.

3.2.2 Free-Free Resonance Testing

To perform free-free resonance (FFR) testing, cylinders were removed from the plastic sealing bags and placed (one at a time) on a foam sheet. Each cylinder was subjected to an axial impulse load (via a tap using a wood block) (Figure 3.8a) to induce longitudinal free vibration. Each cylinder was subjected to five impacts resulting in five acceleration vs. time history records (Figure 3.8b). A Tukey window was applied to these time history records to remove any forced vibration induced by the source impact. Windowed time histories were then subjected to a fast Fourier transform (FFT) and the five resulting frequency spectrums averaged for resonant frequency identification (Figure 3.8c). Using the cylinder's mass density, the resonant frequency is used to estimate seismic Young's modulus using Equation 3.1

$$E_0 = \rho(2f_{rp}L)^2 = \rho(V_p)^2 \tag{3.1}$$

where:

E_0 = seismic Young's modulus (MPa)

ρ = mass density (kg/m^3)

f_{rp} = longitudinal resonant frequency (Hz)

L = cylinder length (m)

V_p = material p-wave velocity (m/s)

As a general note, SeisNDT requires inputs (and exports results) in SI units, so both FFR and surface wave results are exported in this form.

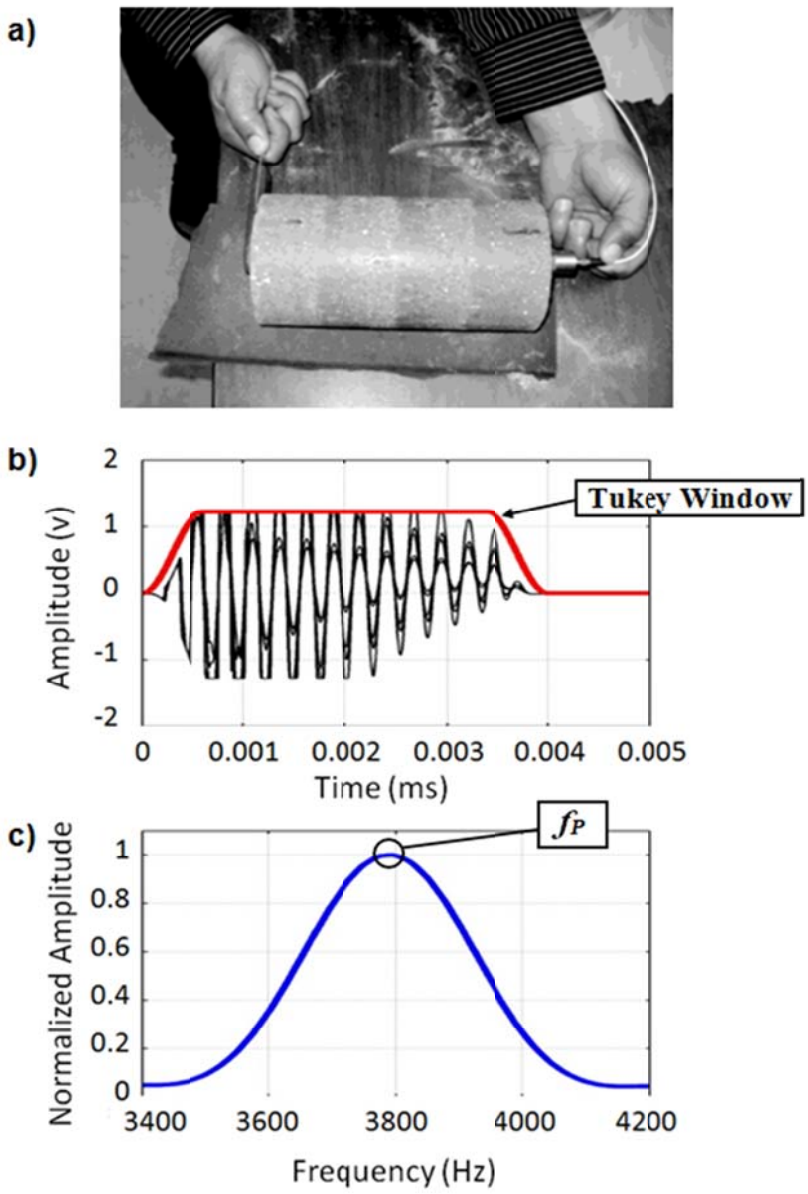

Figure 3.8: (a) Cylinder, accelerometer, and impact orientation for FFR longitudinal excitation with (b) corresponding windowed time history, and (c) frequency spectrum with selected resonant frequencies.

3.3 Field Test Program

3.3.1 Principles of Surface Wave Testing

Material characterization via surface wave testing is based on the propagation of various wave types in an elastic medium. The two fundamental types of body (or bulk) waves are compressional (P) and shear (S) waves (Figure 3.9). Surface waves are stress waves that travel along the free surface of a material. These waves have velocities that are dependent on the elastic

properties of the material (Ryden, 2004). Determination of P and S wave velocities as a function of a material's elastic properties is shown in Equations 3.2 and 3.3. The full derivation of this theory is presented in Ryden (2004). In layered media, guided waveforms can be generated by the interaction of P and S waves at the material layer interface (i.e., the interface between LSS and the unstabilized material below). One special type of guided wave is the Rayleigh wave generated from reflections and mode conversions of body waves (i.e., P and S waves) at the free surface (Rayleigh, 1885). Estimation of Rayleigh wave speed as a function of material properties is shown in Equation 3.4.

$$V_p = \sqrt{\frac{E(1-\upsilon)}{\rho(1+\upsilon)(1-2\upsilon)}} \tag{3.2}$$

$$V_s = \sqrt{\frac{E}{2\rho(1+\upsilon)}} \tag{3.3}$$

$$V_R = \frac{V_s}{(1.13-0.16\upsilon)} \tag{3.4}$$

where:

V_p is the material's p-wave velocity (m/s)

V_s is the material's s-wave velocity (m/s)

V_R is the material's Rayleigh wave velocity (m/s)

E is the material's Young's modulus (MPa)

ρ is the material's mass density (kg/m^3)

υ is the material's Poisson's ratio (unitless)

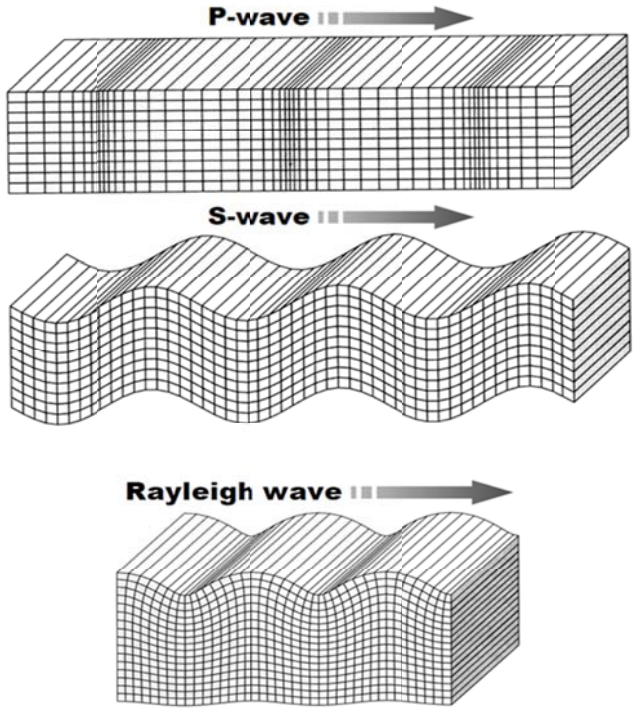

Figure 3.9: Particle motion for propagating P waves, S waves , and Rayleigh waves (modified from Ryden (2004)).

When an impulse source acts on the surface of a homogeneous halfspace, P, S, and Rayleigh waves are generated. However, 67% of the energy induced by this source impulse propagates as a Rayleigh wave (Richart et al. 1970). Rayleigh waves have significantly larger amplitude than body waves when measured from the material surface, and for this reason, they are often the easiest to measure with surface wave testing. Rayleigh waves travel through a depth zone of approximately one wavelength (Graff, 1975), meaning that the frequency of the source impulse is very important (i.e., longer wavelengths/lower frequencies interrogate a greater depth than shorter wavelengths/higher frequencies).

The results of surface wave measurements can be interpreted either through time domain analysis or frequency domain (spectral) analysis. Figure 3.10 illustrates an example experimental setup and the resulting time domain results. By picking the first arrival time of a wave form at a minimum of two locations, the wave velocity in the material can be estimated if the separation distance between the two measurement locations is known. Rayleigh waves are often the target of this type of analysis because of their larger amplitude, but lower amplitude P waves are sometimes detected as well (in which case, V_P can be directly estimated). Once material wave

velocity has been appropriately identified, the seismic Young's modulus of the material can be estimated using Equation 3.1 and the material's mass density.

In general, time domain analysis is sufficient for characterization of LSS. It is a faster and simpler procedure than spectral analysis. However, spectral analysis can also estimate the thickness of the top layer of material (e.g., field-constructed LSS). The underlying theory and data processing for spectral analysis are significantly more complicated than the time domain approach, and are therefore not discussed in detail here. Full detail on the theoretical background and data processing are discussed in Ryden (2004). However, some commercially available software automatically performs spectral analysis from raw data and may therefore be a more desirable approach if LSS layer thickness is also desired. Several commercially available surface wave setups are discussed in Section 2.3.

Basic time domain analysis of surface wave data involves the identification of Rayleigh (and possibly P) waves and picking their subsequent arrival times. Figure 3.10 illustrates the most basic experimental setup and corresponding time histories. As seen in Figure 3.10b and c, arriving P waves have significantly smaller amplitude than Rayleigh waves from the same time history. If P waves can be readily identified in the time histories, V_p can be estimated directly using Equation 3.5.

$$V_p = \frac{x_2 - x_1}{t_{P2} - t_{P1}} \tag{3.5}$$

$$V_R = \frac{x_2 - x_1}{t_{R2} - t_{R1}} \tag{3.6}$$

$$V_P = [2(1+\nu)] \cdot [V_R(1.13 - 0.16\upsilon)] \tag{3.7}$$

where:

t_{R1} is the first arrival time of the Rayleigh wave in record 1 (s)

t_{R2} is the first arrival time of the Rayleigh wave in record 2 (s)

t_{P1} is the first arrival time of the P-wave in record 1 (s)

t_{P2} is the first arrival time of the P-wave in record 2 (s)

x_1 is the source to receiver distance for record 1 (m)

x_2 is the source to receiver distance for record 2 (m)

However, if only Rayleigh waves are present, V_p should be estimated using Equations 3.6/ 3.7 and the material's Poisson's ratio. Poisson's ratio for LSS typically ranges between 0.2 and 0.4. If the value is not known, 0.3 is a valid assumption.

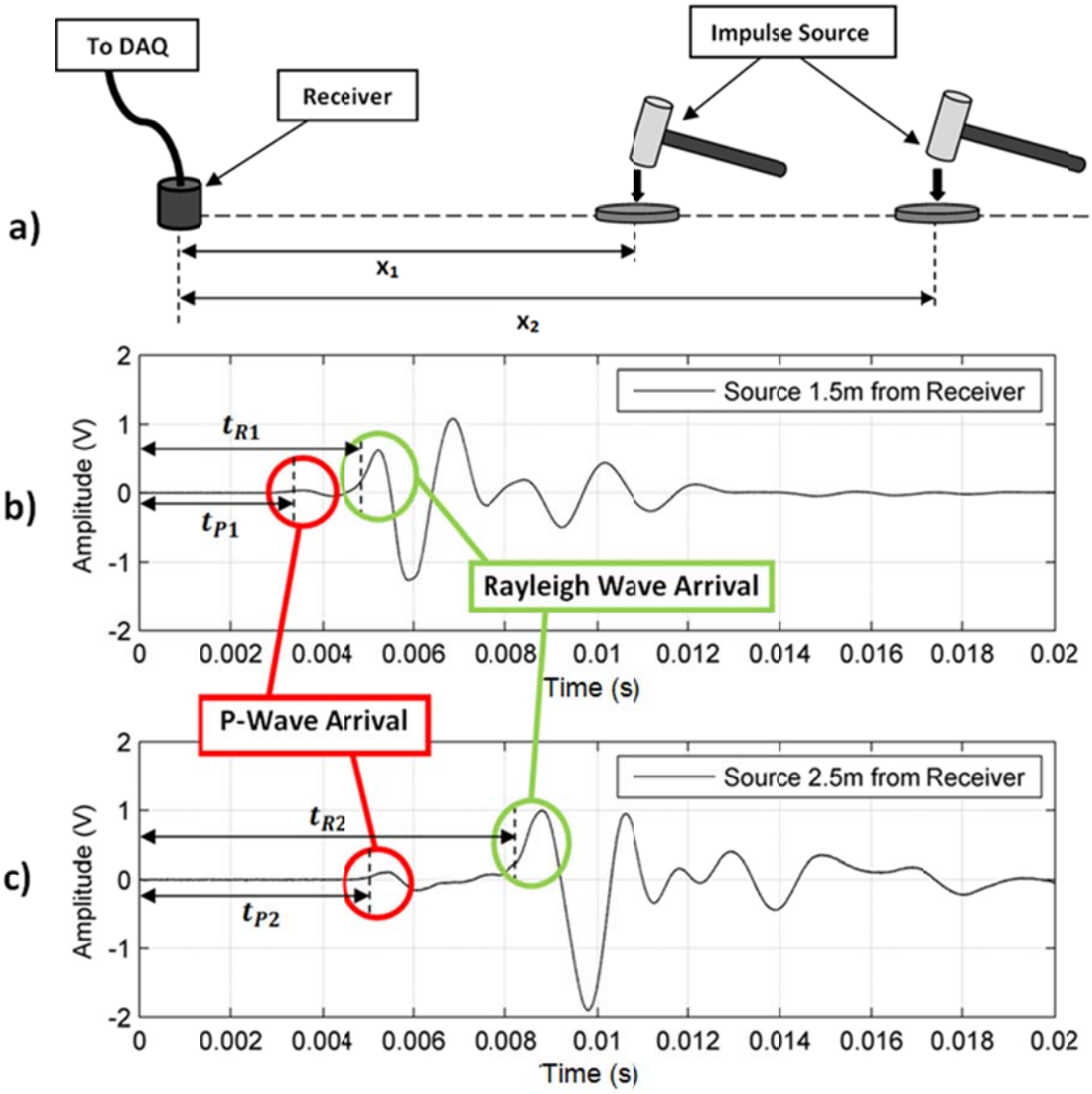

Figure 3.10: (a) Source and receiver configuration for simple surface wave testing, (b) waveform identification for example record 1, and (c) waveform identification for example record 2.

Frequency domain (spectral) analysis of surface waves is a complicated process requiring specialized test equipment and data processing algorithms. For this reason, the details of spectral analysis are not discussed here (i.e., spectral analysis is often performed by pre-constructed

software and would not be done manually). A detailed description of the underlying assumptions and mathematics is presented in Ryden (2004). Ideally, this software would import raw time history data traces and convert them into a dispersion curve. Both time domain and spectral analysis was performed (via SeisNDT) on surface wave data, and interpretation of spectral results is discussed in Appendix C.

3.3.2 Experimental Setup and Interpretation of Surface Wave Data

This research utilized a more complex surface wave testing program in the interest of obtaining more robust data sets for spectral analysis. The setup used for field testing is shown in Figure 3.11. Test arrays were either 1 m (at TCA) or 3 m (all other sites) in length. Wave behavior as a function of source to receiver distance is more readily visible in 3m array results, and therefore, discussion of spectral analysis will use 3m test array data. An example test protocol for a 3m test array is shown in Figure 3.12a. Note that for the multiple source one receiver (MSOR) approach, one accelerometer receives signal from 30 separate impacts (i.e., multiple sources). These individual records are superimposed (Figure 3.12b) to simulate multichannel analysis of surface waves (i.e., a system with 1 source and 30 receivers). Example data from a 3m array test is shown in Figure 3.12b and (amplified for wave identification) c. Again, note that in the un-amplified record, P waves are somewhat difficult to identify. For this reason, it is often necessary to amplify raw time histories to identify P waves (if they are present at all).

Figure 3.11: SeisNDT experimental surface wave test setup.

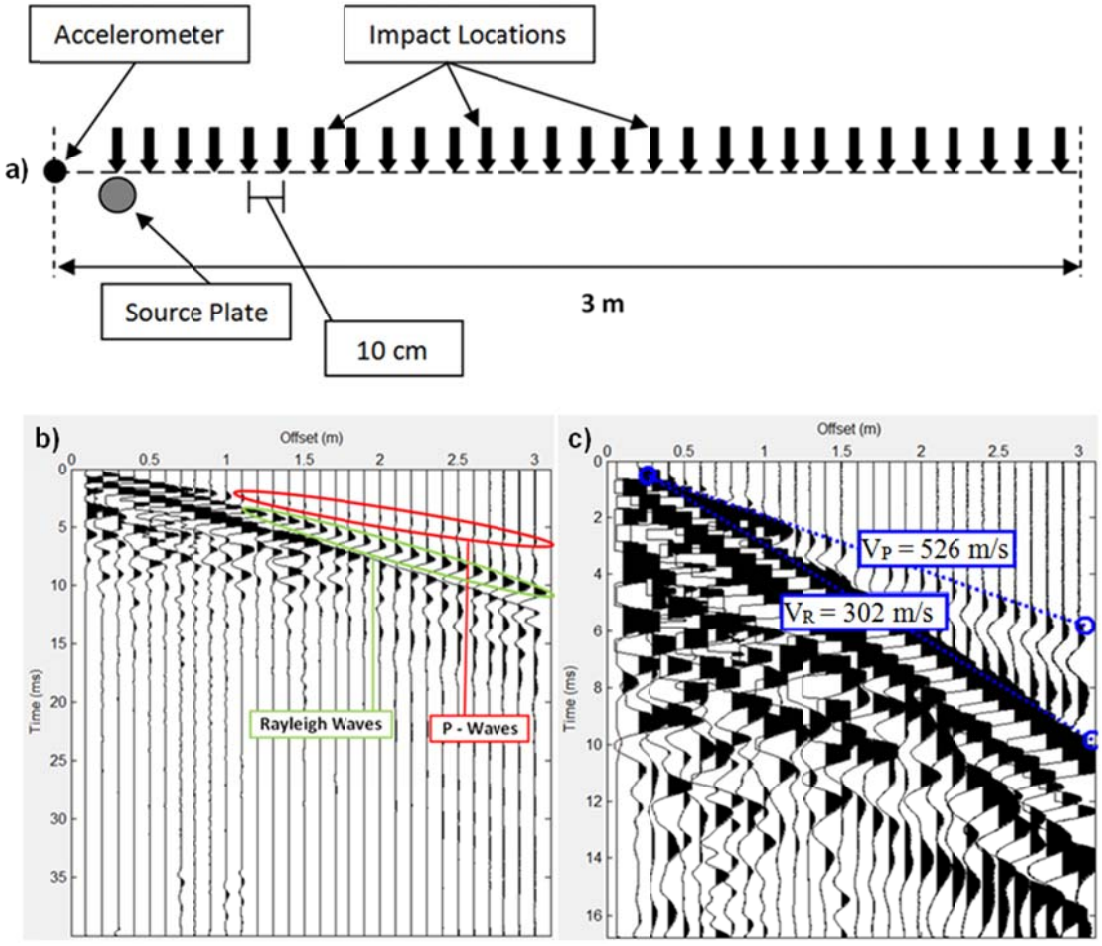

Figure 3.12: (a) Surface wave testing setup utilized in this research, (b) raw time domain data from one of these tests, and (c) magnified raw time domain data for easier identification of waveforms.

3.3.3 Additional Considerations for Testing on Field LSS

The field-constructed LSS at all three test sites was for low volume residential roads, and therefore, recommended guidelines for LSS preparation were not always followed. Specifically, sections were not always compacted within the recommended time frame after final remix and final surface grading (Figure 3.14a) was conducted post compaction day (i.e., day 3, 5, or 7). These practices resulted in disturbance of the curing LSS. If not compacted within the allowable time frame (i.e., Section 307 of CDOT's specification on Lime Stabilized Subgrade states that compaction should begin immediately after final remix), LSS may not be compacted at optimum moisture content, and will therefore underperform. Sections compacted below optimum moisture content often undergo significant surface cracking (Figure 3.14b). Large cracks in the field-constructed LSS surface result in extreme attenuation of surface waves, making this method less

effective. In addition, post compaction day grading (Figure 3.14a) disturbs the chemical reactions within the curing LSS, causing it to underperform or halt performance entirely. For these reasons, surface wave test results from this research often predicted lower modulus values compared to FFR results. This lack of agreement is due to differences in construction practice, not testing equipment or procedure. That is to say, FFR cylinders were compacted immediately after final remix and not damaged or disturbed post-compaction, and therefore, better performance would be expected compared to the corresponding field-constructed LSS. Differences between FFR and surface wave results are discussed in greater detail in section 4.3.

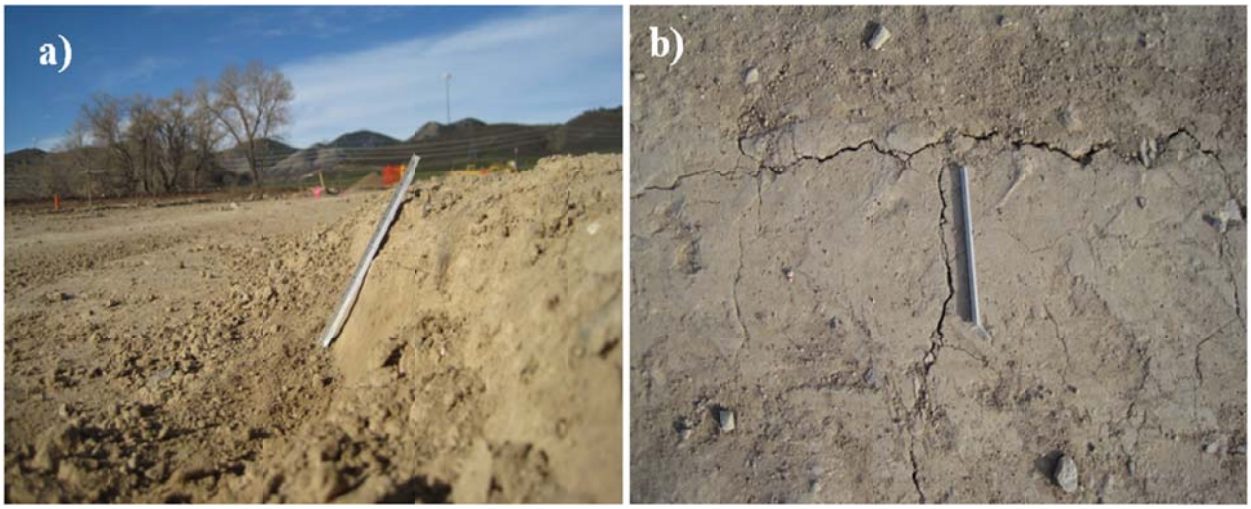

Figure 3.13: Illustration of field condition variability – (a) significant post-compaction grading, and (b) surface cracking. Note the reference ruler in these images is 10 cm in length.

This study proposed the use of cored LSS cylinders from field compacted sections for verification of performance via FFR and UCS testing. While several attempts were made to core field LSS, the resulting cylinders were disturbed and not testable. For this reason, FFR and UCS results from these cylinders would not be representative of expected LSS behavior. To this end, it is not realistic to obtain undisturbed LSS cylinders from field coring, and therefore, no UCS testing was performed. The study also proposed FFR testing (followed by UCS testing) of remolded Proctor specimens from field mixed LSS. A thorough literature review revealed that FFR testing should only be performed on specimens with a 2:1 (or greater) specimen height to diameter ratio. As Proctor specimens do not meet this criterion (i.e., Proctor specimens have a 1.15:1 height to diameter ratio), FFR testing of these specimens is not valid. Resonance testing

on Proctor specimens generated modulus results inconsistent with 2:1 specimens based on the FFR modulus equation (3.1). Additional research and finite element modeling would be necessary to validate the expected resonant frequency behavior of specimens with a height to diameter ratio less than 2:1. Toohey, Mooney, and Bearce (2013) suggest that the UCS values obtained from testing on standard Proctor specimens exhibit an approximately 1:1 correlation to UCS values obtained from testing on 4 in x 8 in cylindrical specimens. Furthermore, Toohey and Mooney (2012) suggest a correlation between E_0 and UCS q_u (both obtained from 4 in x 8 in specimens) shown in Equation 3.9. If a correlation to q_u is desired, Equation 3.9 should be used.

$$E_0(MPa) = 1735 * q_u(MPa) - 225(MPa) \tag{3.9}$$

CHAPTER 4: RESULTS

4.1 Temperature Raw Data

Because curing temperature must be considered to appropriately predict seismic modulus growth in LSS, the temperature curing regimes for each site are discussed first to lend context to FFR and surface wave seismic modulus results. To characterize the temperature dependence of LSS curing, FFR cylinder sets were cured at constant temperatures of 8°C/46°F, 23°C/73°F, and 41°C/105°F (in the laboratory) and at variable temperature regimes in the field. Curing regimes for each cylinder set are summarized in Table 3.2. Note that the constant temperatures used for laboratory curing are not arbitrary. 23°C/73°F is the temperature specified for normal curing in the laboratory and 41°C/105°F is the temperature specified for accelerated curing in the laboratory. 8°C/46°F is representative of decelerated curing, as Mallela et al. (2004) notes that LSS reactions are decelerated below a temperature of 13°C/55°F.

In the field, ambient (air) temperature, soil trench temperature (i.e., Figure 3.7), and field-constructed LSS temperature were monitored using TinyTag 2.0 temperature sensors (Figure 4.1). Ambient temperature was recorded directly on the sensor, while soil temperatures were measured by a removable in-situ probe shown in Figure 4.1. Measured field temperatures for TCA 2011, TCA 2012, Candelas, and Solterra are shown in Figures 4.2, 4.3, 4.4, and 4.5, respectively.

Figure 4.1: TinyTag 2.0 Temperature sensory and in-situ soil probe used for temperature measurement.

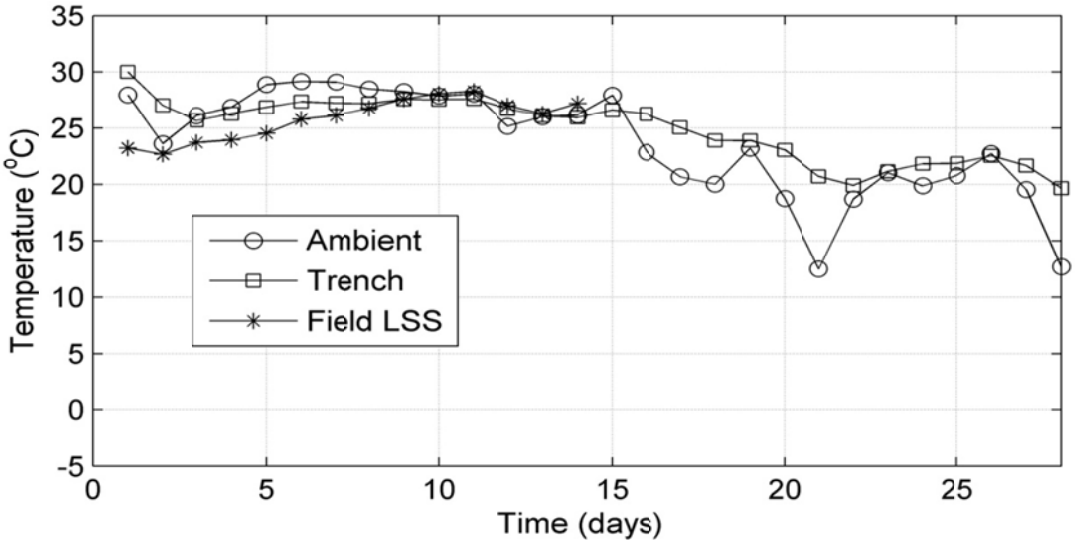

Figure 4.2: Ambient, trench, and field-constructed LSS temperature history for TCA 2011.

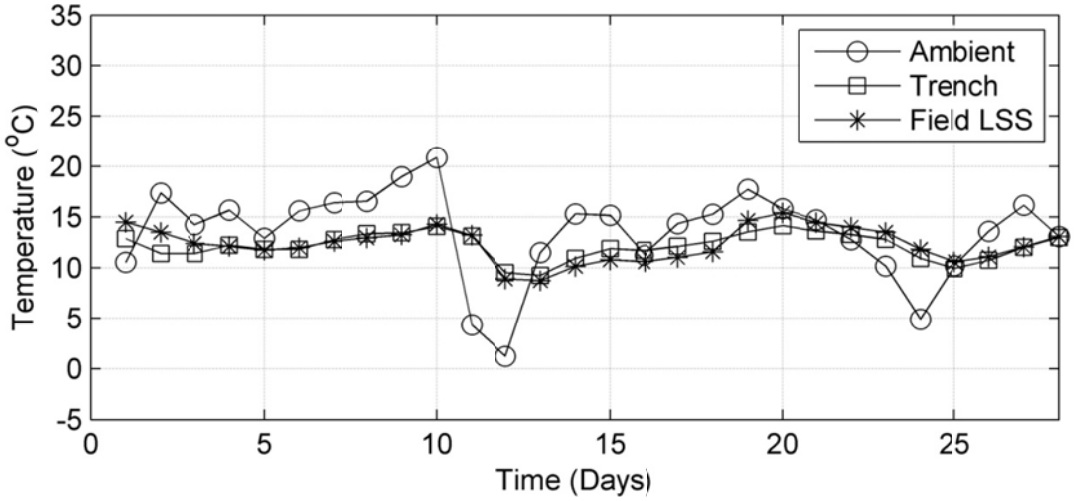

Figure 4.3: Ambient, trench, and field-constructed LSS temperature history for TCA 2012.

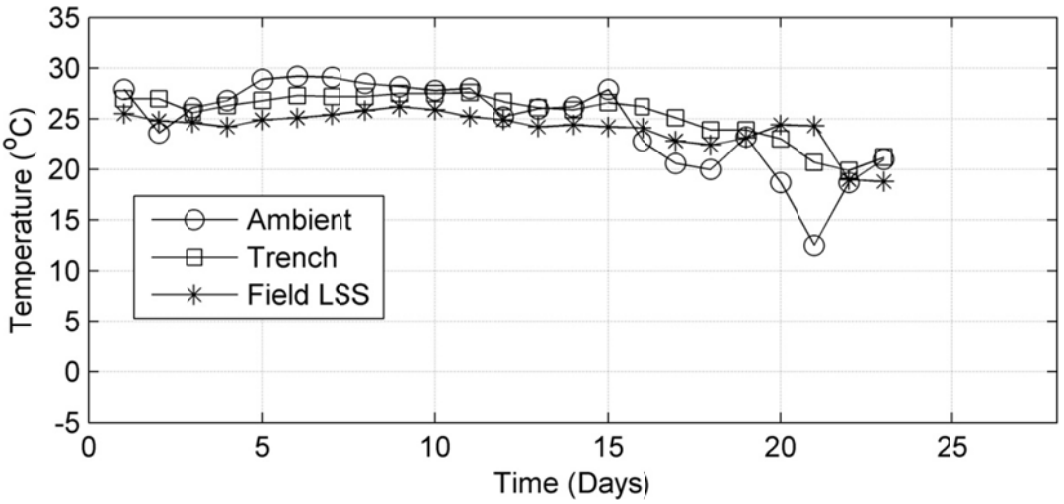

Figure 4.4: Ambient, trench, and field-constructed LSS temperature history for Candelas.

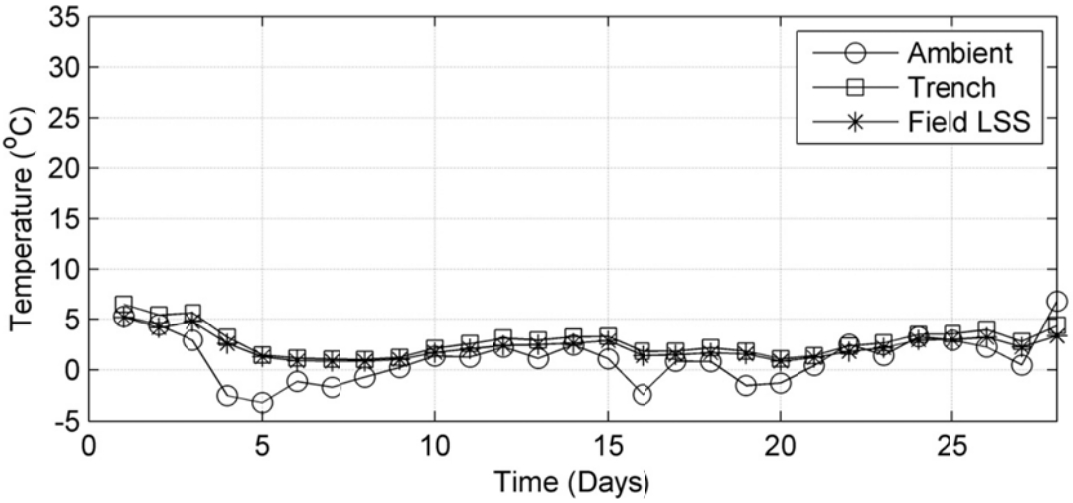

Figure 4.5: Ambient, trench, and field-constructed LSS temperature history for Solterra.

For all sites, the general trend in temperature behavior suggests that ambient temperature undergoes the most extreme variation and oscillates on either side of the less variable temperatures measured in the cylinder storage trench and field-constructed LSS layer. Furthermore, the temperature in the cylinder storage trench was greater than or equal to field-constructed LSS layer temperature. One possible explanation for this discrepancy is that the probe in the field constructed LSS was compacted into the layer, whereas the storage trench probe was simply mounded with loose soil. Probe depth for the storage trench is known, but final depth of the probe in compacted LSS is not known exactly (i.e., the probe was placed in the

loose, remixed LSS and compacted into the layer). Because of this variation between temperatures, Figure 4.6 suggests a correlation between ambient temperature and field-constructed LSS layer temperature. This correlation is implemented in the pilot LSS seismic QA spec (Section 5.1) so that soil temperature can be inferred from ambient temperature in the event that it is not measured directly.

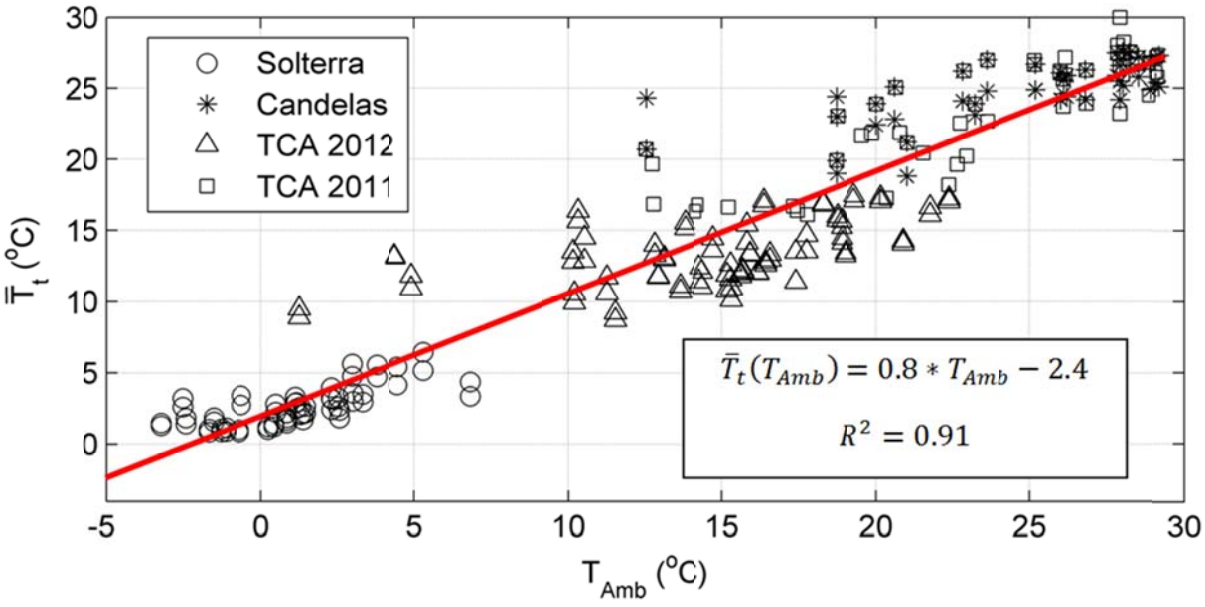

Figure 4.6: Correlation between ambient and LSS soil temperature.

4.2 Free-Free Resonance Results

This section summarizes the FFR test results from all test sites and zones. For each site, the seismic Young's modulus ($E_{0\,FFR}$) is plotted vs. curing time. For TCA 2011, each cylinder exhibits modulus gain over 28 days with low range/mean values (i.e., < 0.1 for all cylinder sets at day 28). There is a small (but noticeable) difference in the modulus growth of field cured vs. laboratory cured cylinders. As expected, the higher temperatures in the field, particularly early on, induce greater modulus growth than in the laboratory cylinders. The effects of temperature on LSS curing are significant, and are addressed in detail in Section 4.4. $E_{0\,FFR}$ data for TCA 2011 (Zone 1) is shown in Figure 4.7a, with field temperature regime shown in 4.7b and $E_{0\,FFR}$ range/mean for the 5 specimens in 4.7c. TCA Zone 2 cylinders were only subjected to laboratory curing and results are presented in Figure 4.8a with range/mean values in Figure 4.8b.

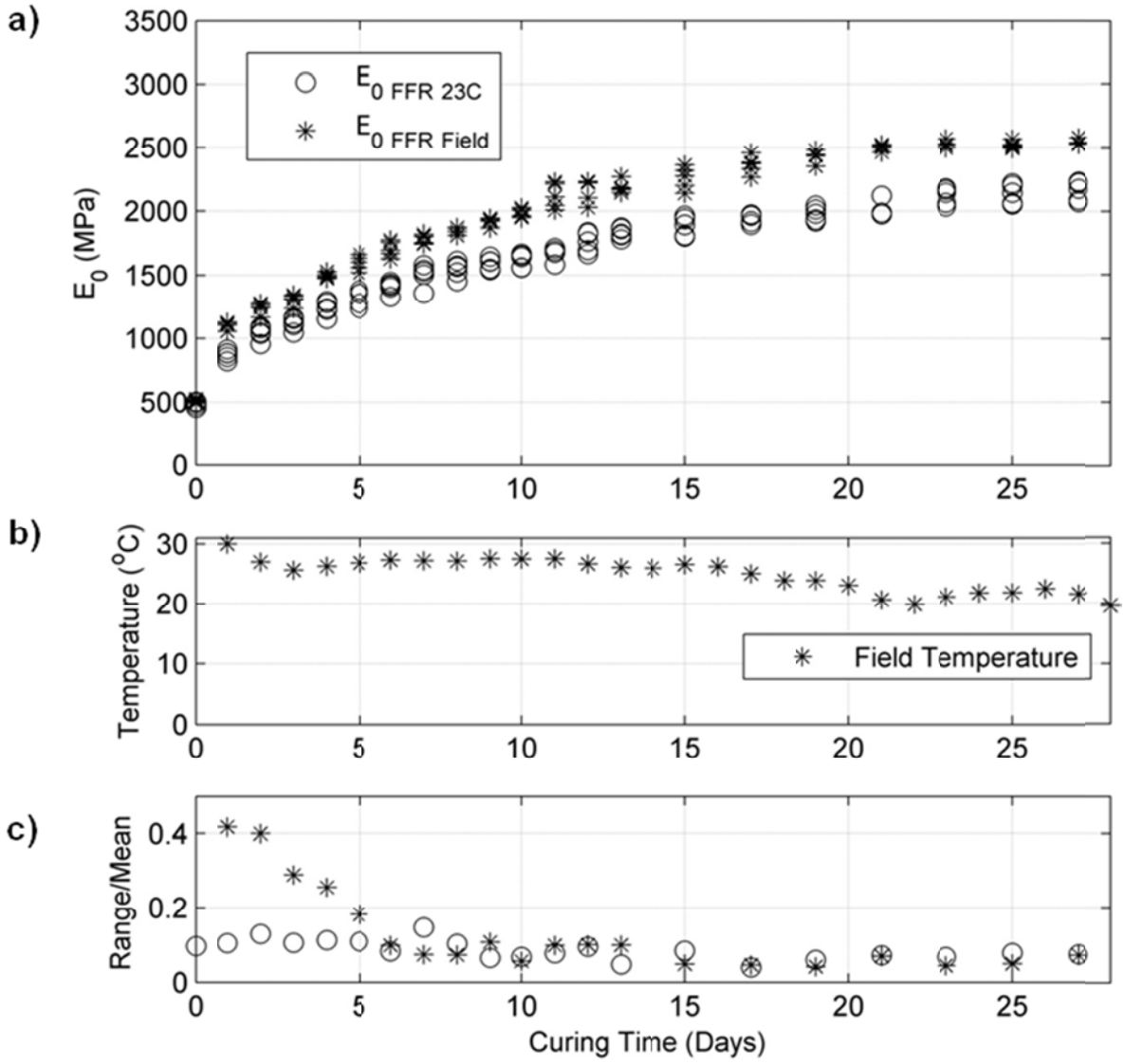

Figure 4.7: (a) Seismic Young's modulus vs. curing time for TCA 2011 – Zone 1, (b) curing temperature regime for field cylinders, and (c) range/mean for the data in (a).

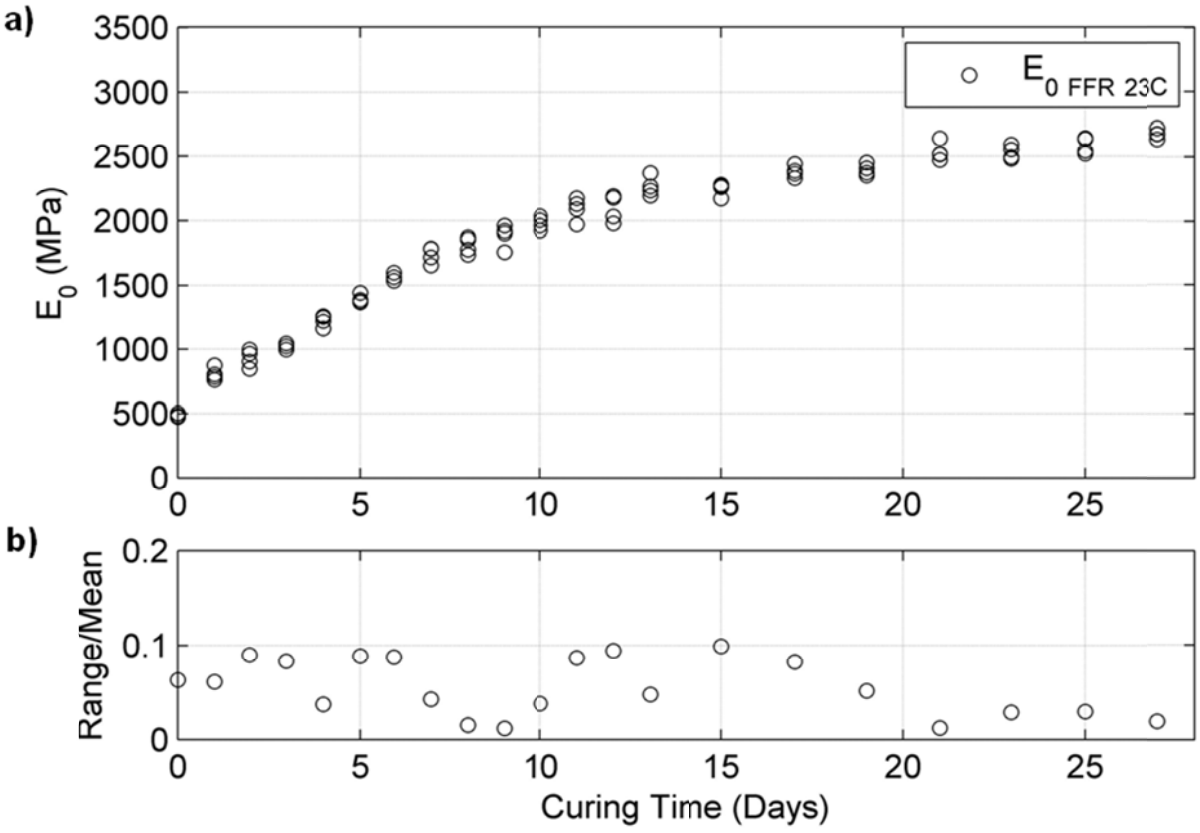

Figure 4.8: (a) Seismic Young's modulus vs. curing time and (b) range/mean of data for TCA 2011 – Zone 2.

$E_{0\ FFR}$ data for Candelas (Zone 1) is shown in Figure 4.9.a with TCA 2011, each cylinder shows modulus gain over all 28 days, but each data set displays greater variation (range/mean) set than TCA data. Range/mean for this data is consistent with typical geotechnical data in the literature (i.e., < 0.25 for all cylinder sets at day 28). The larger range/mean values for these cylinders may be a result of field mixing (i.e., these soils were mixed on a large scale in the field, as opposed to a laboratory mix with precisely weighed proportions of lime/soil/water).

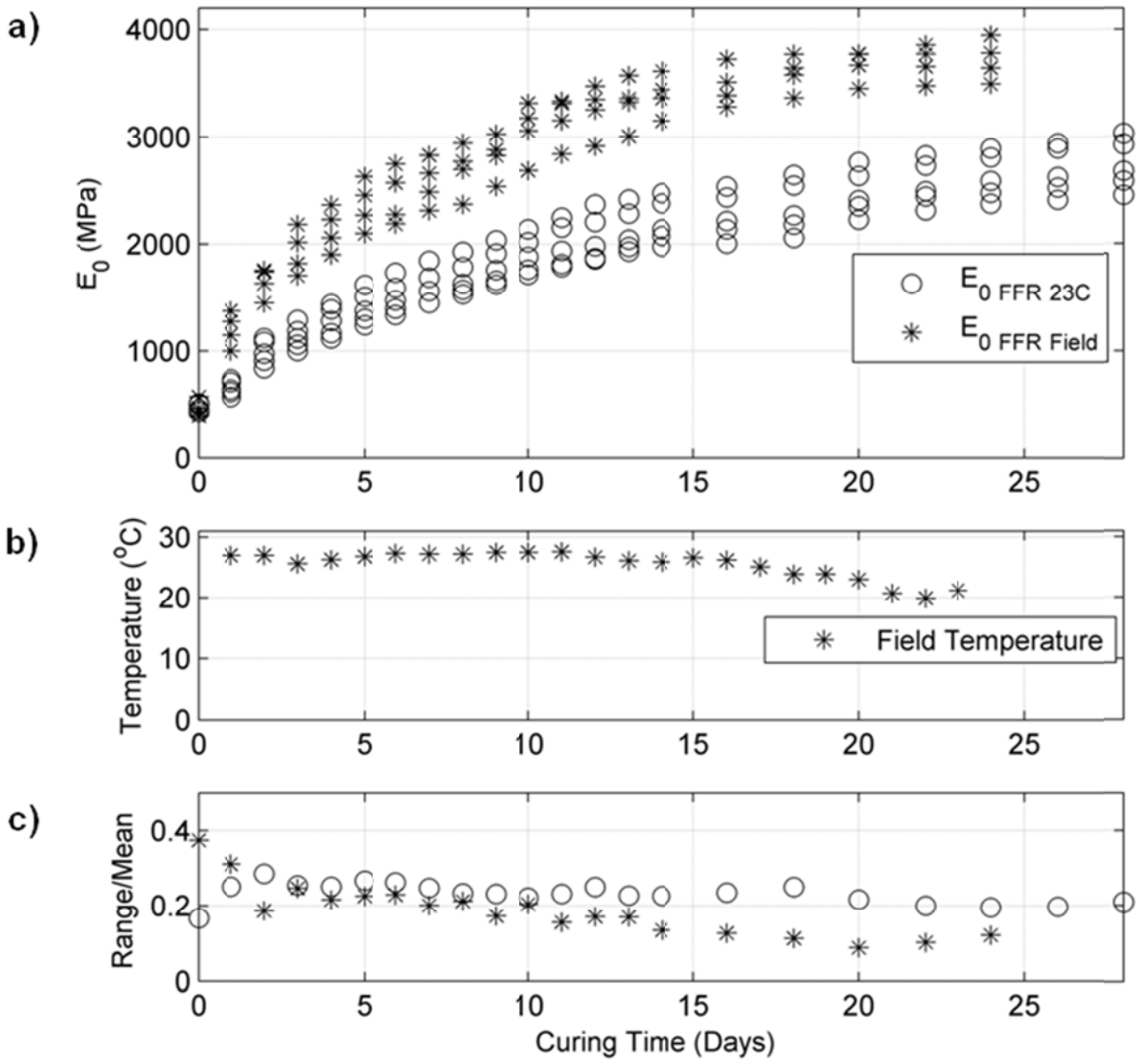

Figure 4.9: (a) Seismic Young's modulus vs. curing time for Candelas– Zone 1, (b) curing temperature regime for field cylinders, and (c) range/mean for the data in (a).

TCA 2011 data showed that temperature has a significant effect on seismic modulus growth, and therefore, one goal for Candelas testing was to cure FFR cylinders at different constant temperatures. For Candelas Zone 2, four FFR cylinder sets were tested (Figure 4.10a). The variation in modulus growth behavior for this zone is significant (e.g., see $E_{0\ FFR\ 8C}$ compared to $E_{0\ FFR\ 41C}$). All cylinders exhibit modulus growth over 28 days with range/mean values that are notably higher than TCA, but comparable to Candelas Zone 1. $E_{0\ FFR\ 41C}$ ceased modulus gain after approximately 5 days. Mallela *et al.* (2004) states that LSS curing at temperatures above 41°C/105°F may induce reactions that are not present in lower temperature curing. To this end,

$E_{0\,FFR\,41C}$ may undergo reactions not present in the other cylinders which could explain the difference in behavior (i.e., halt of reaction/modulus gain).

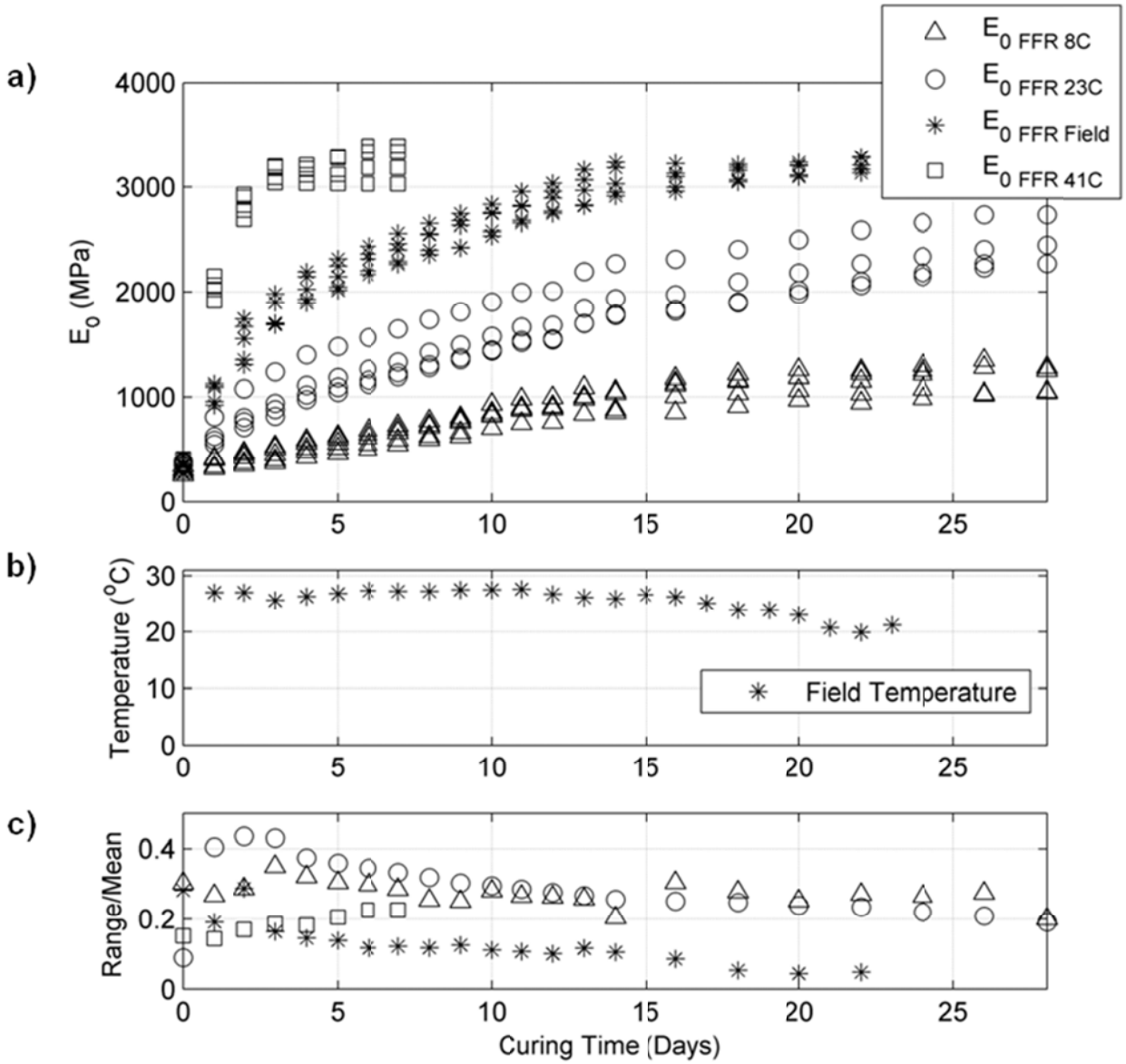

Figure 4.10: (a) Seismic Young's modulus vs. curing time for Candelas – Zone 2, (b) curing temperature regime for field cylinders, and (c) range/mean for the data in (a).

$E_{0\,FFR}$ data for Solterra are shown in Figure 4.11. As expected, modulus gain at lower temperatures is lower than at higher temperatures. All cylinders exhibit modulus gain over 28 days with low range/mean values (i.e., < 0.11 for all cylinder sets at day 28). Note that one cylinder cured at 41°C/105°F has a significantly lower modulus than the other cylinders in the set. Because these data values are more than three standard deviations from the mean, it is

assumed that this cylinder underwent disturbance not experienced by the other cylinders. To this end, the cylinder is not included in average data calculations. After approximately 13 days, Solterra $E_{0\ FFR\ 41C}$ exhibited similar behavior to $E_{0\ FFR\ 41C}$ from Candelas Zone 2 (i.e., halted modulus gain). Again, the specific reason for this halt in reaction is not known, but elevated curing temperature is a probable cause. This collective data set is especially interesting because the field construction occurred in November (i.e., field curing temperature regime was notably lower than sections prepared in summer/fall months). Note that the field-cured cylinders behave very similarly to the 8°C/46°F laboratory-cured cylinders. This further supports the need for treating LSS modulus growth as a maturity function instead of just a function of curing time.

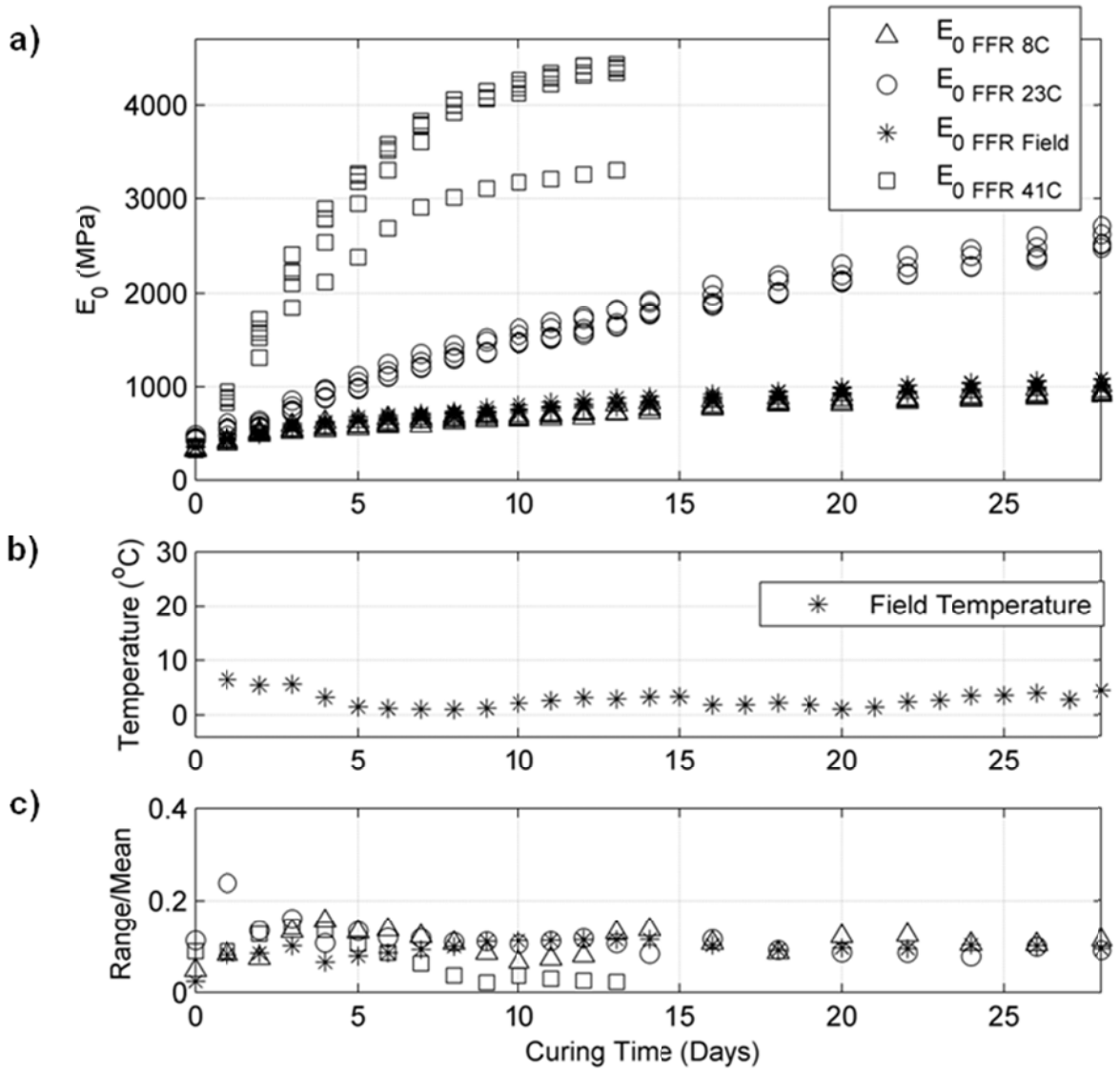

Figure 4.11: (a) Seismic Young's modulus vs. curing time for Solterra, (b) curing temperature regime for field cylinders, and (c) range/mean for the data in (a).

4.3 Surface Wave Test Results

This section discusses the modulus results obtained from surface wave testing on all three test sites and explores the reasons for any differences between surface wave and corresponding FFR results. The first site considered is Candelas, where seismic modulus values for the locations undergoing meaningful growth showed good agreement to corresponding FFR values. A total of thirteen locations were tested from days 1-4 (Figure 4.12). Of the thirteen locations tested, only four experienced meaningful modulus growth. Locations with seismic modulus corresponding to unstabilized soil are not plotted as they do not provide any useful information to inform curing behavior. The four modulus-gaining locations were all in Zone 2 (Figure 3.3). On the day of final compaction for Zones 1 and 3, an equipment breakdown occurred, resulting in significant delay between final remix and compaction. It should be noted that each section was prepared 1 day apart (i.e., Zones 1 and 3 underperformance was the result of two equipment breakdowns), and explains why Zone 2 did not suffer from this issue.

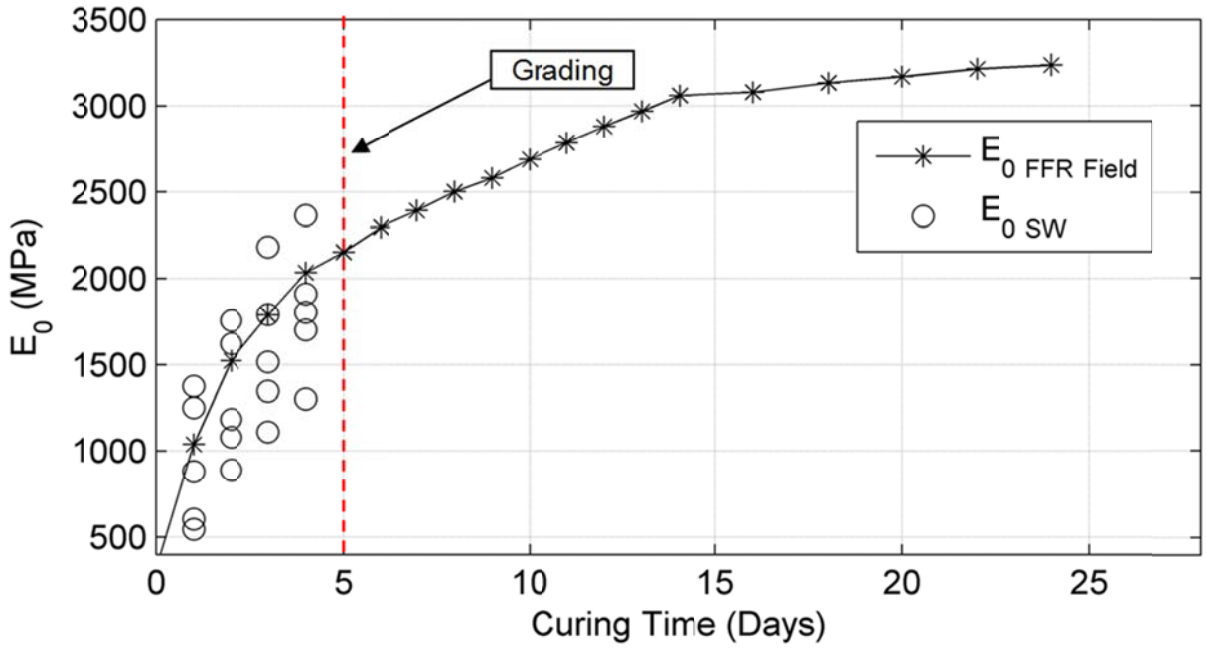

Figure 4.12: Seismic Young's modulus (Surface Wave vs. FFR) for Candelas.

Surface wave based E_0 values from five test locations at the Solterra site exhibited linear growth over 8 days of testing (Figure 4.13). All five locations evaluated showed meaningful

modulus growth and the surface wave values agreed reasonably well with FFR values over this time frame. Solterra E_0 values are much lower than other sites due to the low temperatures, further indicating that differences in curing temperature must be considered to appropriately predict seismic modulus behavior. Grading on day 9 induced modulus loss (or at the very least, a halt in modulus growth), and therefore, surface wave data obtained post grading is not displayed.

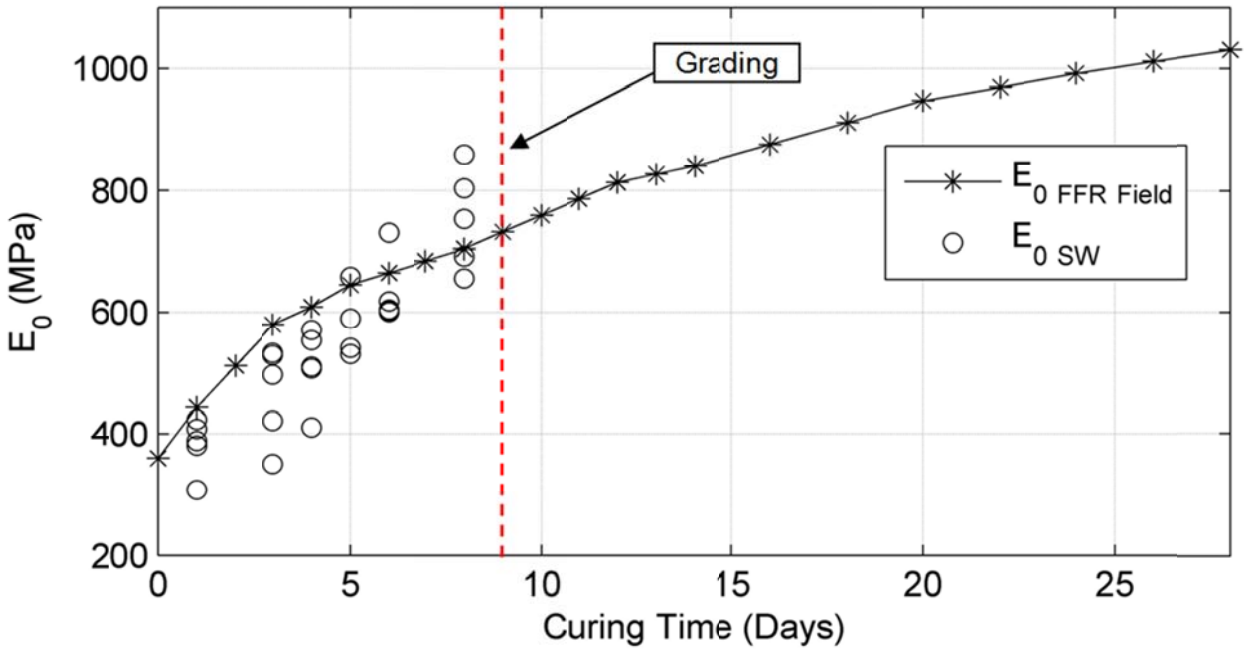

Figure 4.13: Seismic Young's modulus (Surface Wave vs. FFR) for Solterra.

For TCA 2011 (Zone 1), seven of the twelve locations evaluated underwent meaningful modulus growth (i.e., five locations remained in the 300-500 MPa range, consistent with the seismic modulus of unstabilized soil for this site). For Zone 1, surface wave testing was conducted from days 2-10, but grading on day 7 induced significant modulus loss at several locations. In Zone 2 (Figure 4.15), four of twenty locations experienced meaningful modulus growth. Due to significant grading on day 6, post-grading data is not displayed. Chronologically, TCA 2011 was the first field test site and utilized 1m long test arrays (compared to Candelas and Solterra, which used 3m test arrays). Therefore, significantly more locations were tested at these sites. However, initial testing at TCA revealed a noticeable difference between FFR and surface wave test results (with FFR reporting significantly higher modulus values than surface waves tests). To this end, 1 m test arrays may not be sufficient for LSS characterization as dispersion

between P and R waves does not always occur within the first meter of source to receiver separation. To improve the data quality and robustness, 3 m test arrays were used on later test sites. However, the results obtained from TCA are not necessarily invalid and the field-constructed LSS may have underperformed for construction related reasons.

For TCA 2012 (Zone 3), surface wave testing was performed on days 2-9 (Figure 4.16) and halted after grading. FFR cylinders from this round of testing did not experience meaningful modulus gain and therefore, no comparison is available. However, surface wave results from TCA 2012 are compared to $E_{0\ FFR\ Field}$ from TCA 2011 (i.e., same soil/mix design, different temperature curing regime) in Figure 4.16a. Differences in curing temperature are illustrated in Figure 4.16b, and convey the reason for the difference in modulus performance. It should also be noted that the location from which FFR cylinder soil was gathered corresponded with a surface wave test location that underwent no modulus gain. While the reason for this lack of performance is not known, it is noteworthy that both FFR and surface wave testing predicted the same result.

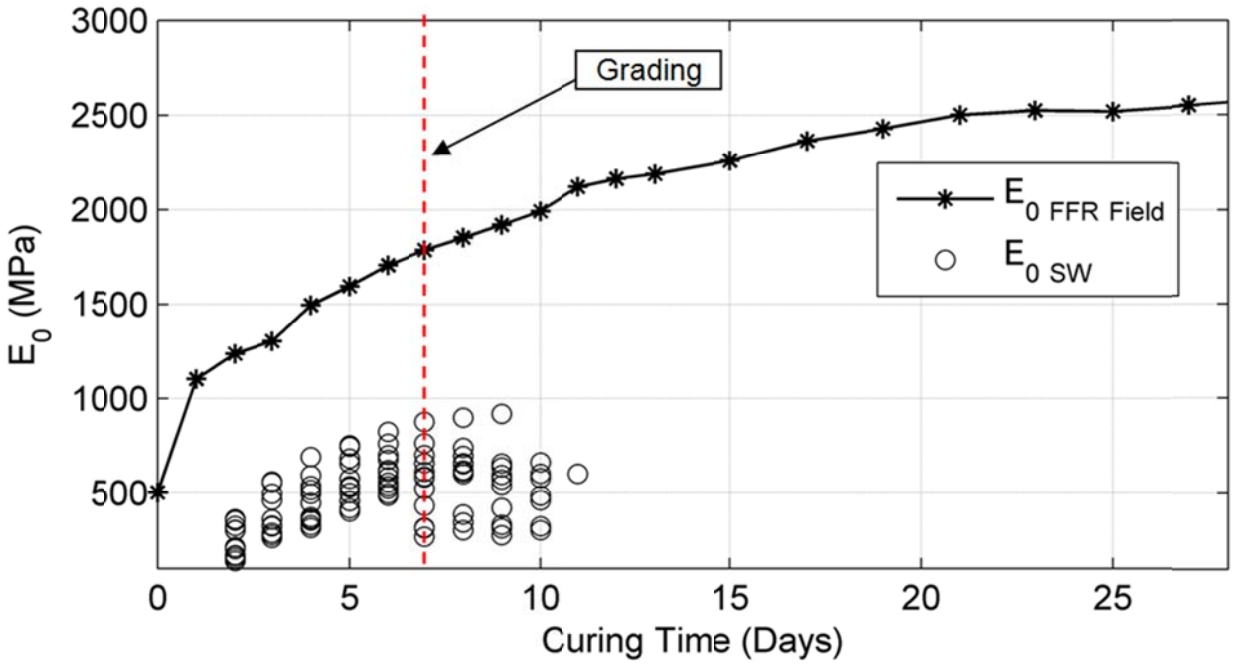

Figure 4.14: Seismic Young's modulus (Surface Wave vs. FFR) for TCA 2011 – Zone 1.

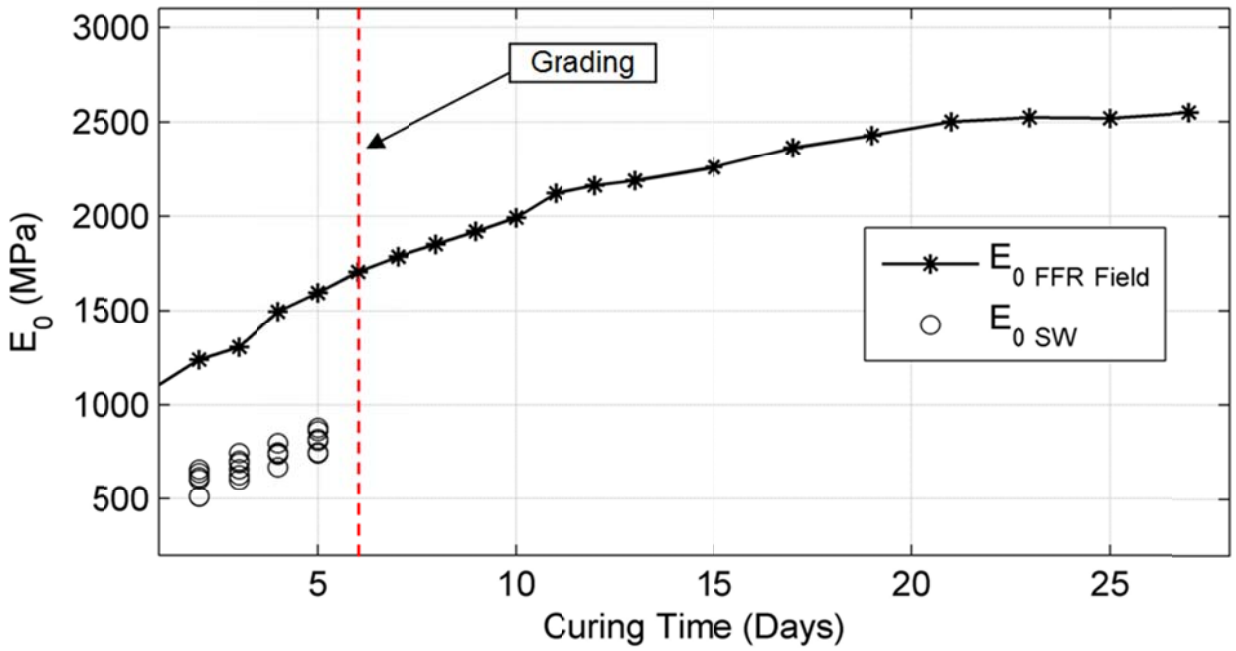

Figure 4.15: Seismic Young's modulus (Surface Wave vs. FFR) for TCA 2011 – Zone 2.

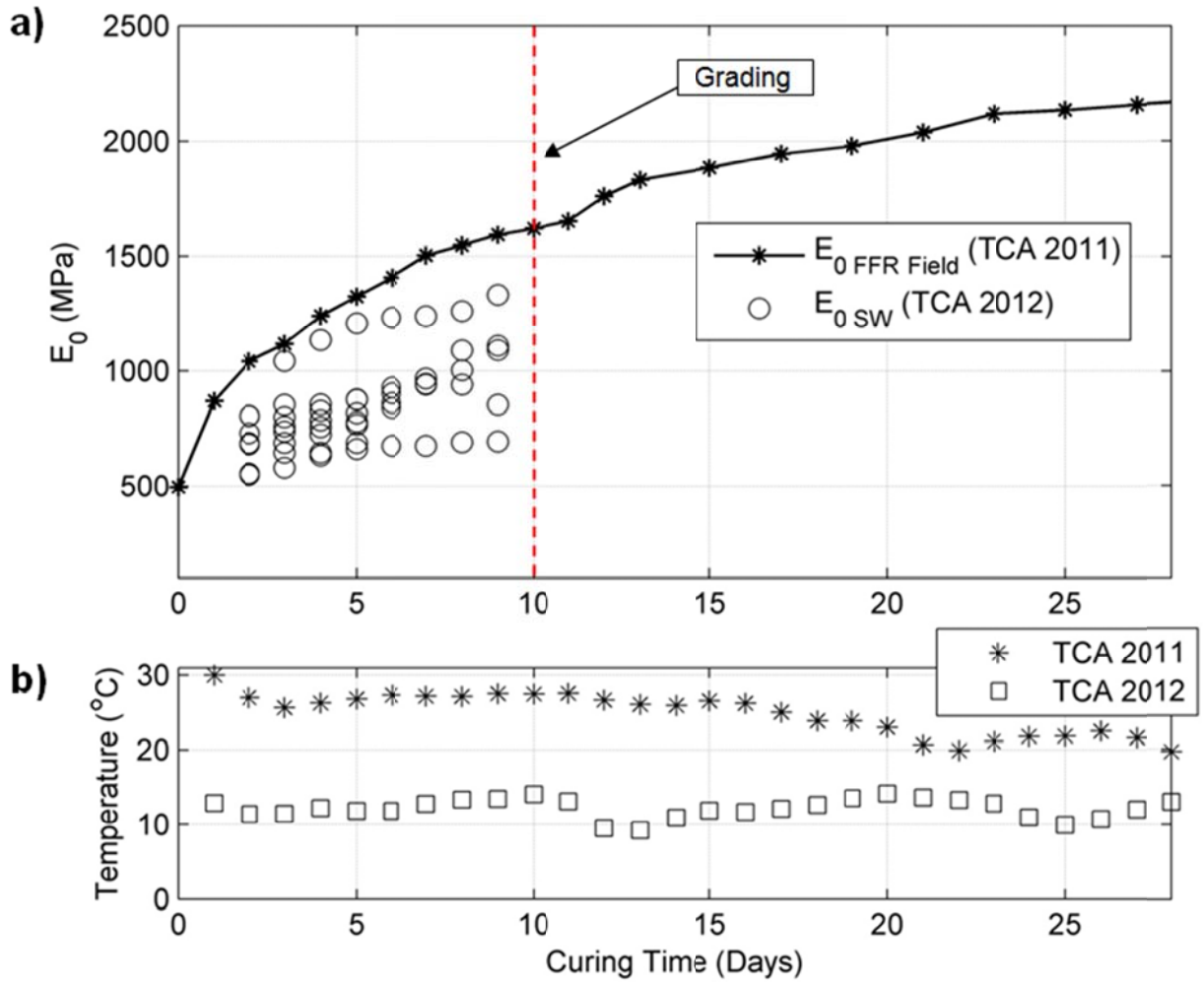

Figure 4.16: (a) Seismic Young's modulus (Surface Wave) for TCA 2012 – Zone 3 compared to FFR from TCA 2011 (Zone 2), and (b) corresponding field temperature curing regimes.

4.4 Development of a Maturity Index for LSS

Given the observed behavior of LSS cured under varying temperature conditions, it is clear that modulus growth in LSS must be characterized as a function of both curing time and curing temperature, i.e., via a time and temperature maturity index. A simple approach to characterizing LSS maturity is the linear maturity index applied to concrete, shown in Equation 4.1.

$$M(t, T_a, T_0) = \sum (T_a - T_0)t \tag{4.1}$$

where:

M = maturity (^{o}C * days)

T_a = average temperature during each time interval, e.g., one day (^{o}C)

T_0 = temperature below which cement hydration is assumed to cease (^oC)
t = curing time, elapsed from initial compaction (days)

FFR data from each cylinder set was averaged and is presented vs. curing time in Figures 4.17a, 4.18a, and 4.19a for TCA, Candelas, and Solterra, respectively. Equation 4.1 is applied to this data and the resulting maturity relationships are shown in Figures 4.17b, 4.18b, and 4.19b, for TCA, Candelas, and Solterra, respectively. After applying Equation 4.1 to the FFR data, it is clear that a linear maturity index does not adequately capture LSS modulus growth, i.e., if a linear maturity index was applicable to LSS, the E_0 curves in Figures 4.17b, 4.18b, and 4.19b would plot on top of one and other.

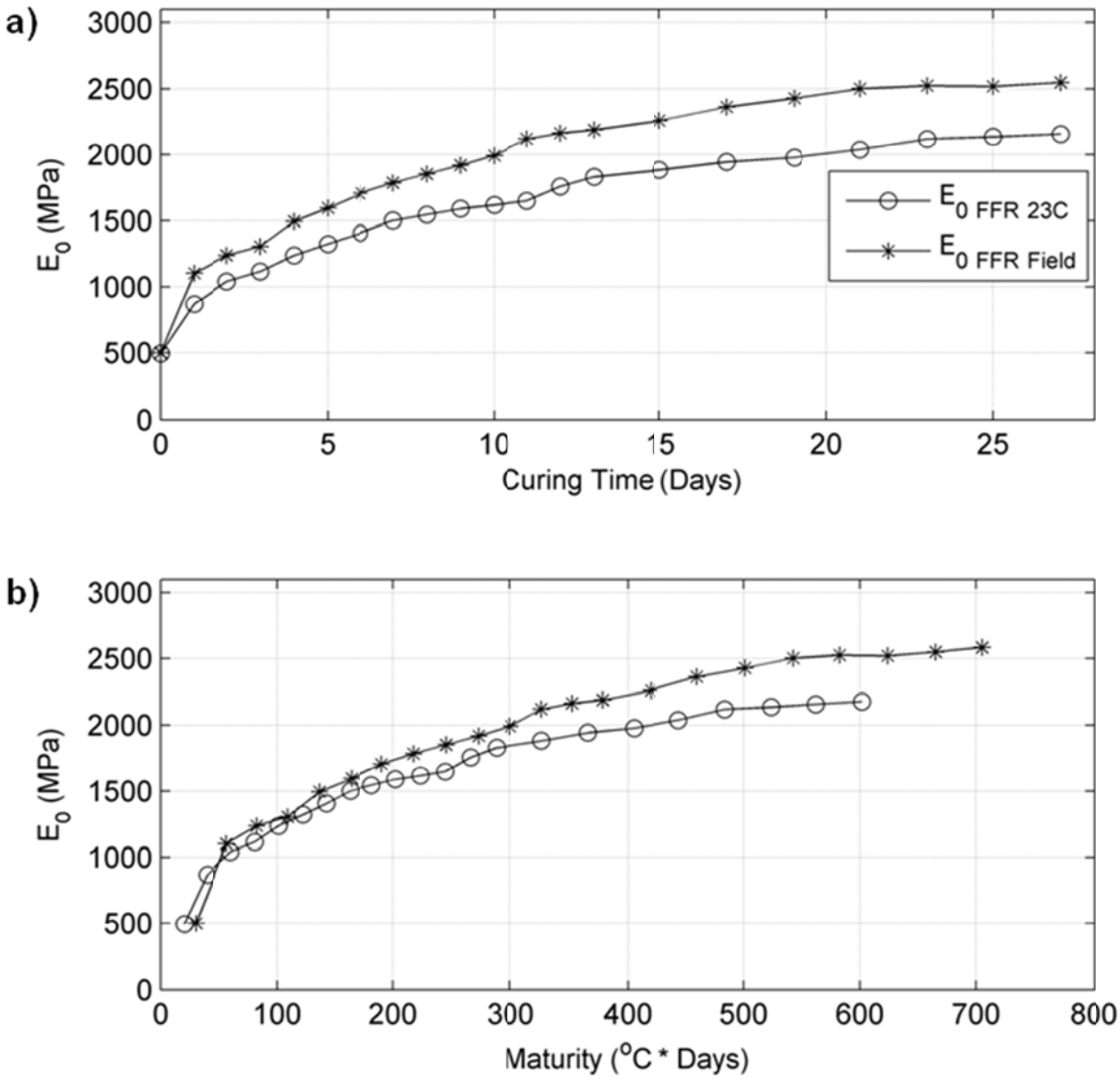

Figure 4.17: Seismic Young's modulus vs. (a) curing time and (b) maturity index for TCA 2011 – Zone 1.

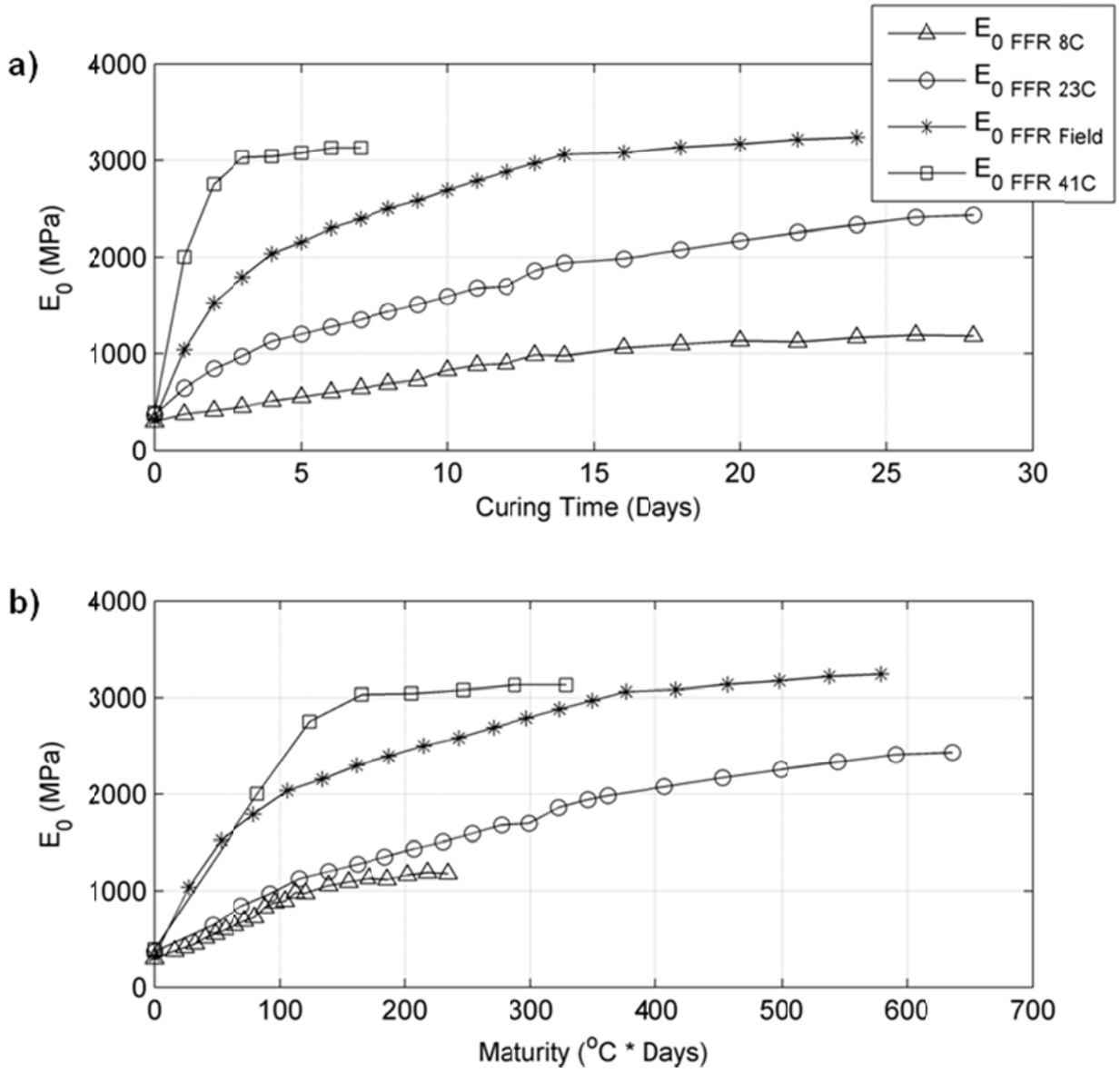

Figure 4.18: Seismic Young's modulus vs. (a) curing time and (b) maturity index for Candelas.

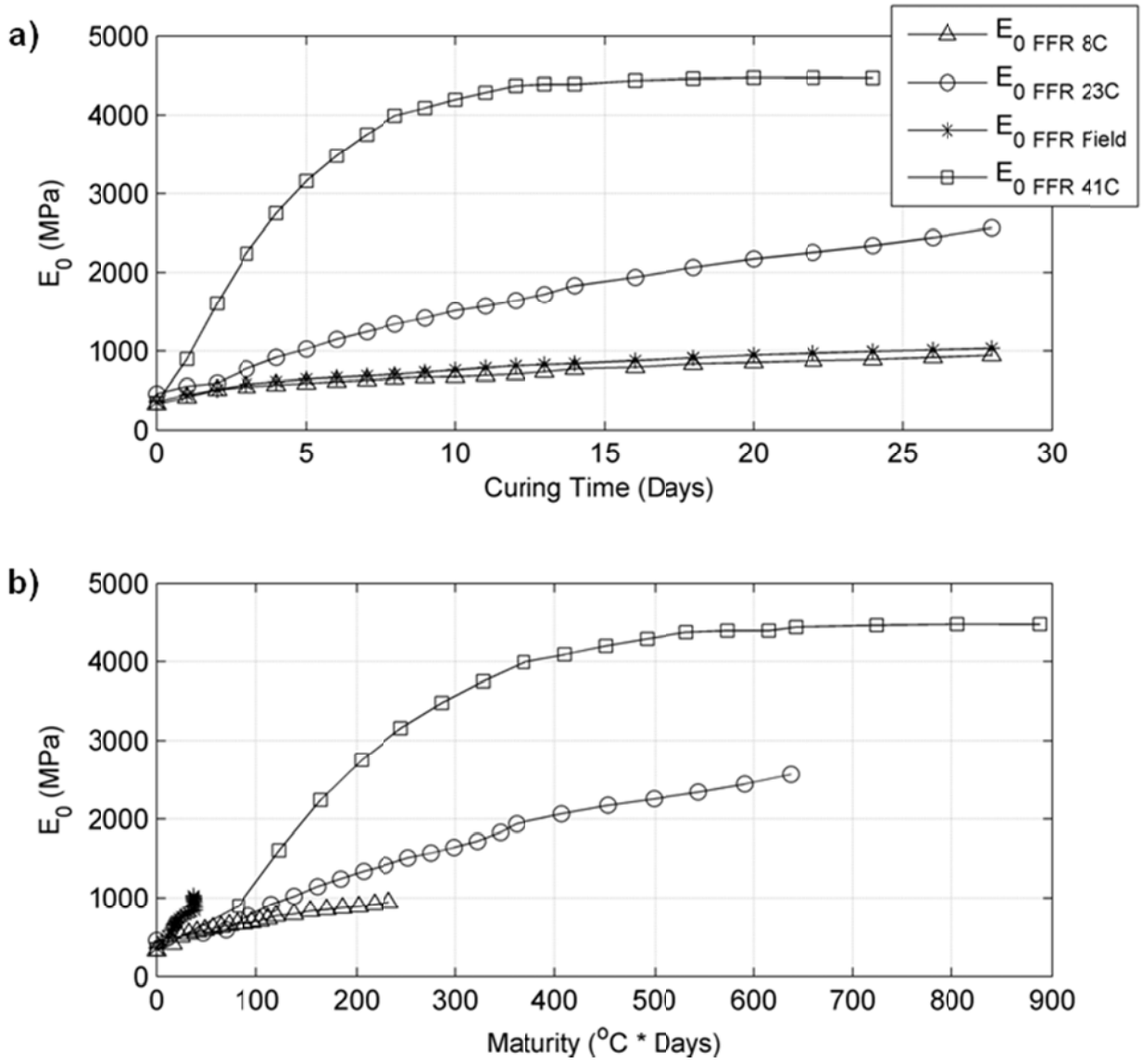

Figure 4.19: Seismic Young's modulus vs. (a) curing time and (b) maturity index for Solterra.

To assess the non-linearity of the LSS maturity index, E_0 is first characterized as individual functions of both curing time (t) and cumulative average curing temperature ($\bar{T}_t$) from inception through day t. To isolate the two functions governing LSS maturity, a correlation plot between E_0 and $\bar{T}_t$ is generated for each t (days 1-28). An example of the correlation between E_0 and $\bar{T}_t$ (for days 3, 7, 14, and 28) is shown in Figure 4.20, and correlation plots for all 28 days are shown in Appendix D.

The general form of this expression is shown in Equation 4.2,

$$E_0(\bar{T}_t) = \eta_t \, e^{\beta \bar{T}_t} \tag{4.2}$$

where:

$\bar{T}_t$= cumulative average temperature from days 1-t (^{o}C)

β = a constant empirical parameter (0.05 $\pm$ 0.002) (unitless)

η_t = a varying empirical parameter related to *t* (see Figure 4.21, Equation 4.3) (unitless).

Per analysis of the data, η_t changes as a function of *t* (Figure 4.21). Fitting the array of $\eta_t$values suggests that η_t follows a power model (Equation 4.3),

$$\eta_t \, (t) = \alpha * t^{\gamma} \tag{4.3}$$

where t = curing day, α = 241 and γ = 0.349. Essentially, η_t is a power model function that describes the development of E_0 as a function of *t* only. This is an expected result and was demonstrated in Toohey and Mooney (2012), (i.e., E_0 development in cylinders cured under constant temperature followed a power model as a function of *t*). The empirical parameter β in Equation 4.2 was found to remain constant (β = 0.05 $\pm$ 0.002) as shown in Figure 4.22.

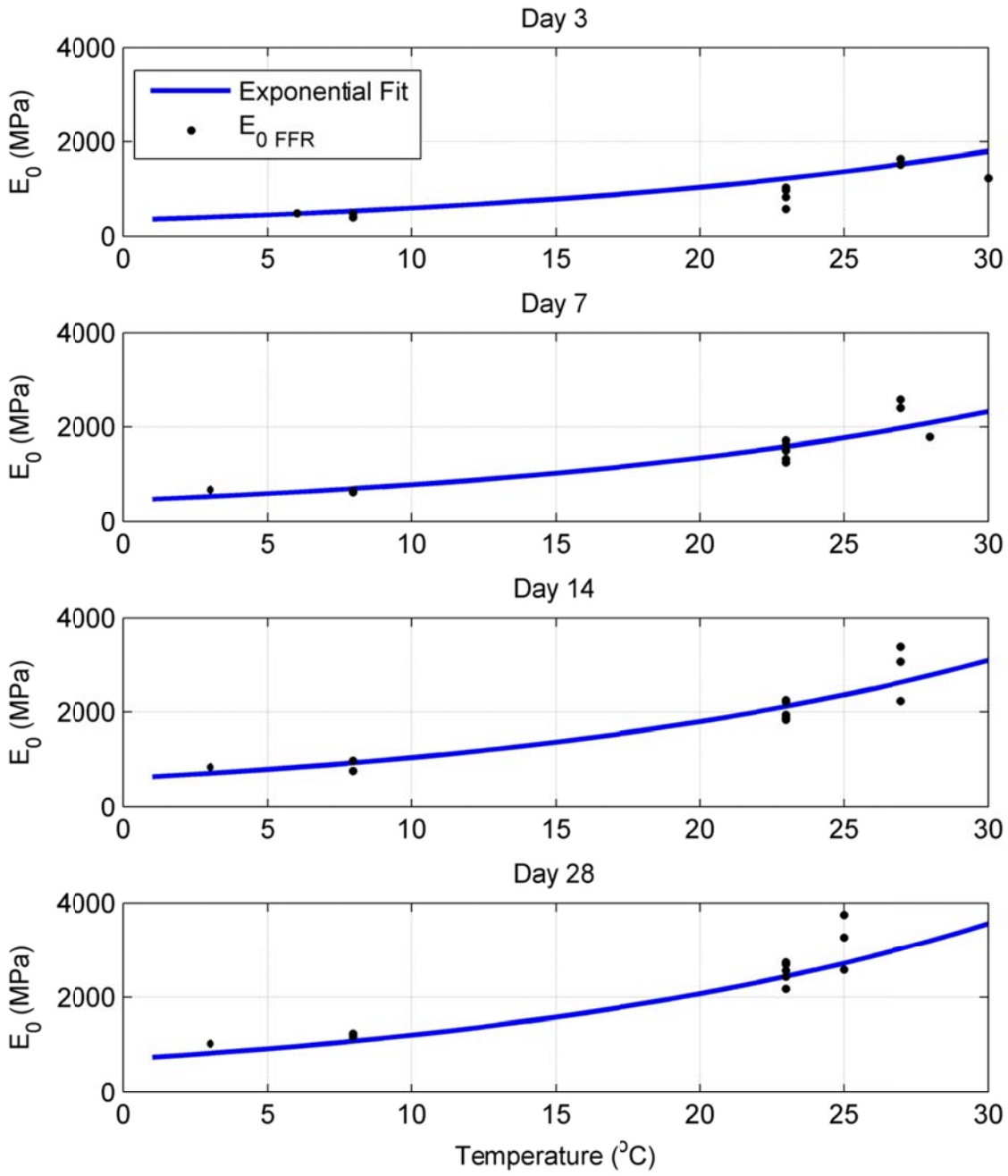

Figure 4.20: Correlation between E_0 and $\overline{T}_t$ for days 3, 7, 14, and 28.

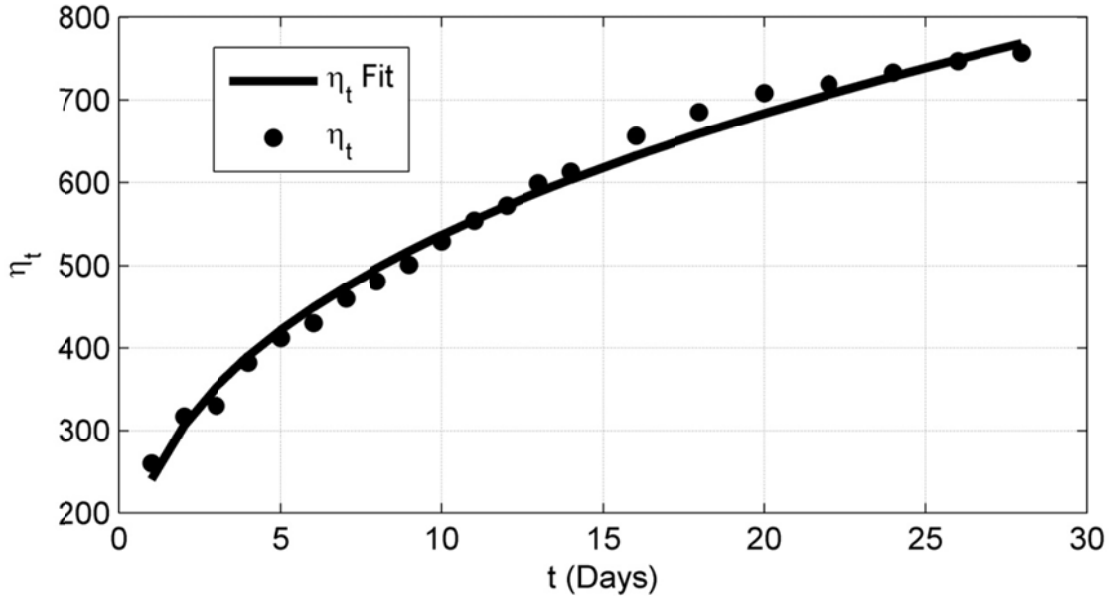

Figure 4.21: η_t as a function of curing day (*t*) with best fit equation.

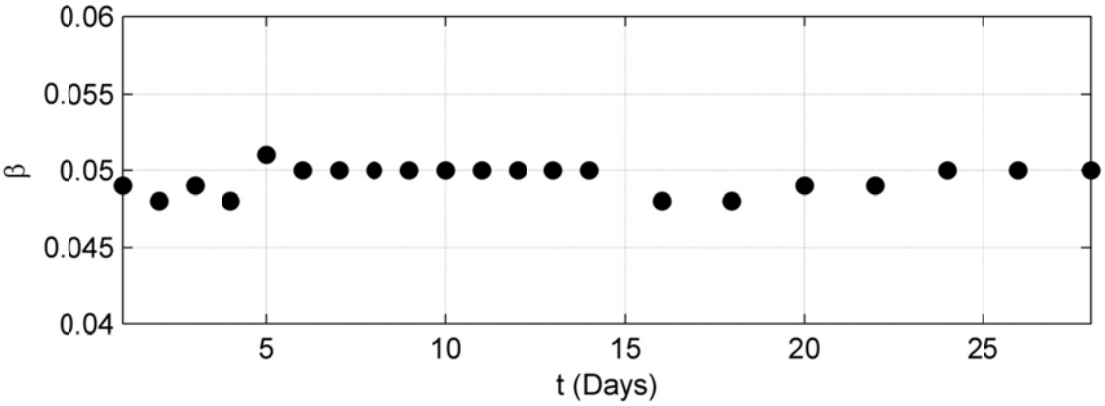

Figure 4.22: β as a function of curing day (*t*).

Next, the two functional components (exponential behavior in $\bar{T}_t$, power model behavior in *t*) are combined to assess LSS maturity as a function of both curing time and temperature (Equation 4.4). Plotting Equation 4.4 generates a family of curves (Figure 4.23c), where each curve represents E_0 behavior on a particular curing day and varies as a function of $\bar{T}_t$ for that day. For a constant $\bar{T}_t$ throughout each curing day, e.g., lab curing at 23°C/73 °F, the expected E_0 values are columns in the curve family as shown in Figure 4.23c.

$$E_0(t, \bar{T}_t) = (\alpha t^{\gamma}) * (e^{\beta \bar{T}_t}) \quad (4.4)$$

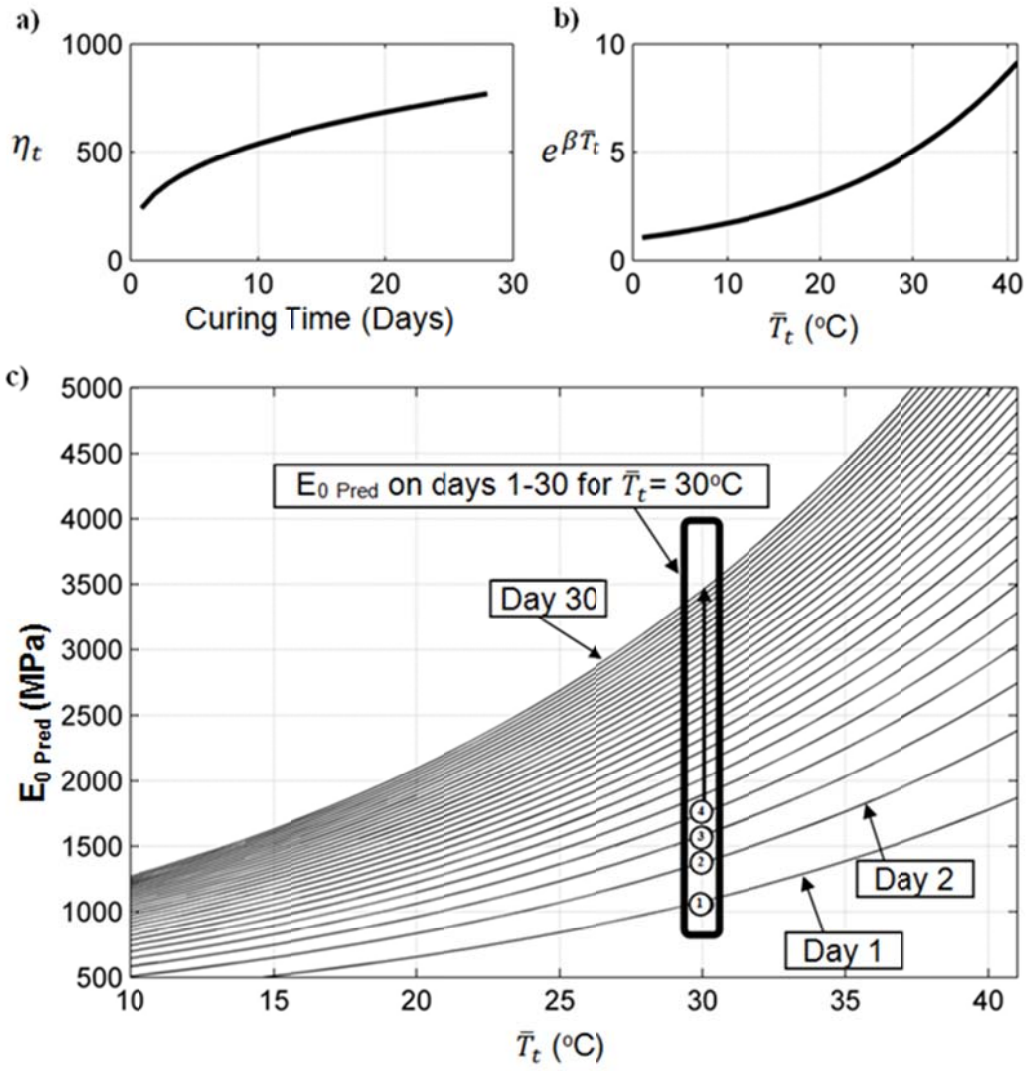

Figure 4.23 Plots of (a) η_t, (b) $e^{\beta \bar{T}_t}$, and (c) the family of curves generated by multiplying the two together.

The validity of the non-linear LSS maturity index (Equation 4.4) is first examined using experimental data at constant curing temperatures. The seismic Young's modulus predicted by the LSS maturity index ($E_{0\ Pred}$) for temperatures ranging from 4-40°C at 4°C intervals is presented in Figure 4.24. Average $E_{0\ FFR}$ values for all constant-temperature cured data sets are also plotted to illustrate the general agreement between experimental data and $E_{0\ Pred}$ from the maturity index.

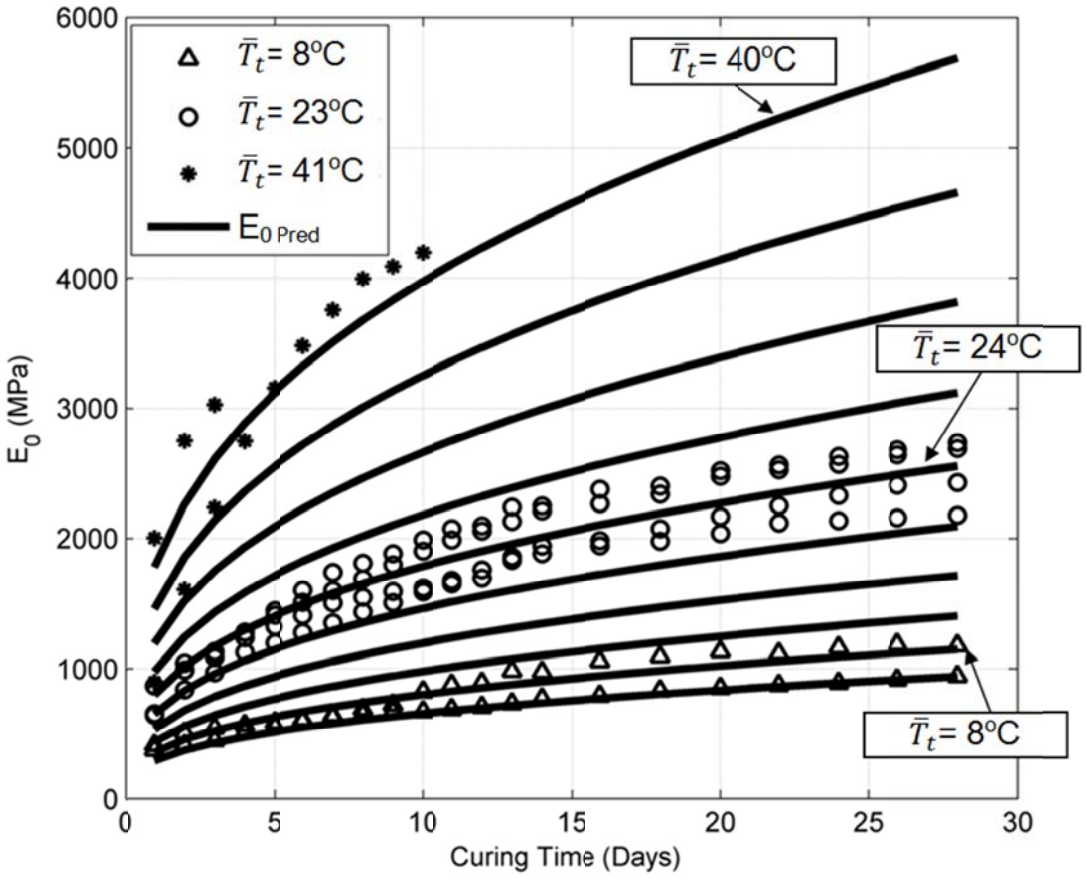

Figure 4.24: Averaged E_0 data sets at constant curing temperatures compared to E_{Pred} (4°C intervals) generated using Equation 4.4.

Results from individual FFR cylinders are shown for each constant temperature curing regime in Figure 4.25 and suggest that the LSS maturity index is accurate for fitting individual FFR data sets cured at constant temperature. Both $E_{0\ Pred\ 8C}$ and $E_{0\ Pred\ 23C}$ show very good agreement for days 1-28. $E_{0\ Pred\ 41C}$ overestimates the experimental data for days 1-3, but agrees quite well on day 4 and higher.

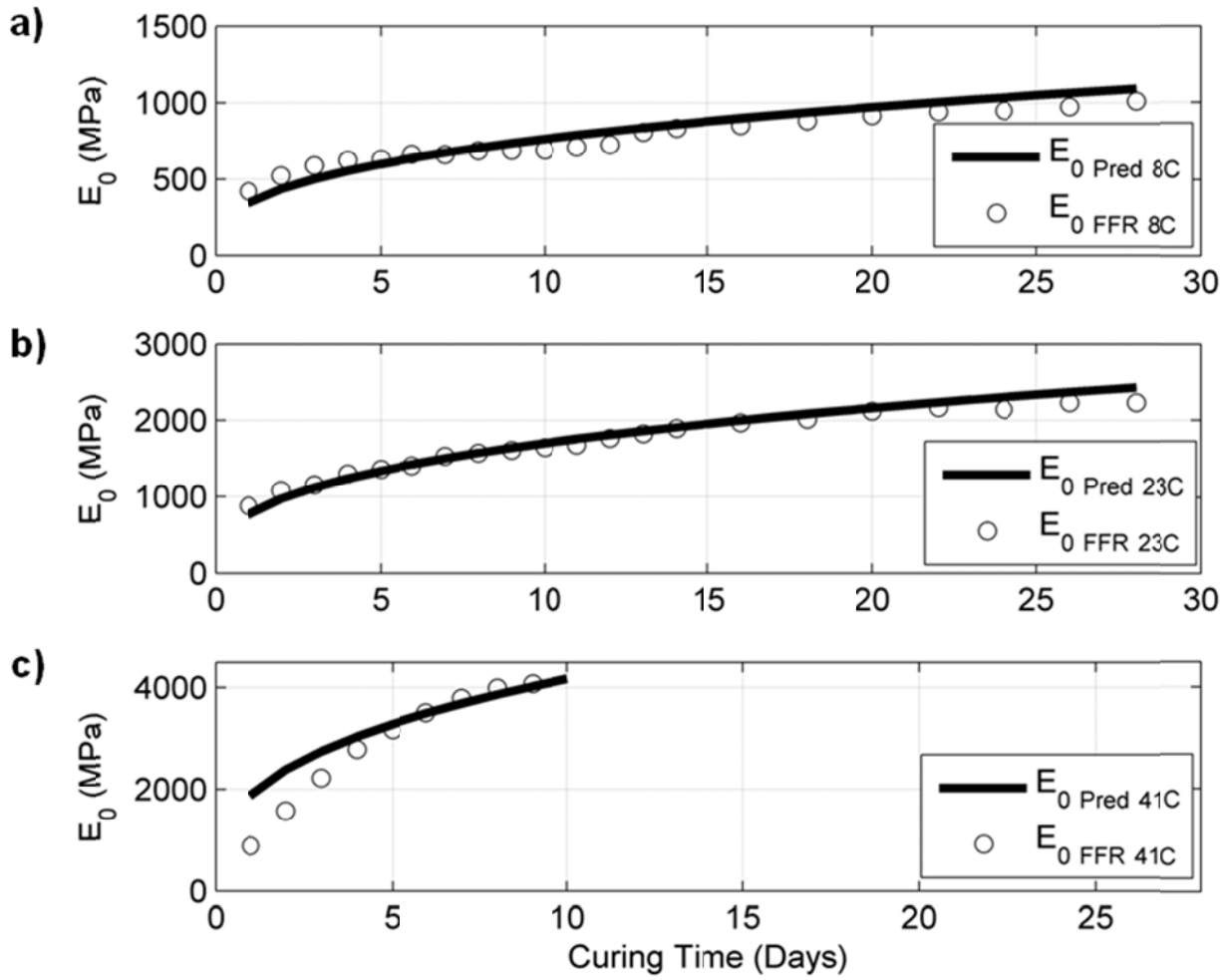

Figure 4.25: Individual FFR data sets compared to E_{Pred} from the maturity index for (a) $\bar{T}_t$ = 8°C, (b) $\bar{T}_t$ = 23°C, and (c) $\bar{T}_t$ = 41°C.

The non-linear maturity index is next applied to cylinders cured in the field under variable temperature conditions. Because the field temperature is not constant, the assessment of curing temperature must be considered with different interpretations of $\bar{T}_t$ (e.g., daily average, cumulative average, etc.). Assuming $\bar{T}_{t=}\bar{T}_{t\,sum}$ for variable temperature curing regimes (see Appendix E for derivation), the resulting $E_{0\ Pred}$ is shown through the family of maturity curves for days 1-28 via red arrows (Figure 4.27a) with corresponding $\bar{T}_t$ (Figure 4.27b). This figure is analogous to Figure 4.23, but a single temperature column cannot be used because $\bar{T}_t$ varies. $E_{0\ FFR}$ for the cylinders cured under this temperature regime (Figure 4.27b) is compared to $E_{0\ Pred}$ (Figure 4.27a) in Figure 4.28.

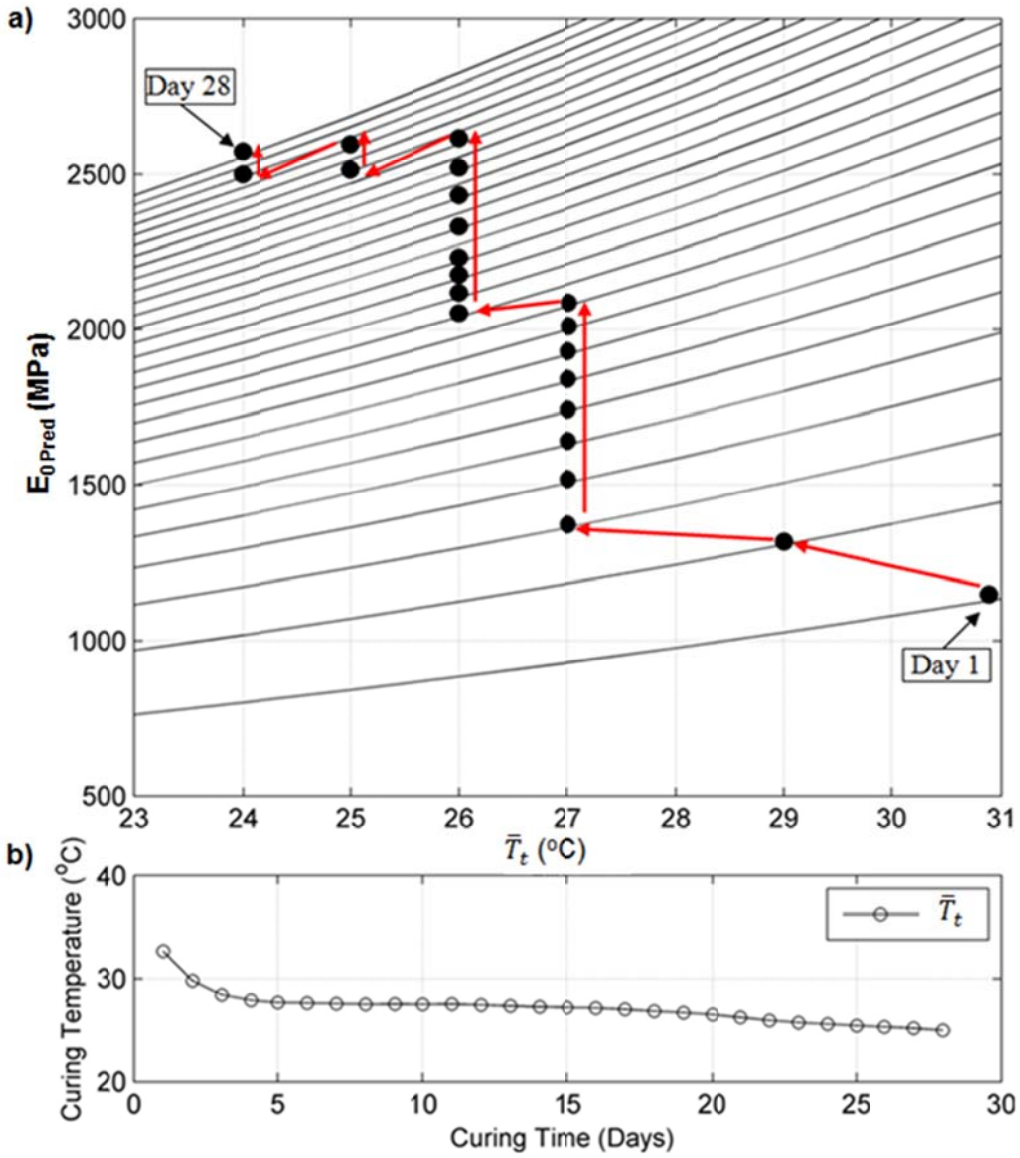

Figure 4.26: (a) Development of E_{Pred} expressed through maturity curves, and (b) $\bar{T}_t$ used to obtain the results in part (a).

The non-linear maturity index predicts experimental LSS behavior for variable temperature curing regimes quite well (Figure 4.28). Although small decreases in modulus are occasionally observed (e.g., days 11, 20, etc.), these are a result of $\bar{T}_t$ being rounded to the nearest degree. The solution curve family could be reconstructed for inputs with 0.1°C resolution to reduce/remove this effect, but would also imply that $\bar{T}_t$ is known to 0.1°C precision.

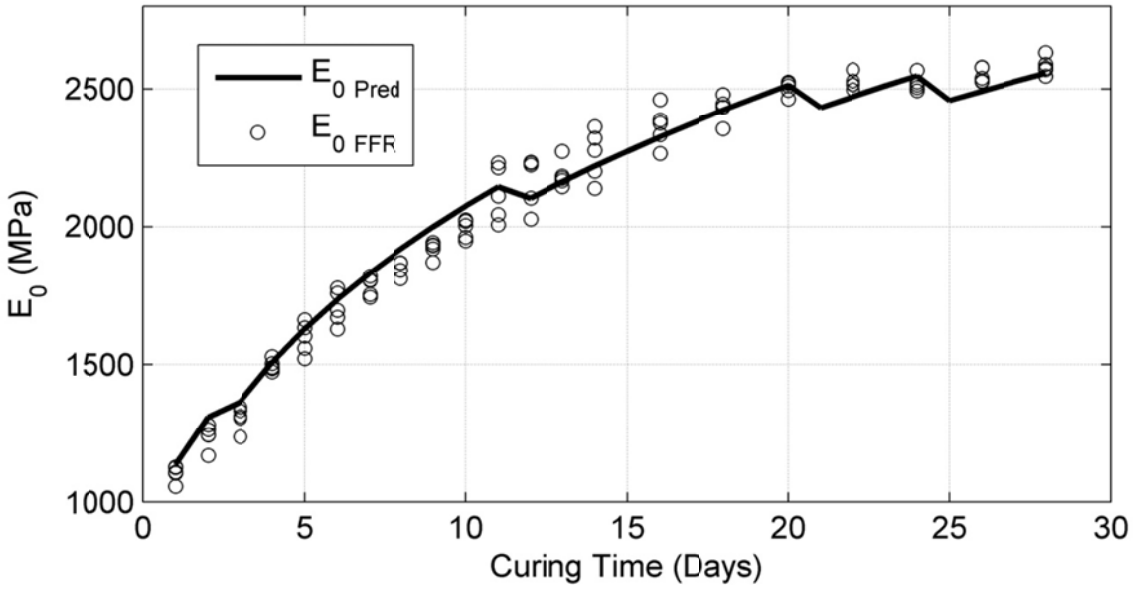

Figure 4.27: E0 compared to EPred for the $\bar{T}_t$ regime shown in Figure 4.26b.

4.5 Comparison of FFR and Surface Wave Data Using LSS Maturity Index

With a developed and validated time and temperature dependent LSS maturity index, we can now directly compare E_0 data across variable temperature (field) regimes in the interest of developing a pilot specification for seismic LSS QA. As the pilot specification seeks to expedite construction (or at least allow acceptance/rejection within the same time frame as current QA), data are compared over the first 4-8 days of curing. Because temperature differences existed between field-stored cylinders (FFR) and field-constructed LSS (surface wave), the LSS maturity index-predicted modulus differs. In some cases, this temperature difference helps to explain the lack of agreement between FFR and surface wave results.

All field-cured LSS (both FFR cylinders and surface wave tests results) are compared to the LSS maturity index on a site to site basis. TCA 2011 (Zone 1) results show good agreement between FFR data and the LSS maturity index (Figure 4.28). The maturity index-predicted modulus for the field-constructed LSS is less than that of the trench-cured LSS (a result of temperature difference), but experimental surface wave data suggests modulus values in the field much lower than the corresponding FFR. Surface wave results from TCA 2012 show good agreement to the LSS maturity index (i.e., surface wave results have significant scatter, but the maturity index predicts a good average value) (Figure 4.29). Note that this figure lacks FFR data

because FFR cylinders prepared for this section did not undergo meaningful modulus growth. The reason for lack of performance with FFR cylinders is unknown.

For Candelas field data, the LSS maturity index slightly underpredicts both FFR and surface wave surface wave data (Figure 4.31), but the difference is comparatively small (i.e., compared to TCA 2011 surface wave results). For the Solterra field data, the LSS maturity index shows good agreement to experimental data for both FFR and surface wave results (Figure 4.32). In general, the LSS maturity index shows relatively good agreement to FFR data for all sites However, the LSS maturity index sometimes disagrees with surface wave data. This lack of agreement does not imply limitations to either the testing procedure or the LSS maturity index. Rather, this results from lack of field-constructed LSS performance. From a QA standpoint, sections in which surface wave modulus is significantly lower than LSS maturity index-predicted modulus would likely be rejected.

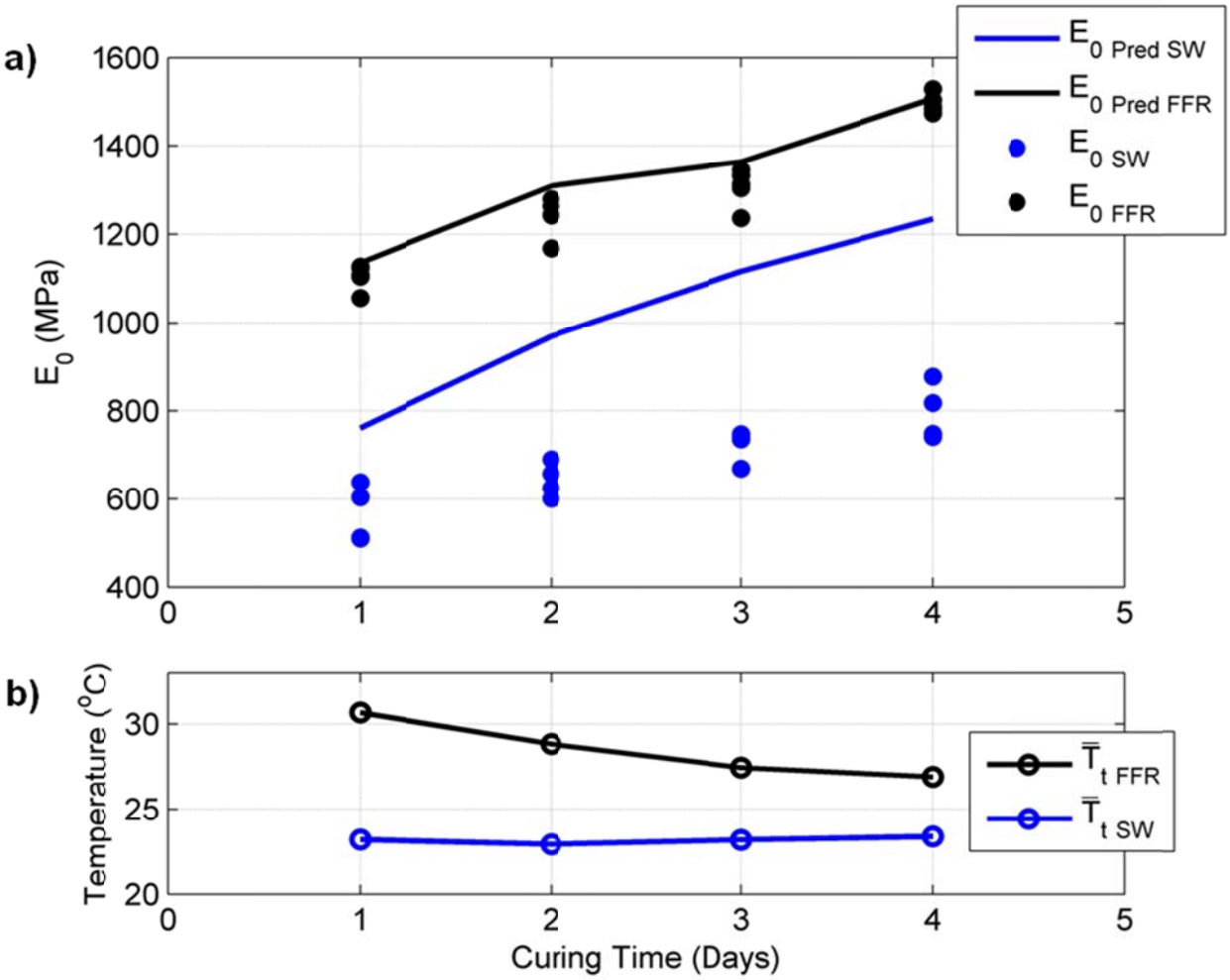

Figure 4.28: (a) Experimental surface wave and FFR results compared to EPred for respective curing regimes, and (b) corresponding $\overline{T}_t$ data for TCA 2011.

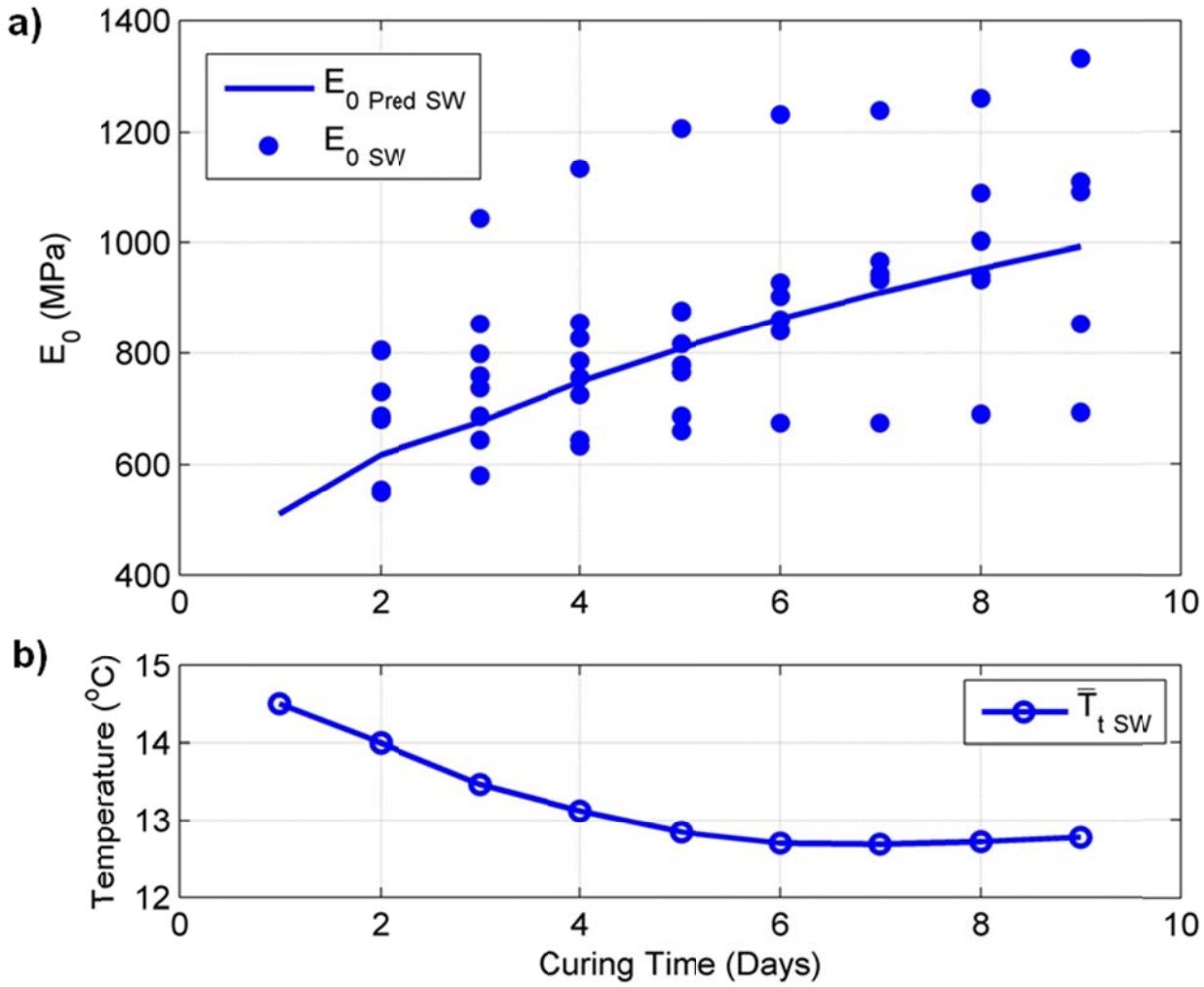

Figure 4.29: (a) Experimental surface wave and FFR results compared to EPred for respective curing regimes, and (b) corresponding $\overline{T}_t$ data for TCA 2012.

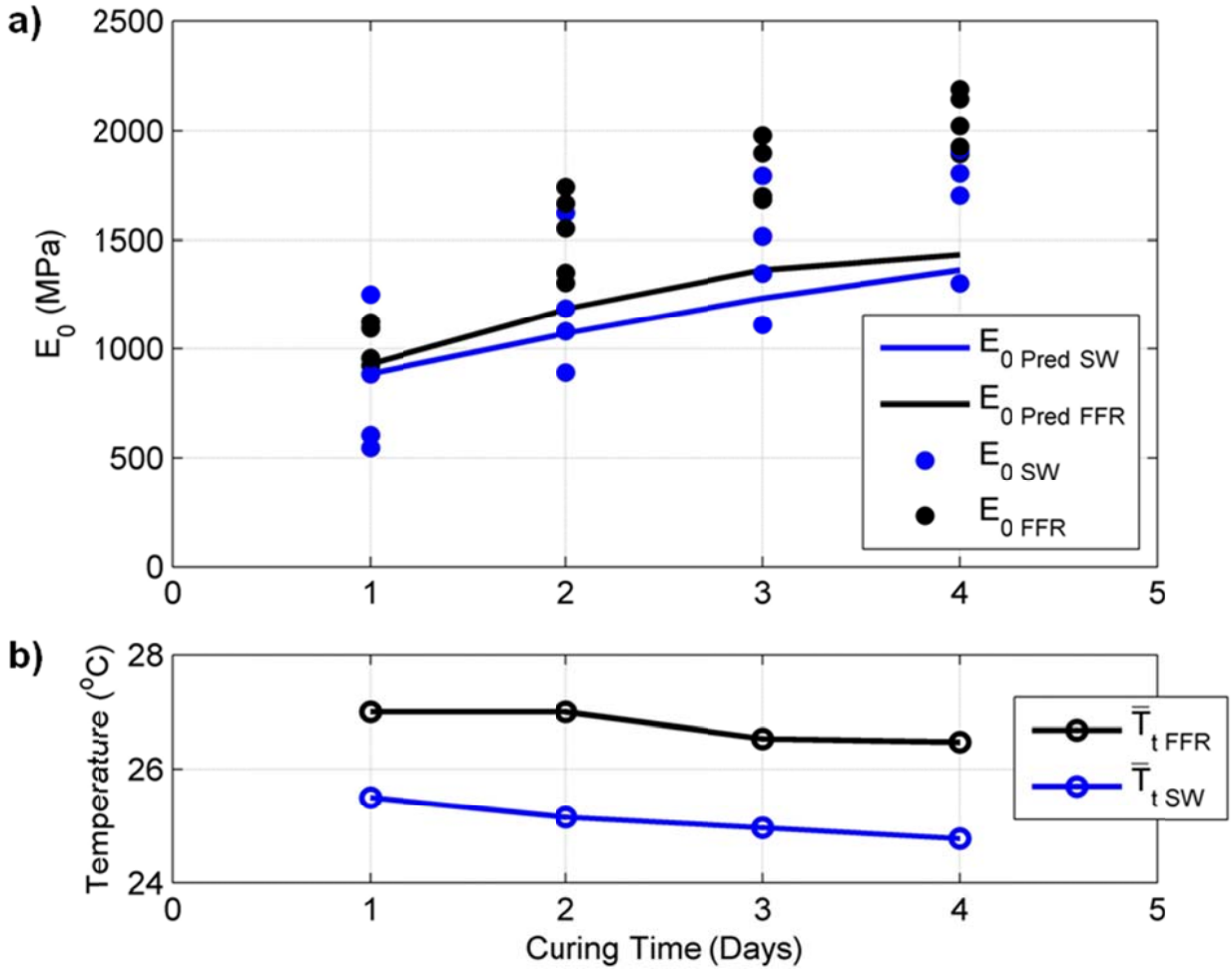

Figure 4.30: (a) Experimental surface wave and FFR results compared to EPred for respective curing regimes, and (b) corresponding $\overline{\overline{T}}_t$ data for Candelas.

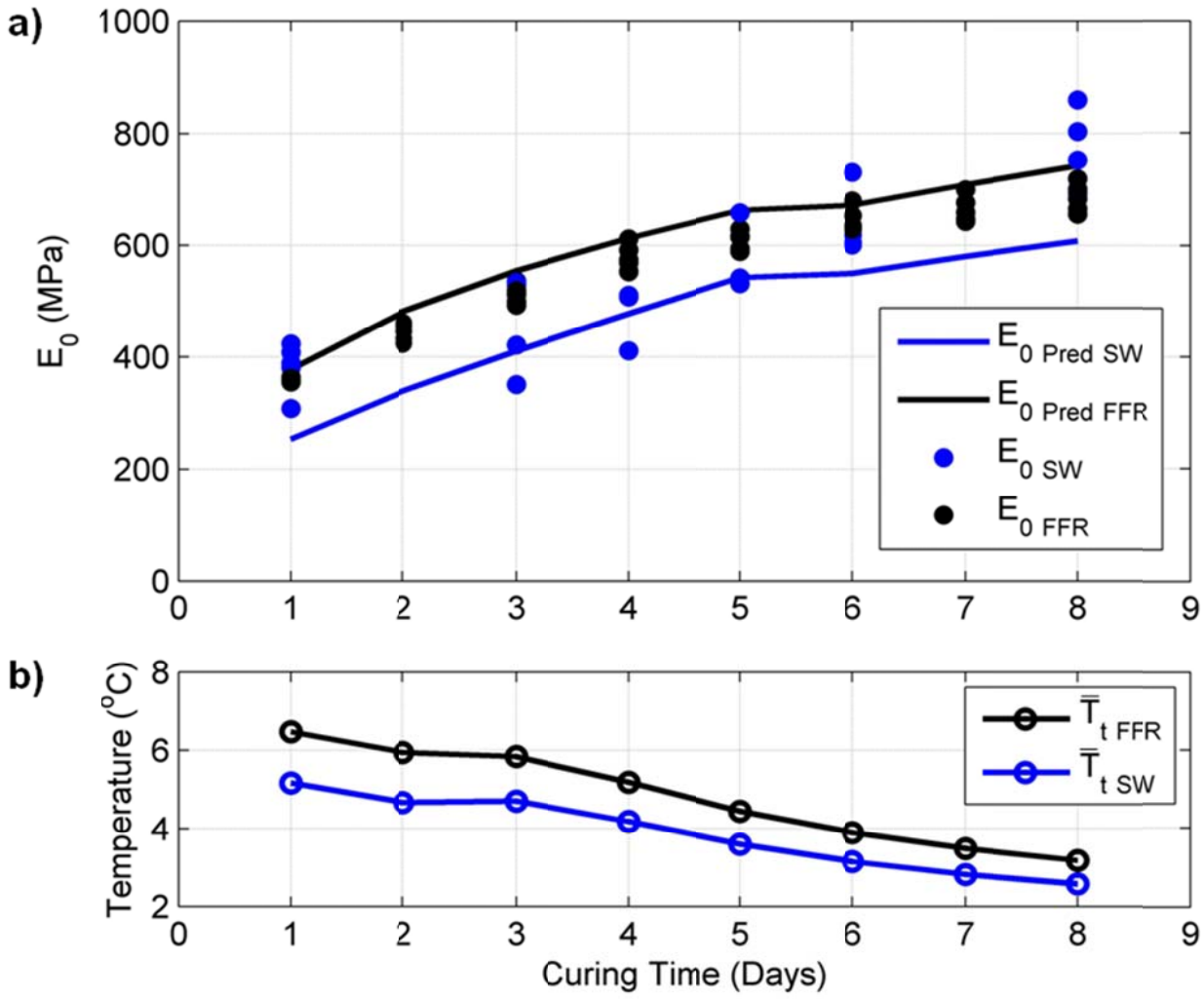

Figure 4.31: (a) Experimental surface wave and FFR results compared to EPred for respective curing regimes, and (b) corresponding $\overline{T}_t$ data for Solterra.

4.6 Conclusions

Based on the results of the experimental test program conducted in this study, the following conclusions can be formed:

1. Temperature has a significant impact on LSS modulus growth with curing time. The growth of modulus was found to vary as a non-linear function of both temperature and curing time. The specific function was inferred from the fitting of constant and variable curing temperature free-free resonance data, and is a seismic modulus maturity index for LSS.

2. The LSS maturity index is a function of soil temperature, not ambient (air) temperature. Both LSS and air temperature were monitored during field construction, and a correlation between the two is obtained. This correlation can simplify the implementation of the LSS maturity index pilot specification as only air temperature needs to be obtained.

3. Differences in modulus growth between free-free resonance (cylinders) and surface wave (field-constructed LSS) data can be attributed to construction-related issues, and are not the result of testing equipment/practice. To this end, the study supports the recommendations of the CDOT specification for LSS (Section 307) in that grading should be performed immediately after construction. Grading conducted on later days (i.e., days 4-8) resulted in significant seismic modulus loss on field-constructed LSS.

4. The study supports the use of cylinder and surface wave seismic testing for the QA of LSS. As the goal of LSS QA should be to evaluate the actual field-constructed LSS, either method is valid as long as appropriate LSS field construction procedure is followed.

5. The study recommends the use of the seismic LSS maturity index developed herein. Results suggest that significant differences in LSS seismic modulus behavior occur due to curing temperature variation. For this reason, acceptance via seismic QA on field-constructed LSS must consider curing temperature.

6. A draft specification for QA of LSS via seismic testing is developed in Chapter 5. This specification allows for the use of either cylinder or surface wave testing to determine the seismic modulus of field-constructed LSS. Experimental results are statistically adjusted based on % confidence criteria, and acceptance/rejection is verified via the field curing temperature and the LSS maturity index.

7. In the event that simultaneous acceptance via unconfined compressive strength (UCS) testing is desired, a correlation between seismic modulus and UCS is recommended. Attempts to core field-constructed LSS for UCS testing were not successful, and this approach is not recommended.

CHAPTER 5: PILOT SPECIFICATION

A pilot specification was developed for the use of nondestructive seismic testing for quality assurance (QA) of lime-stabilized soil (LSS). This pilot specification details the procedure for QA of LSS via seismic testing and maturity index – based acceptance criteria. Seismic modulus of LSS is assessed using one of two experimental methods: Method A (seismic testing of reconstituted cylinders) or Method B (surface wave testing of field-constructed LSS). A target modulus value is obtained from a time/temperature dependent LSS maturity index (Section III, and finally, experimental data are statistically adjusted (based on desired % confidence) and compared to the target modulus value for acceptance/rejection (Section IV). Note that some figures/equations from earlier chapters of the report are repeated here in the interest of making this a standalone pilot specification.

I: Experimental Testing- Method A

***Description*:** Method A specifies the experimental procedure for field LSS assessment via seismic testing of reconstituted, field-mixed cylinders.

***Required Materials*:** hand shovel, full size shovel, soil storage container, airtight plastic bags, 4 in (diameter) x 8 in (height) cylindrical soil compaction mold, hammer and tamper, free-free resonance experimental setup.

***Procedure I - Specimen Preparation*:** On the day of final field remix/compaction of an LSS field section, gather machine-mixed LSS for specimen preparation. LSS should ideally be gathered immediately after final remix but must be obtained prior to field compaction. At each soil gather location, obtain enough loose LSS to prepare five cylinders. Cylinders are reconstituted with a 4 in diameter by 8 in height soil compaction mold, using four hand-tamped 2 in layers of predefined soil mass (Figure 5.1).

Figure 5.1: (a) FFR cylinder preparation and (b) example cylinder.

Immediately after preparation, the reconstituted LSS cylinders should be sealed in individual plastic bags (one per specimen) and placed in a soil trench on site (Figure 5.2a). This trench should be approximately 6 in deep, 10 in wide, and long enough to accommodate the desired number of cylinders (approximately 24 in per five cylinders). Once all cylinders are prepared, the trench should be covered with loose soil, mounded to a height approximately 10 cm above the ground surface (Figure 5.2b). If possible, ground temperature within the trench should be continuously monitored (e.g., with an in-situ temperature probe).

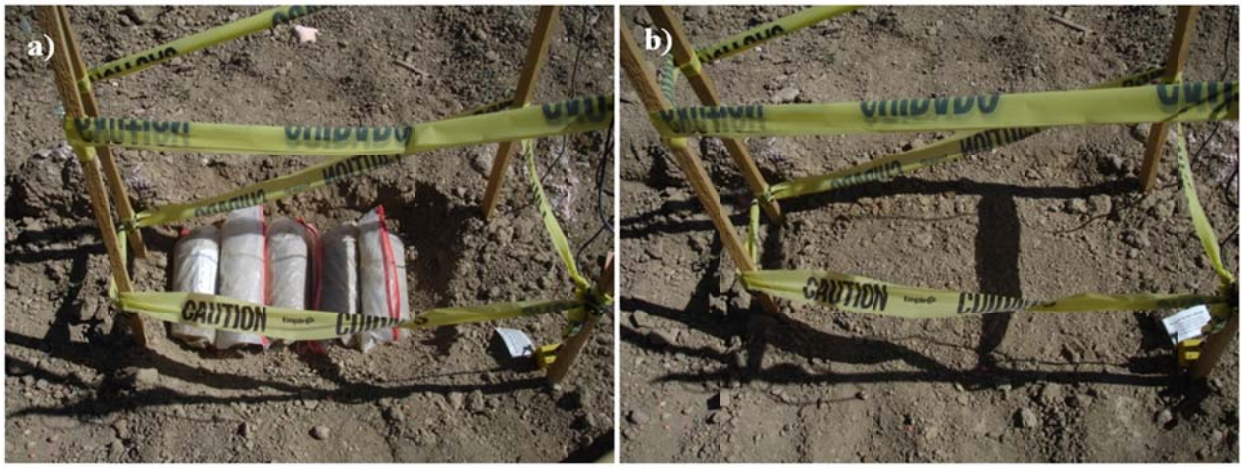

Figure 5.2: (a) FFR field cylinder storage trench uncovered and (b) covered.

Procedure II - Free-Free Resonance Testing: Free-free resonance (FFR) testing should be performed on each cylinder after 3, 5, or 7 days of curing. There is no ASTM standard for free-free resonance testing, but the methodology used herein mimics that found in literature (e.g., Ryden *et al*., 2006, Ahnberg and Holmen, 2008, Toohey and Mooney, 2010). Cylinders should be removed from the earthen trench, taken out of the plastic sealing bags, and placed (one at a time) on a foam sheet. Each cylinder is then subjected to longitudinal excitement via a tap (Figure 5.3) to estimate seismic Young's modulus. Each cylinder should be subjected to five impacts (taps). A miniature accelerometer is used to record the resultant free vibration of the cylinder. After data processing, the resonant frequency and the cylinder's mass density are used to determine seismic Young's modulus using Equations 5.1.

$$E_0 = \rho(2f_{rp}L)^2 = \rho(V_p)^2 \tag{5.1}$$

where:

E_0 = seismic Young's modulus (MPa)

ρ = mass density (kg/m^3)

f_{rp} = longitudinal resonant frequency (Hz)

L = cylinder length (m)

V_p = material p-wave velocity (m/s)

For each set of five cylinders, determine the mean (μ) and standard deviation (σ) of E_0 for acceptance verification in Section V of the specification. Each cylinder should be placed back in the bag and in the trench for future testing, if desired.

Figure 5.3: Free-free resonance testing with longitudinal excitation.

II: Experimental Testing- Method B

***Description*:** Method B specifies the experimental procedure for LSS assessment via seismic surface wave testing of field-compacted LSS surfaces.

***Materials*:** Surface wave testing equipment (e.g., D-SPA, SeisNDT, etc.).

***Procedure*:** Surface wave testing should be performed after 3, 5, or 7 days of curing on at least five locations per LSS section (depending on desired coverage and equipment efficiency, more locations may be tested). There is no ASTM standard for seismic surface wave testing, but from a procedural standpoint, the experimental method used herein is similar to that of the ASTM standard for seismic reflection testing (ASTM D7128-05). The procedure for data processing/analysis is adopted from literature (e.g., Nazarian *et al*., 2004, Ryden 2004, Ryden *et al*., 2006). To conduct surface wave testing, an accelerometer (or array of accelerometers) is coupled to the LSS surface via industrial grease (Figure 5.4b) or in-ground spikes (Figure 5.4c). A source impact (Figure 5.4a) is made adjacent to the accelerometer and the resulting waves are measured (Figure 5.5). In the development of this specification, the accelerometer used was the PCB 393A03 by PCB Piezotronics. The direct spike method was used as the grease provided less efficient coupling due to loose surface grains on the field-constructed LSS surface. The source

hammer was a PCB 086D05 instrumented hammer (by PCB Piezotronics) which was tapped against a metal plate (4in diameter, 0.4in thickness) to generate the waves measured by the accelerometer.

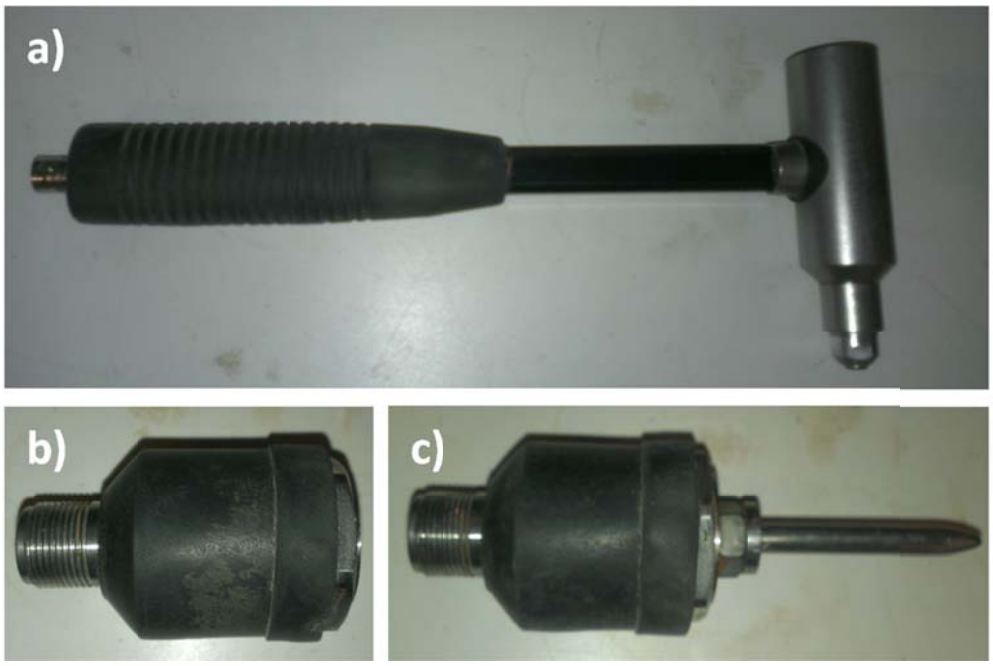

Figure 5.4: (a) instrumented hammer used as source impact, (b) accelerometer with no spike for greased coupling, and (c) accelerometer with ground spike for direct coupling.

Each impact generates an acceleration vs. time history that is used to estimate wave velocities in LSS using a known source to receiver distance. The minimum number of records necessary to evaluate a single location is two; however, more can be used to improve the quality of the result. Each record will have visibly identifiable waveforms of different varieties. The first arrival times for Primary (P) waves and/or Rayleigh (R) waves are extracted from the raw data (Figure 5.5b, c). P waves often have comparatively lower amplitudes than R waves and are sometimes difficult to identify. If P waves are visible, Equation 5.3 should be used to determine V_P.

$$V_p = \frac{x_2 - x_1}{t_{P2} - t_{P1}} \tag{5.3}$$

$$V_R = \frac{x_2 - x_1}{t_{R2} - t_{R1}} \tag{5.4}$$

$$V_P = [2(1+\nu)] \cdot [V_R(1.13 - 0.16\upsilon)] \quad (5.5)$$

where:

t_{R1} is the first arrival time of the Rayleigh wave in record 1 (s)

t_{R2} is the first arrival time of the Rayleigh wave in record 2 (s)

t_{P1} is the first arrival time of the P-wave in record 1 (s)

t_{P2} is the first arrival time of the P-wave in record 2 (s)

x_1 is the source to receiver distance for record 1 (m)

x_2 is the source to receiver distance for record 2 (m)

If P waves are not visible, V_P is determined using V_R (from Equation 5.4) and the material's Poisson's ratio (ν) using Equation 5.5. Poisson's ratio for LSS generally ranges from 0.2-0.4, so if the actual value is not known, use $\nu = 0.3$.

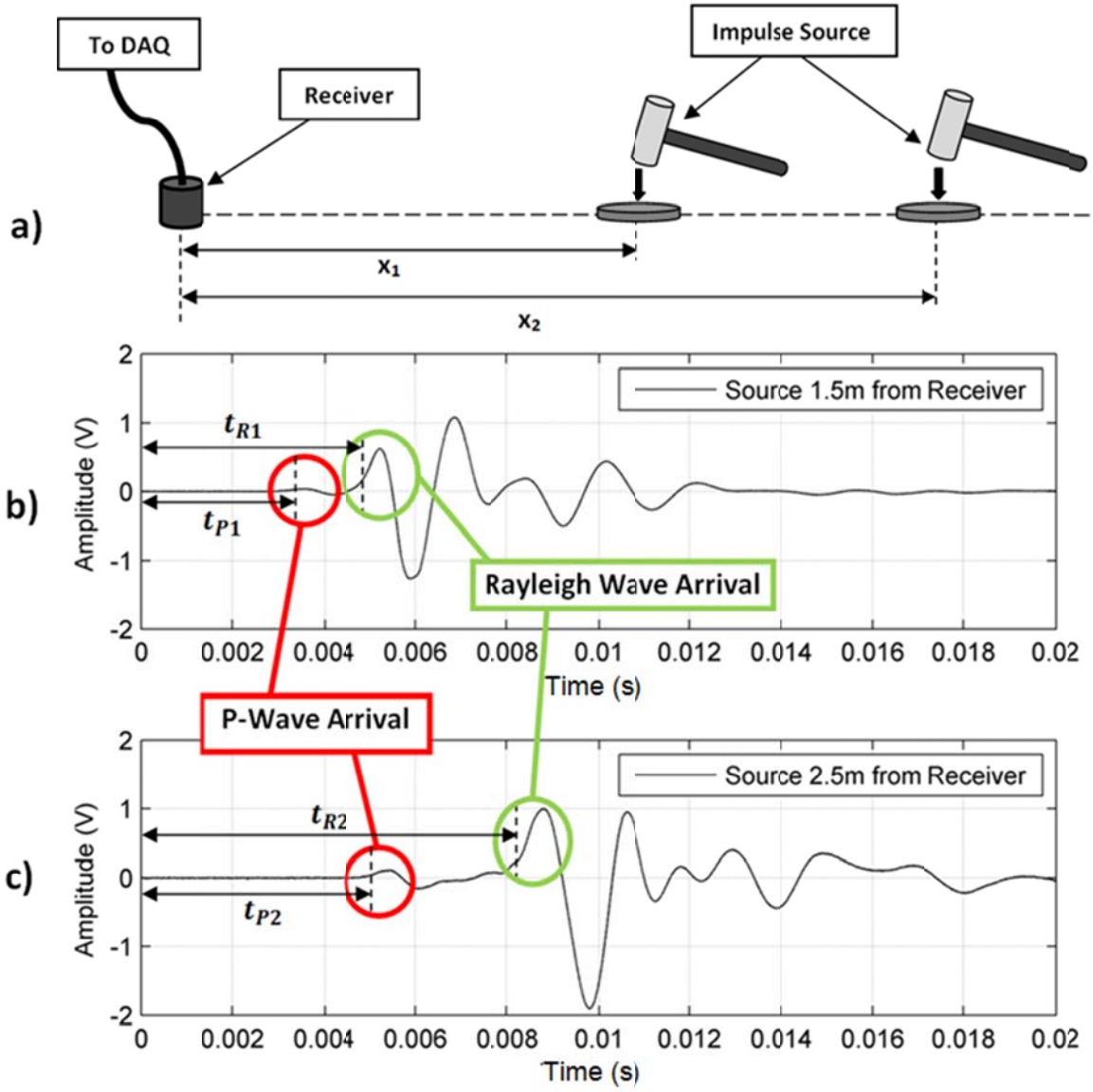

Figure 5.5: (a) Source and receiver configuration for simple surface wave testing, (b) waveform identification for example record 1, and (c) waveform identification for example record 2.

Once V_P has been obtained (from Equation 5.3 or 5.5), determine E_0 using the soil's mass density and Equation 5.1. If field density tests have been performed (e.g., nuclear density gauge), this value of density should be used. If field density tests have not been performed, standard Proctor density should be used (i.e., assuming a mix design study was conducted for the LSS section, standard Proctor density for optimum mix design should be available). Finally, determine the mean (μ) and standard deviation (σ) of E_0 (for each LSS section) for acceptance verification in Section V.

III: Determination of Target Seismic Modulus from LSS Maturity Index

Because LSS maturity is a time and temperature dependent reaction, the LSS temperature must be monitored in the field (or inferred from ambient temperature). If the average daily soil temperature ($\bar{T}_{t\ Day}$) was directly recorded via a temperature probe, determine the average curing temperature ($\bar{T}_t$) using Equation 5.6. If soil temperature was not directly recorded, first determine $\bar{T}_{t\ Day}$ with ambient (air) temperature and Equation 5.7.

$$\bar{T}_t(t, \bar{T}_{t\ Day}) = \frac{\sum_{i=1}^{t} \bar{T}_{t\ Day(i)}}{t} \tag{5.6}$$

$$\bar{T}_{t\ Day}\ (T_{Amb}) = 0.8 \cdot T_{Amb} + 2.8 \tag{5.7}$$

where:

T_{Amb} = the average ambient (air) temperature over 1 day of curing (^{o}C)

$\bar{T}_{t\ Day}$ = the average soil (LSS) temperature over 1 day of curing (^{o}C)

$\bar{T}_t$ = the cumulative average soil temperature over *t* days of curing (^{o}C)

The LSS maturity index –based target modulus (E_{Tar}) is determined using Equation 5.8, $\bar{T}_t$ (Equation 5.7), and the curing day on which experimental testing was performed (*t*).

$$E_{Tar}(t, \bar{T}_t) = (\alpha t^{\gamma}) * (e^{\beta \bar{T}_t}) \tag{5.8}$$

where:

E_{Tar} = target E_0 based on maturity index (MPa)

t = curing day (days)

$\bar{T}_t$ = average temperature for day 1 through the day being estimated (^{o}C)

α = 241

γ = 0.349

β = 0.05

IV: Acceptance Criteria for LSS

To evaluate acceptance of LSS sections, a statistically-based confidence interval approach is recommended. Field data exhibits scatter. A typical Gaussian (normal) distribution of field data is shown in Figure 5.5 where μ and σ are the mean and standard deviation of the field-measured E_0 values. The criteria for acceptance should be adjusted to suit the desired confidence interval. For example, the criteria for acceptance $\mu \geq E_{Tar}$ would insure that 50% of the E_0 values meet or exceed E_{Tar} (Figure 5.6a). This is termed a 50% confidence interval. If a greater confidence interval is required, the acceptance criteria are adjusted. For example, $(\mu - \sigma) \geq E_{Tar}$ implies 84% confidence (Figure 5.6b) and $(\mu - 2\sigma) \geq E_{Tar}$ implies 98% confidence (Figure 5.6c). The term E_{Acc} is introduced to establish the desired criteria as shown in Equations 5.9-5.11.

$$E_{Acc\ 50\%} = \mu \tag{5.9}$$

$$E_{Acc\ 84\%} = (\mu - \sigma) \tag{5.10}$$

$$E_{Acc\ 98\%} = (\mu - 2\sigma) \tag{5.11}$$

The acceptance criteria is therefore $E_{Acc} \geq E_{Tar}$. :

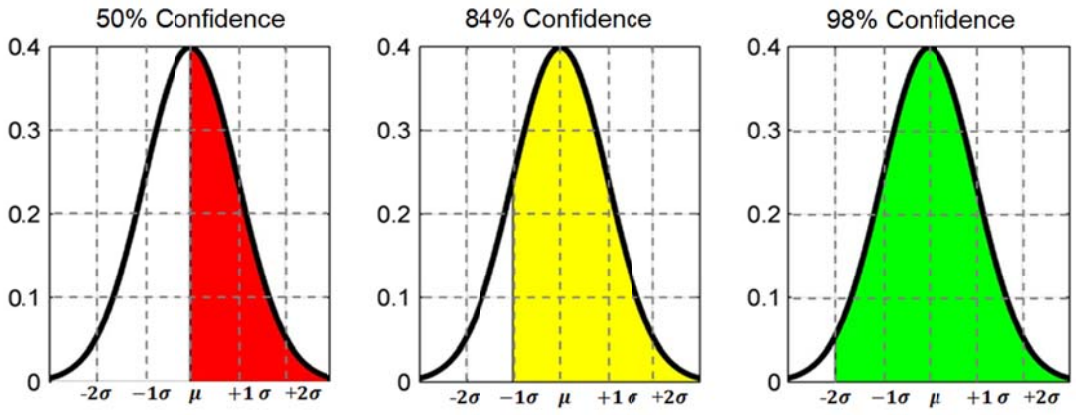

Figure 5.6: LSS acceptance intervals assuming normally distributed data.

Acceptance can be verified on days 3, 5, or 7. Once a section has met acceptance, no additional testing is required. A flowchart of the QA acceptance procedure is illustrated in Figure 5.7.

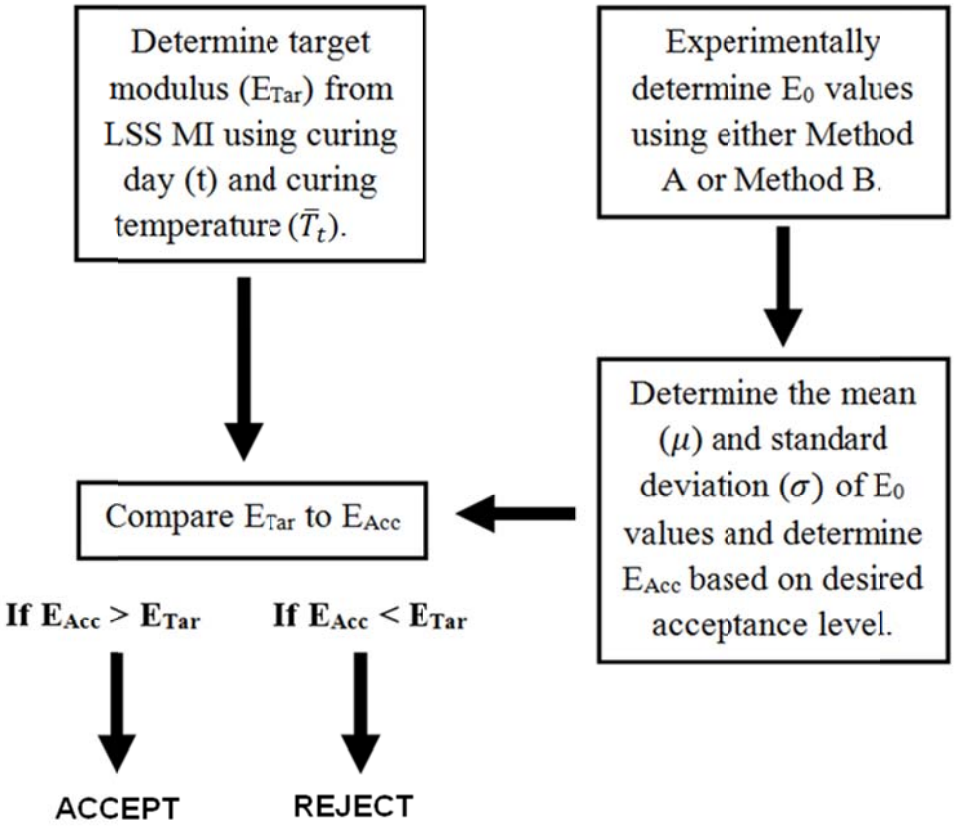

Figure 5.7: Flow chart for LSS QA specification.

V: Synthetic Data Example

To illustrate the procedure for LSS acceptance using this specification, a synthetic data example is presented below. The example site contains 3 sections experimentally evaluated using Method B (surface wave testing). Assuming thorough testing coverage is desired, ten locations per section were evaluated (Figure 5.8). In addition, assume the desired confidence level is 84%, i.e., that 84% of the measured E_0 values must exceed the E_{Tar} (Figure 5.6, Equation 5.10). Note that as this is synthetic data, E_0 values for days 3, 5, and 7 are presented for each section. For an actual application of this specification, subsequent tests would not be conducted after section acceptance has been met.

Step 1: Compute the mean and standard deviation of E_0 for each LSS section

Following the procedure in Section III of the pilot specification, raw surface wave data is converted to E_0 data. Because different testing setups provide different results (i.e., some may require manual picking of arrival times while others may give direct wave velocity/modulus

results), this process is not reiterated here, and thus synthetic E_0, μ, and σ data are presented in Tables 5.1 and 5.2.

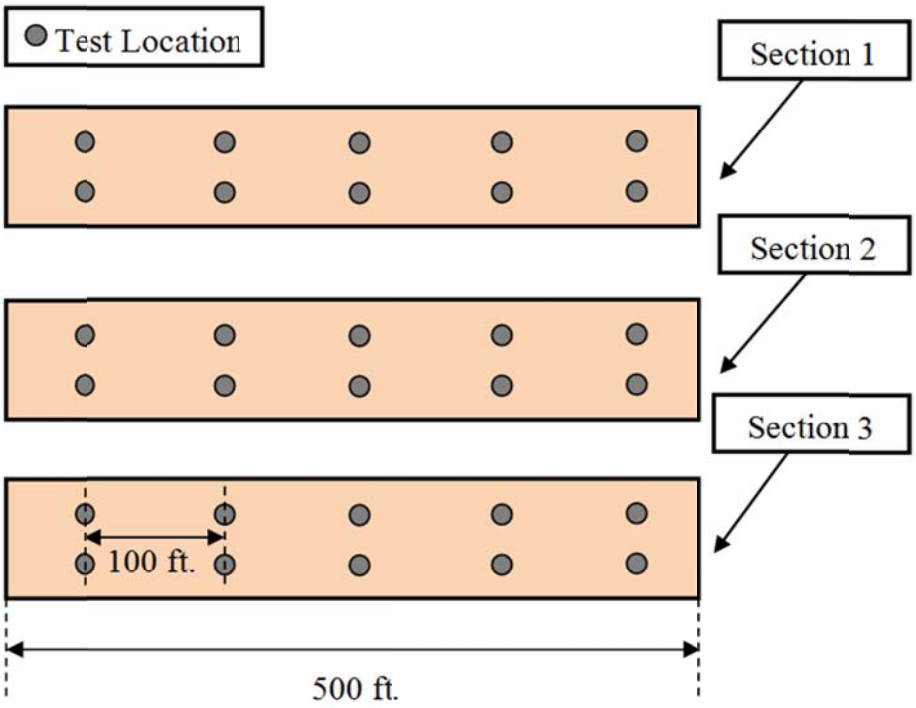

Figure 5.8: Synthetic data LSS site with 3 mixed sections and ten surface wave tests per section.

Table 5.1: Synthetic surface wave E_0 data from section 1-3 on days 3, 5, and 7.

Section 1				Section 2				Section 3			
Test Loc.	E_0 (MPa) Day 3	Day 5	Day 7	Test Loc.	E_0 (MPa) Day 3	Day 5	Day 7	Test Loc.	E_0 (MPa) Day 3	Day 5	Day 7
1	2120	2050	2160	1	1920	1740	1900	1	1490	1990	2100
2	1540	1970	2340	2	1570	2100	1990	2	1570	2180	1960
3	1710	2140	2470	3	1680	1990	1940	3	1820	1940	2280
4	1350	1650	2010	4	1520	2120	2210	4	1630	2360	1910
5	1450	1710	2060	5	1620	1900	2460	5	1660	1790	2220
6	1490	1600	2280	6	1760	1730	2240	6	1800	2220	2210
7	1530	1850	2330	7	1230	1910	2510	7	1650	1910	1940
8	1840	2120	1870	8	1690	2160	2060	8	1750	2080	2240
9	1730	1850	2240	9	1540	2060	2210	9	1250	2100	2080
10	1550	1790	2130	10	1440	1910	1920	10	1650	1890	1900

Table 5.2: μ and σ for each data set presented in Table 5.1.

Section	E_0 (MPa) Day 3		Day 5		Day 7	
	μ	σ	μ	σ	μ	σ
1	1629	226	1873	192	2188	179
2	1598	187	1963	151	2145	219
3	1627	166	2046	173	2084	148

Step 2: Determine $\bar{T}_t$ for each section

For simplicity sake, assume all three sections (Figure 5.8) were mixed on the same day (i.e., $\bar{T}_t$ is the same for all sections). The average daily air temperature (T_{Amb}) is used to estimate average daily soil temperature ($\bar{T}_{t\,Day}$) using the correlation shown in Equation 5.7. $\bar{T}_{t\,Day}$ is then used to determine the cumulative average temperature ($\bar{T}_t$) for each day (Equation 5.6, shown in Table 3). As an example, the calculation of $\bar{T}_t$ for day 3 is shown below.

$$\bar{T}_{1\,Day} = 0.8\,(34^oC) + 2.8^oC = 30^oC$$
$$\bar{T}_{2\,Day} = 0.8(33^oC) + 2.8^oC = 29^oC$$
$$\bar{T}_{3\,Day} = 0.8(35^oC) + 2.8^oC = 30^oC$$

$$\bar{T}_3 = \frac{\bar{T}_{1\,Day} + \bar{T}_{2\,Day} + \bar{T}_{3\,Day}}{3} = \frac{30^oC + 29^oC + 30^oC}{3} = 30^oC$$

Table 5.3: Average daily ambient temperature, average daily soil temperature, and cumulative average temperature for synthetic data example.

Day	T_{Amb} (°C)	$\bar{T}_{t\,Day}$ (°C)	$\bar{T}_t$ (°C)
1	34	30	30
2	33	29	30
3	35	31	30
4	31	28	29
5	32	28	29
6	31	27	29
7	30	27	29

Step 3: Determine E_{Tar} for each section

Using Equation 5.8, determine the target modulus (E_{Tar}) using $\bar{T}_t$ and *t* (the curing day that E_0 data was acquired). Calculation of E_{Tar} for days 3, 5, and 7 (with corresponding $\bar{T}_t$ values) is shown below. Note that the empirical parameters α, γ, and β are equal to 241, 0.349, and 0.05, respectively. These parameters were determined by correlating seismic modulus values (obtained via FFR) to curing day and curing temperature. This procedure is described in detail in CDOT Report 2013, Evaluation of Seismic Testing for Quality Assurance of Lime-Stabilized Soil.

$$E_{Tar}(3{,}30) = (\alpha(3)^{\gamma}) * \left(e^{\beta(30)}\right) = 1584\ MPa$$
$$E_{Tar}(5{,}29) = (\alpha(5)^{\gamma}) * \left(e^{\beta(29)}\right) = 1801\ MPa$$
$$E_{Tar}(7{,}29) = (\alpha(7)^{\gamma}) * \left(e^{\beta(29)}\right) = 1926\ MPa$$

Step 4: Assess acceptance for each section

Because 84% confidence is desired, E_{Acc} should be calculated using Equation 5.10. The comparison of E_{Acc} to E_{Tar} for each test day and section is summarized in Table 5.4. Results indicate that Section 1 does not meet acceptance on days 3 or 5 but is acceptable on day 7. E_{Acc} for Section 2 is below the E_{Tar} on days 3, 5, and 7, and should therefore be rejected. Section 3 meets acceptance on day 5, and while the synthetic day 7 data is presented, day 7 testing would not be required based on day 5 acceptance. Additional testing could be performed on rejected sections (e.g., Section 2) on later days, but post 7-day acceptance testing is not generally feasible for construction schedules.

Table 5.4: Evaluation of acceptance criteria for synthetic LSS data set.

Section	$E_{Acc\ 84\%}$ (MPa) Day 3	Day 5	Day 7	Acceptance
1	1400	1680	2010	Accept on Day 7
2	1410	1790	1900	Reject
3	1460	1870	1940	Accept on Day 5
E_{Tar}	1580	1800	1930	

Visual representations of the acceptance criteria for Sections 1, 2, and 3 are shown in Figures 5.9, 5.10, and 5.11, respectively. These figures help to convey the relationship between raw E_0 data and the different acceptance levels, and how these values compare to the expected LSS E_0 behavior (i.e., E_{Tar}).

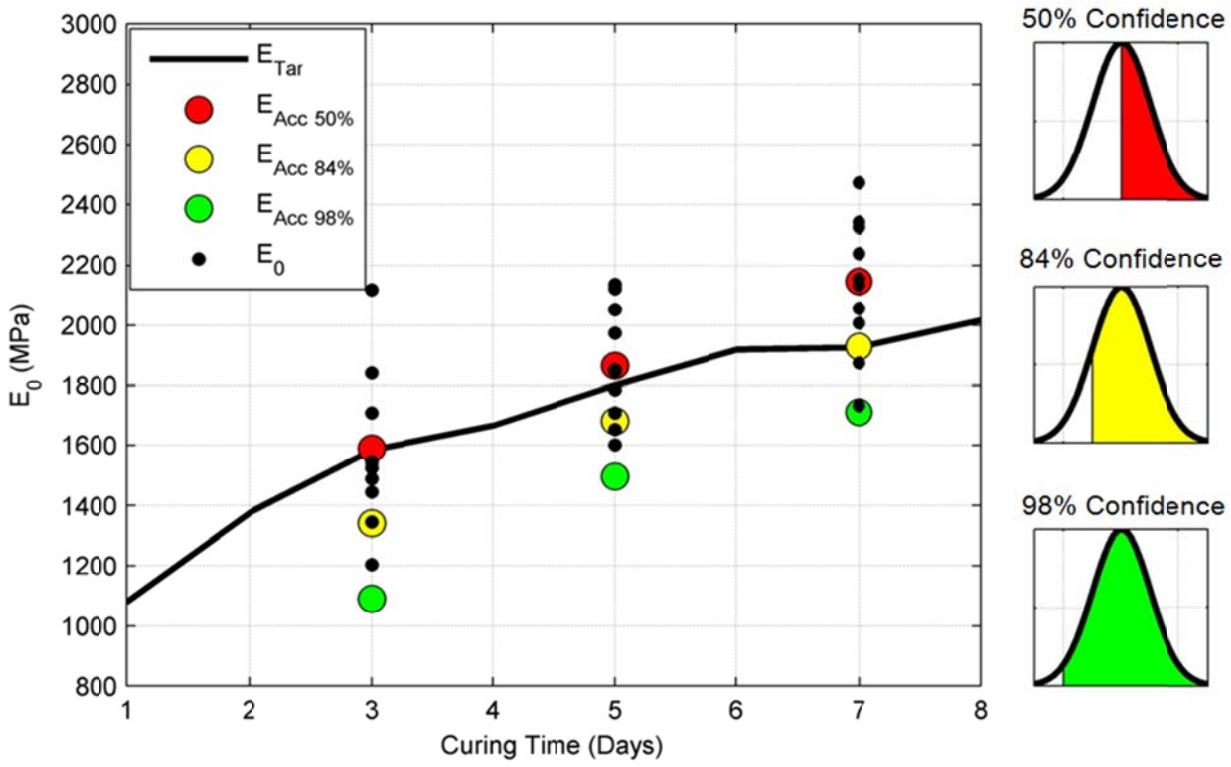

Figure 5.9: Visual representation of unaveraged E_0 data, E_{Tar}, and various acceptance levels for Section 1.

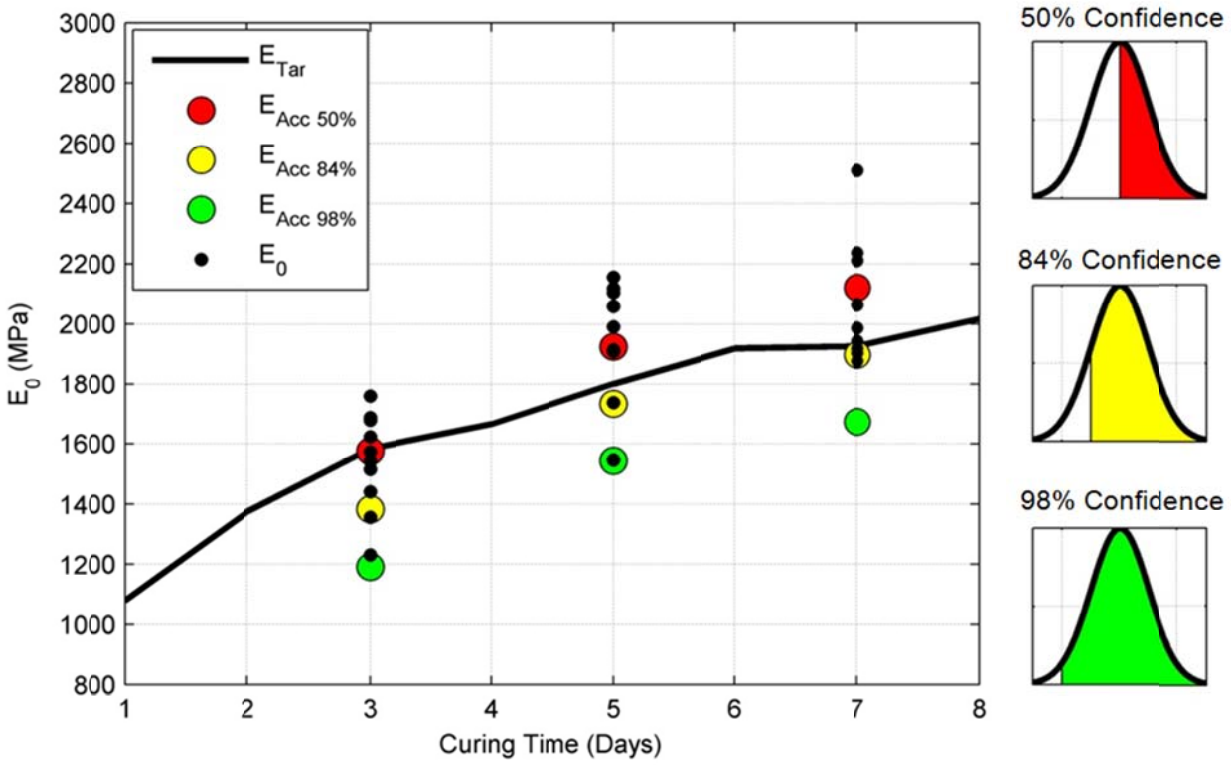

Figure 5.10: Visual representation of unaveraged E_0 data, E_{Tar}, and various acceptance levels for Section 2.

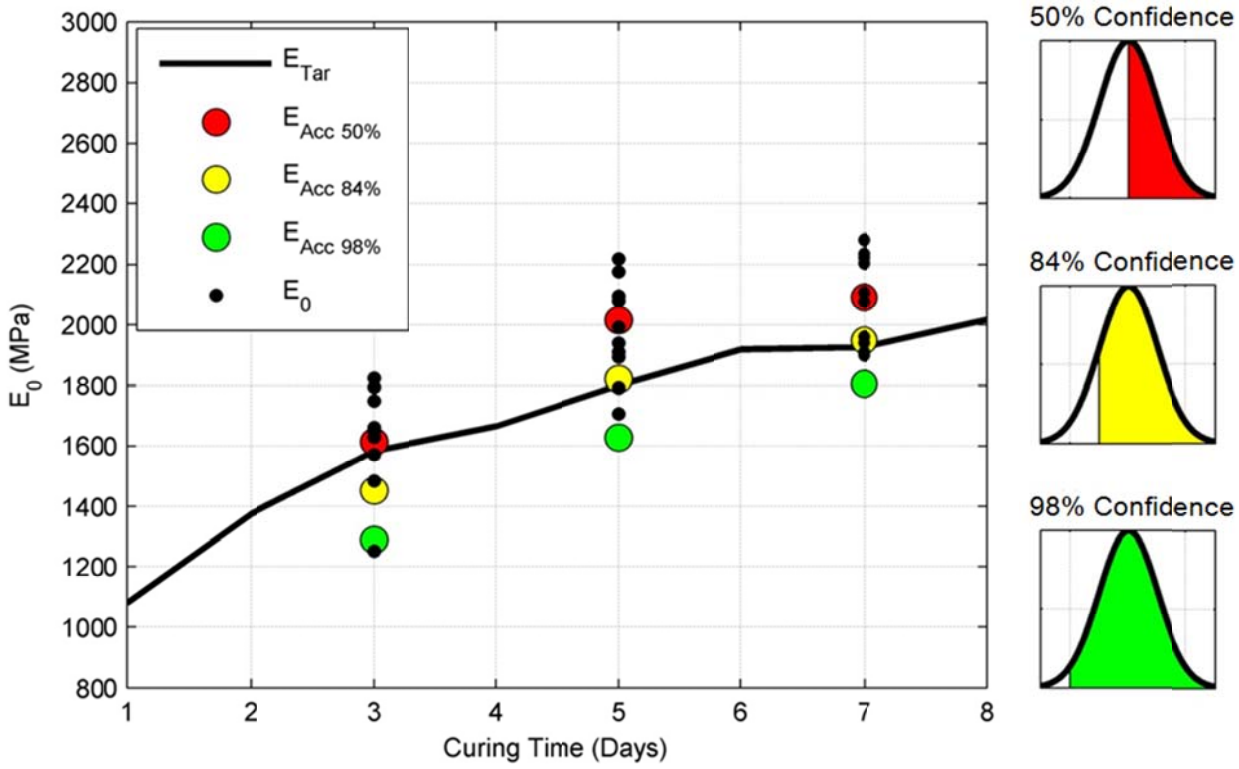

Figure 5.10: Visual representation of unaveraged E_0 data, E_{Tar}, and various acceptance levels for Section 3.

REFERENCES

AASHTO T294. (1994). "Standard Method of Test for Resilient Modulus of Unbound Granular Base/Subbase Materials and Subgrade Soils." American Association of State Highway and Transportation Officials, Washington, D.C.

Ahnberg, H. and Holmen, M. (2008). “Laboratory determination of small-strain moduli in stabilized soils,” Swedish Geotechnical Institute, Sweden.

ASTM D7128-05 (2005 – reapproved in 2010). Standard Guide for Using the Seismic-Reflection Method for Shallow Subsurface Investigation. ASTM International, West Conshohocken, PA

CDOT Construction Specifications (2005), “Lime Treated Subgrade,” Section 307.

Heisey, J. S. (1982). *Determination of in situ shear wave velocities from spectral analysis of surface waves.* Austin: Bureau of Engineering Research-University of Texas.

Kim, D.S., Shin, M.K., & Park, H.C. (2001). Evaluation of Density in Layer Compaction using the SASW Method. *Soil Dynamics and Earthquake Engineering* , 39-46.

Mallela, J., VonQuintus H., and Smith, K.L. (2004). “Consideration of Lime-Stabilized Layers in Mechanistic-Empirical Pavement Design.” Prepared for The National Lime Association.

Mechanistic-Empirical Pavement Design Guide (MEPDG): A Manual of Practice, July 2008 Interim Edition. (2008). American Association of State Highway and Transportation Officials, Washington, D.C.

Nazarian, S. (1984). *In-Situ Determination of Soil Deposits and Pavement Systems by Spectral Analysis of Surface Waves (Ph.D. Thesis).* Austin: University of Texas.

Nazarian, S., Yuan, D., and Arellano, M., (2002). "Quality Management of Base and Subgrade Materials with Seismic Methods," *Transportation Research Record* 1786, Journal of Transportation Research Board, TRB, National Research Council, Washington D.C., pp.3-10.

Nazarian, S., Yuan, D., and Tandon,V. (1999). "Structural Field Testing of Flexible Pavement Layers with Seismic Methods for Quality Control," *Transportation Research Record* 1654, Transportation Research Board, Washington D.C., pp. 50-60.

Olson Engineering, Inc. (2013) Spectral Analysis of Surface Waves. Technical Brief. www.OlsonEngineering.com

Park, C., Miller, R., & Xia, J. (1997). *Multi-Channel Analysis of Surface Waves.* Lawrence: Kansas Geological Survey.

Ryden, N. (2004). *Surface Wave Testing of Pavements.* Doctoral Thesis. Department of Engineering and Geology. Lund University.

Ryden, N., Ekdahl, U., and Lindh, P., (2006). "Quality Control of Cement Stabilised Soils using Non-Destructive Seismic Tests," Advanced testing of fresh cementitious materials, Lecture 34, August 3-4, 2006. Stuttgart, Germany.

Ryden, N., & Park, C. (2006). Fast Simulated Annealing Inversion of Surface Waves. *Geophysics*. Vol. 71, N0. 4, July – August.

Ryden, N., Park, C., Ulriksen, P., & Miller, R. (2004). Multi Model Approach to Seismic Pavement Testing. *J. Geotech. and Geoenvir. Engineering* , 636-645.

Stokoe, K. H., Wright, S. G., Bay, J. A., & Roesset, J. M. (1994). *Characterization of Geotechnical Sites by SASW Method.* Oxford.

Toohey, N.M. (2009). "Determination of Strength and Modulus Gain for Lime-Stabilized Soils", M.S. Thesis, Colorado School of Mines, pp. 93.

Toohey, N.M. and Mooney, M.A. (2012) Seismic Modulus Growth of Lime-Stabilised Soil during Curing. *Geotechnique* 62, No. 2, 161-170

APPENDIX A – TABULAR SEISMIC MODULUS DATA (FFR)

TABLE A1: SEISMIC MODULUS VALUES OBTAINED VIA FFR FOR SOLTERRA (DAYS 1-10).

Specimen	Curing Temp (°C)	Seismic Young's Modulus (MPa) for each day										
		0	1	2	3	4	5	6	7	8	9	10
1	23	460	483	616	792	959	1049	1162	1261	1364	1480	1550
2	23	456	562	585	750	889	976	1114	1206	1294	1364	1462
3	23	450	555	558	744	882	983	1105	1209	1293	1370	1477
4	23	488	615	638	853	976	1113	1242	1348	1440	1517	1619
5	23	436	544	572	729	878	989	1105	1200	1312	1359	1459
6	8	337	420	522	590	624	633	664	662	687	690	693
7	8	339	427	526	545	556	587	600	635	639	647	671
8	8	323	393	488	517	536	555	580	585	617	644	650
9	8	324	410	497	534	575	588	622	635	661	700	694
10	8	325	412	512	539	556	581	594	632	655	671	655
11	Field	364	461	536	611	629	680	699	719	738	777	807
12	Field	355	446	519	592	615	653	676	700	723	739	764
13	Field	362	425	499	574	617	635	659	683	708	727	756
14	Field	359	433	493	553	589	630	643	655	668	696	722
15	Field	360	455	512	569	594	629	647	665	683	720	745
16	41	368	831	1309	1840	2118	2381	2685	2907	3010	3106	3171
17	41	347	887	1575	2223	2785	3178	3506	3794	3997	4079	4220
18	41	340	949	1520	2101	2538	2947	3299	3607	3920	4068	4180
19	41	328	887	1612	2228	2785	3244	3583	3829	4057	4146	4266
20	41	359	870	1717	2409	2894	3263	3534	3781	3999	4066	4124

TABLE A2: SEISMIC MODULUS VALUES OBTAINED VIA FFR FOR SOLTERRA (DAYS 11-28).

Specimen	Curing Temp (°C)	Seismic Young's Modulus (MPa) for each day										
		11	12	13	14	16	18	20	22	24	26	28
1	23	1619	1721	1817	1897	1980	2134	2196	2281	2395	2484	2620
2	23	1508	1555	1640	1781	1863	2013	2117	2203	2289	2383	2510
3	23	1528	1578	1674	1803	1899	2008	2121	2201	2282	2392	2518
4	23	1684	1749	1823	1921	2088	2186	2305	2395	2465	2599	2708
5	23	1521	1611	1648	1768	1879	1996	2134	2208	2282	2358	2475
6	8	710	727	808	834	851	882	917	943	950	975	1011
7	8	691	711	723	764	778	810	833	864	895	912	929
8	8	660	670	719	729	774	810	813	835	857	880	904
9	8	703	712	712	766	766	838	866	872	879	917	954
10	8	687	720	717	767	797	824	834	854	875	897	919
11	Field	836	866	881	895	924	952	981	1012	1033	1055	1075
12	Field	790	815	828	841	892	944	996	1017	1045	1064	1081
13	Field	786	815	830	845	876	906	936	950	973	994	1013
14	Field	747	773	786	799	834	869	904	925	943	962	983
15	Field	771	796	808	821	854	888	921	942	965	982	1001
16	41	3206	3255	3301	3379	3474	3555					
17	41	4338	4414	4433	4357	4426	4438					
18	41	4283	4418	4399	4425	4425	4425					
19	41	4304	4341	4341	4364	4403	4485					
20	41	4219	4315	4384	4414	4491	4491					

TABLE A3: SEISMIC MODULUS VALUES OBTAINED VIA FFR FOR TCA 2011-ZONE 1 (DAYS 1-10).

Specimen	Curing Temp (°C)	Seismic Young's Modulus (MPa) for each day										
		0	1	2	3	4	5	6	7	8	9	10
1	23	456	820	957	1046	1240	1358	1448	1579	1612	1646	1669
2	23	501	880	1078	1153	1295	1356	1403	1528	1567	1607	1645
3	23	475	911	1092	1164	1281	1385	1431	1545	1577	1610	1656
4	23	495	853	1047	1122	1155	1240	1420	1506	1524	1542	1558
5	23	504	884	1036	1106	1226	1279	1330	1358	1453	1551	1562
6	Field	513	1056	1168	1236	1484	1603	1671	1745	1843	1943	1950
7	Field	493	1104	1263	1345	1529	1662	1760	1805	1869	1934	2025
8	Field	525	1124	1279	1333	1504	1522	1628	1822	1871	1921	2005
9	Field	501	1108	1244	1304	1474	1559	1778	1808	1869	1932	1962

TABLE A4: SEISMIC MODULUS VALUES OBTAINED VIA FFR FOR TCA 2011-ZONE 1 (DAYS 11-28).

Specimen	Curing Temp (°C)	Seismic Young's Modulus (MPa) for each day										
		11	12	13	14	16	18	20	22	24	26	28
1	23	1714	1836	1871	1965	1974	2043	2123	2145	2219	2221	2197
2	23	1676	1766	1823	1894	1969	2014	2122	2169	2145	2234	2232
3	23	1692	1827	1863	1942	1964	1979	1988	2181	2200	2176	2176
4	23	1586	1698	1783	1812	1920	1936	1975	2066	2063	2087	2151
5	23	1585	1668	1815	1805	1896	1924	1987	2037	2052	2070	2135
6	Field	2044	2028	2167	2139	2265	2354	2494	2515	2524	2578	2632
7	Field	2213	2223	2176	2363	2386	2445	2510	2570	2567	2577	2589
8	Field	2231	2231	2183	2200	2333	2432	2519	2529	2504	2538	2577
9	Field	2111	2233	2272	2320	2460	2480	2525	2497	2493	2528	2546

TABLE A5: SEISMIC MODULUS VALUES OBTAINED VIA FFR TCA 2011-ZONE 2 (DAYS 1-10).

Specimen	Curing Temp (°C)	Seismic Young's Modulus (MPa) for each day									
		0	1	2	3	4	5	6	7	8	9	10
1	Field	474	804	967	1046	1220	1377	1566	1783	1872	1963	2037
2	Field	483	763	846	998	1162	1392	1601	1718	1739	1760	1963
3	Field	499	784	903	1023	1264	1371	1539	1657	1777	1901	1924
4	Field	501	876	997	1046	1253	1445	1600	1786	1854	1923	2004
5	Field	510	1127	1243	1312	1489	1634	1697	1754	1812	1872	2020

TABLE A6: SEISMIC MODULUS VALUES OBTAINED VIA FFR TCA 2011-ZONE 2 (DAYS 11-28).

Specimen	Curing Temp (°C)	Seismic Young's Modulus (MPa) for each day										
		11	12	13	14	16	18	20	22	24	26	28
1	Field	2175	2190	2265	2280	2386	2405	2515	2594	2635	2674	2718
2	Field	2129	1979	2194	2268	2364	2373	2470	2494	2518	2631	2672
3	Field	1970	2033	2233	2170	2331	2350	2517	2554	2643	2717	2763
4	Field	2090	2177	2369	2259	2441	2451	2641	2480	2542	2673	2745
5	Field	2008	2104	2146	2276	2374	2433	2463	2516	2515	2526	2570

TABLE A7: SEISMIC MODULUS VALUES OBTAINED VIA FFR CANDELAS – ZONE 1 (DAYS 1-10).

Specimen	Curing Temp (°C)	Seismic Young's Modulus (MPa) for each day										
		0	1	2	3	4	5	6	7	8	9	10
1	23	434	737	1122	1291	1440	1622	1734	1847	1928	2039	2139
2	23	512	617	912	1062	1168	1304	1398	1451	1573	1660	1763
3	23	457	641	976	1118	1283	1377	1474	1562	1629	1758	1882
4	23	435	572	840	1003	1118	1244	1337	1451	1533	1622	1716
5	23	504	711	1089	1188	1390	1509	1592	1687	1787	1914	2019
6	Field	375	734	1323	1385	1492	1666	1785	1925	2052	2164	2231
7	Field	433	1150	1632	1819	2061	2270	2276	2487	2697	2826	3317
8	Field	573	1003	1450	1707	1903	2099	2189	2313	2371	2539	2689
9	Field	398	1278	1742	2016	2230	2455	2575	2663	2774	2884	3059
10	Field	465	1377	1757	2184	2365	2632	2749	2832	2944	3027	3178

TABLE A8: SEISMIC MODULUS VALUES OBTAINED VIA FFR CANDELAS-ZONE 1 (DAYS 11-28).

Specimen	Curing Temp (°C)	Seismic Young's Modulus (MPa) for each day										
		11	12	13	14	16	18	20	22	24	26	28
1	23	2249	2373	2418	2479	2539	2647	2769	2831	2894	2945	3029
2	23	1815	1857	1976	2077	2139	2184	2353	2448	2482	2531	2589
3	23	1938	1983	2045	2139	2218	2270	2412	2497	2593	2628	2683
4	23	1788	1870	1934	1978	2006	2061	2230	2317	2378	2415	2455
5	23	2156	2207	2285	2383	2437	2548	2640	2735	2811	2894	2930
6	Field	2286	2390	2468	2514	2552	2637	2727	2836	2935		
7	Field	3336	3350	3359	3364	3388	3579	3671	3657	3646		
8	Field	2842	2918	3007	3154	3282	3365	3452	3478	3495		
9	Field	3156	3253	3329	3442	3511	3643	3776	3857	3949		
10	Field	3315	3474	3572	3614	3726	3771	3771	3774	3782		

TABLE A9: SEISMIC MODULUS VALUES OBTAINED VIA FFR CANDELAS – ZONE 2 (DAYS 1-10).

Specimen	Curing Temp (°C)	Seismic Young's Modulus (MPa) for each day										
		0	1	2	3	4	5	6	7	8	9	10
1	8	305	411	469	529	590	631	684	729	773	805	850
2	8	254	317	371	398	477	511	551	590	626	662	702
3	8	344	403	453	504	560	602	647	693	736	779	827
4	8	304	418	423	451	509	558	612	661	715	761	820
5	8	278	337	351	371	426	463	505	546	598	623	934
6	23	293	351	445	521	584	642	705	769	834	897	942
7	23	368	552	711	818	976	1046	1122	1196	1277	1351	1433
8	23	383	626	805	942	1110	1184	1262	1331	1423	1493	1576
9	23	372	590	769	883	1023	1092	1159	1229	1303	1371	1447
10	23	350	812	1077	1235	1398	1478	1563	1645	1734	1808	1903
11	Field	269	923	1350	1685	1894	2015	2167	2264	2357	2423	2534
12	Field	341	956	1304	1692	1926	2045	2201	2288	2398	2421	2578
13	Field	359	1122	1553	1701	2023	2145	2316	2402	2554	2679	2754
14	Field	278	1094	1666	1898	2145	2246	2363	2458	2547	2634	2744
15	Field	343	1098	1742	1978	2191	2315	2436	2556	2651	2745	2835
16	41	353	2023	2779	3199	3212	3278	3339	3339	3339	3339	3339
17	41	401	1914	2689	3090	3177	3295	3394	3394	3394	3394	3394
18	41	403	2066	2930	3188	3114	3120	3185	3185	3185	3185	3185
19	41	387	1861	2461	2635	2658	2661	2689	2689	2689	2689	2689
20	41	413	2150	2902	3039	3035	3031	3029	3029	3029	3029	3029

TABLE A10: SEISMIC MODULUS VALUES OBTAINED VIA FFR CANDELAS – ZONE 2 (DAYS 11-28).

Specimen	Curing Temp	Seismic Young's Modulus (MPa) for each day										
	(°C)	11	12	13	14	16	18	20	22	24	26	28
1	8	901	913	1002	1053	1175	1216	1257	1248	1295	1344	1278
2	8	749	761	837	879	1003	1032	1062	1030	1075	1018	1050
3	8	876	890	980	1034	1134	1159	1184	1150	1215	1278	1248
4	8	884	906	1003	1053	1113	1148	1184	1218	1248	1278	1278
5	8	982	996	1090	854	854	912	972	946	987	1030	1042
6	23	985	989	1076	1122	1278	1288	1468	1553	1627	1701	1730
7	23	1517	1540	1698	1788	1835	1895	2016	2061	2146	2230	2270
8	23	1665	1683	1842	1935	1973	2096	2184	2270	2339	2406	2448
9	23	1536	1552	1699	1772	1814	1903	1978	2099	2184	2270	2270
10	23	1996	2008	2194	2270	2312	2408	2497	2589	2661	2735	2735
11	Field	2657	2746	2820	2912	2957	3047	3096	3135	3178		
12	Field	2681	2768	2826	2946	2995	3068	3113	3166	3199		
13	Field	2812	2893	2966	3029	3098	3158	3234	3289	3339		
14	Field	2821	2959	3067	3185	3130	3187	3208	3209	3212		
15	Field	2956	3035	3165	3234	3222	3214	3202	3283	3264		
16	41	3339	3339	3339	3339	3331	3337	3339				
17	41	3394	3394	3394	3394	3382	3390	3394				
18	41	3185	3185	3185	3171	3199	3189	3185				
19	41	2689	2689	2689	2689	2692	2695	2689				
20	41	3029	3029	3029	3015	3042	3040	3029				

APPENDIX B – TABULAR SEISMIC MODULUS DATA (SURFACE WAVE)

TABLE B.1: SEISMIC MODULUS VALUES OBTAINED VIA SURFACE WAVE TESTING FOR TCA 2011 – ZONE 1.

Test Location	Seismic Young's Modulus (MPa) for each day								
	2	3	4	5	6	7	8	9	10
1	153	327	361	418	760	432			
2	352	322	353	402	485	521	618	655	662
3	203	260	328	753	612	268	301	312	213
4	302	494	315	655	699	312	343		
5	212	322	445	500	536	580	599	635	662
6	361	561	689	746	823	877	900	920	
7	167	462	515	536	675	764	651	331	322
8	304	276	494	527	554	612	658	276	301
9	171	287	361	457	521	586	612	595	601
10	325	494	536	573	622	658	696	570	578
11	165	554	592	682	583	699	738	539	459
12	140	358	371	457	497	317	386	421	485

TABLE B.2: SEISMIC MODULUS VALUES OBTAINED VIA SURFACE WAVE TESTING FOR TCA 2011 – ZONE 2.

Test Location	Seismic Young's Modulus (MPa) for each day			
	2	3	4	5
7	604	657	736	748
8	510	601	669	741
11	512	625	741	878
15	638	690	747	818
19	616	744	796	861
20	655	703	741	809

TABLE B.3: SEISMIC MODULUS VALUES OBTAINED VIA SURFACE WAVE TESTING FOR TCA 2012.

Test Location	Seismic Young's Modulus (MPa) for each day							
	2	3	4	5	6	7	8	9
1	549	645	645	687	675	675	691	694
2	806	853	855	875	903	944	1089	1091
3	730	799	827	877	928	967	1003	1110
4	804	1043	1134	1207	1232	1239	1261	1332
5	682	737	756	779	840	933	933	853
6	555	687	725	766	861	941	941	853
7	687	759	786	817				
8	551	581	634	661				
9	195	271	344	361	368	374	387	366
10	126	412	431	455	460	470	480	570
11	336	358	365	392	392	395	398	442
12	234	287	344	401	415	430	461	461

TABLE B.4: SEISMIC MODULUS VALUES OBTAINED VIA SURFACE WAVE TESTING FOR SOLTERRA.

Test Location	Seismic Young's Modulus (MPa) for each day					
	2	3	4	5	6	7
1	381	422	510	590	730	692
2	423	529	554	542	603	656
3	409	533	411	658	605	804
4	389	497	571	531	601	860
5	308	351	507	590	618	753

TABLE B.5: SEISMIC MODULUS VALUES OBTAINED VIA SURFACE WAVE TESTING FOR CANDELAS.

Test Location	Seismic Young's Modulus (MPa) for each day			
	2	3	4	5
6	547	890	1110	1302
7	1251	1624	1794	1913
8	882	1186	1517	1805
9	605	1080	1348	1704

APPENDIX C – SPECTRAL ANALYSIS OF SURFACE WAVES PROCEDURE

This appendix explains the procedure for spectral analysis of surface wave data via SeisNDT. Beginning with raw data (i.e., superimposed time histories at each spacing) (C1a), SeisNDT's spectral analysis algorithm generates a dispersion curve (Figure C1b). Once the dispersion curve has been generated, wave velocities and layer thickness can be estimated by fitting know symmetric and asymmetric mode shapes to the dispersion generated by the raw data (Figure C1b) While algorithms generate the dispersion curve, it is often necessary for the user to interpret the proper fit of this curve by adjusting V_p, Poisson's ratio, and top layer thickness. Full explanation/derivation of the theory used to predict/interpret these mode shapes can be found in Ryden (2004), but SeisNDT makes these computations automatically.

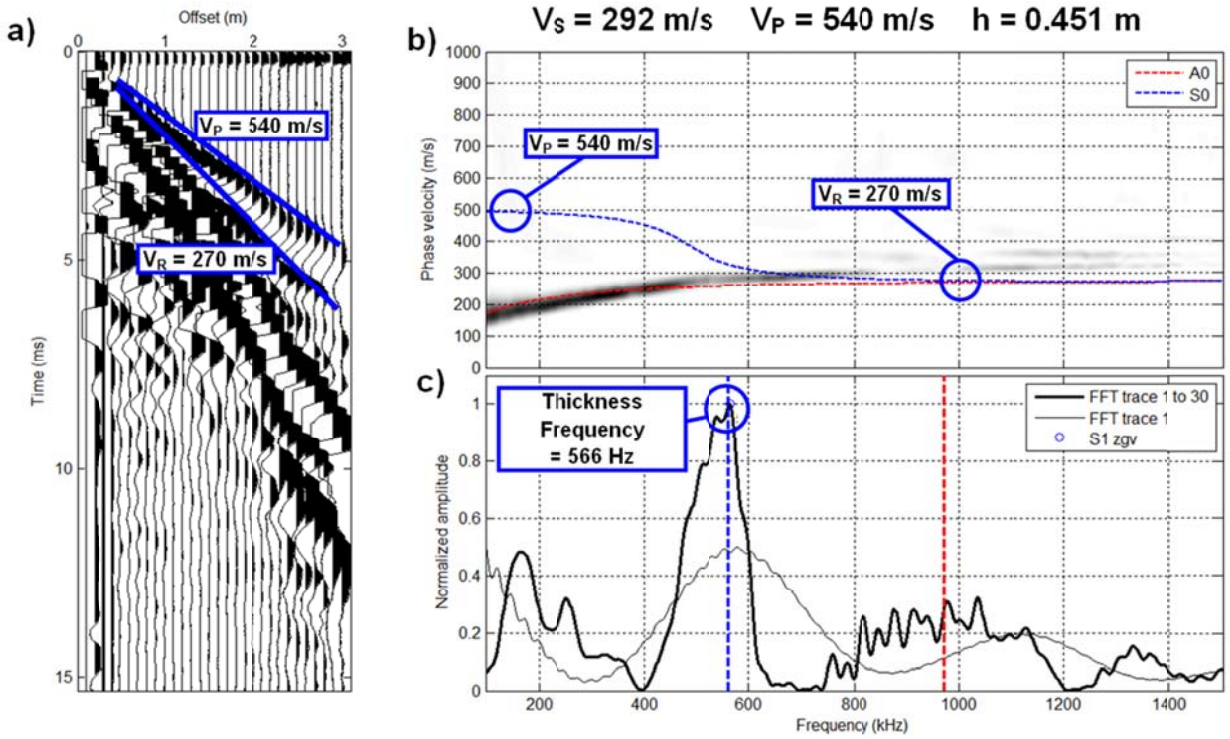

Figure C1: Raw time history data with labeled wave velocities (a), dispersion curve resulting from the raw data in (a) with wave velocities identified (b), and thickness frequency identification from layer interface reflection (c).

APPENDIX D – SEISMIC MODULUS – TEMPERATURE CORRELATION PLOTS

This appendix presents the correlation between E_0 and curing temperature used to develop the LSS maturity index. These data were obtained via FFR.

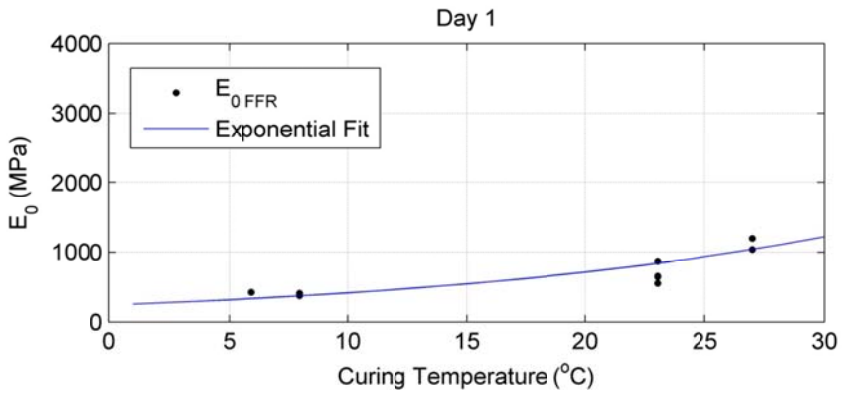

Figure D1: Correlation between E_0 and curing temperature (day 1).

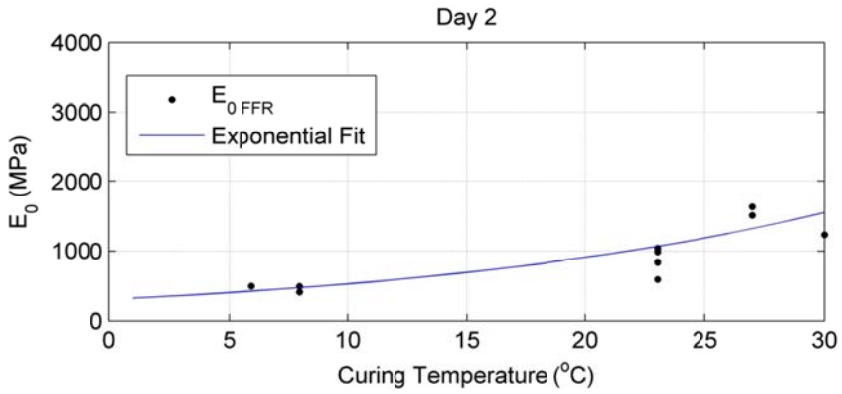

Figure D2: Correlation between E_0 and curing temperature (day 2).

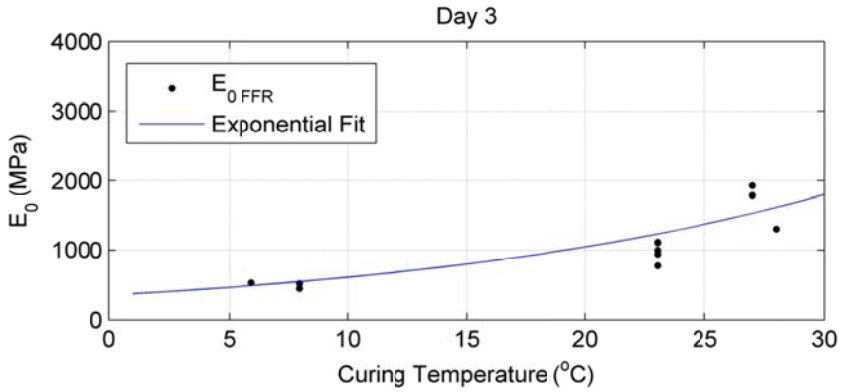

Figure D3: Correlation between E_0 and curing temperature (day 3).

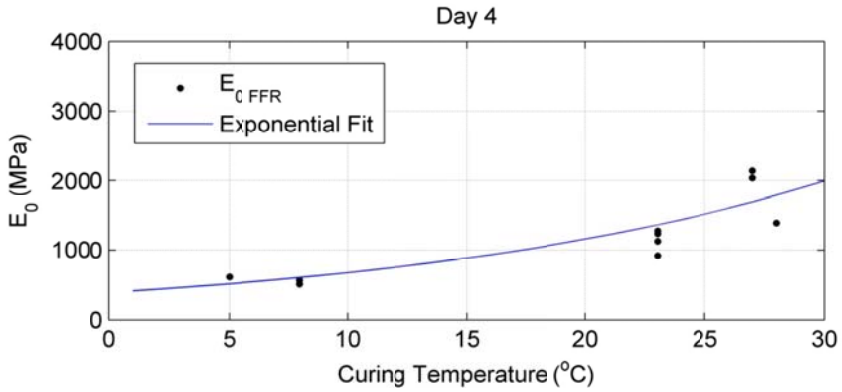

Figure D4: Correlation between E_0 and curing temperature (day 4).

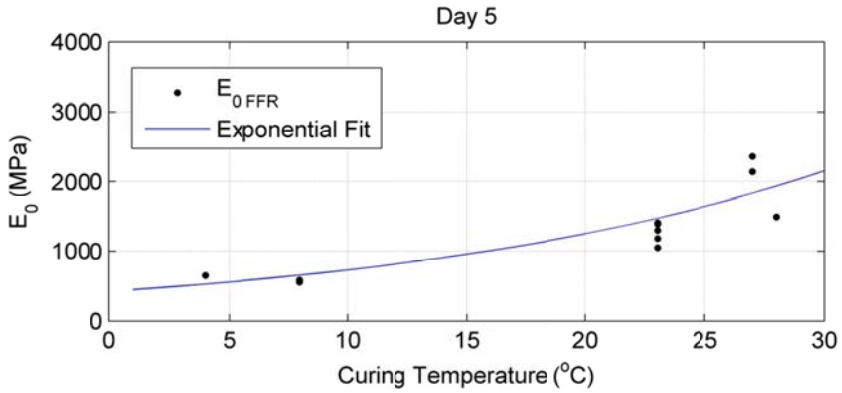

Figure D5: Correlation between E_0 and curing temperature (day 5).

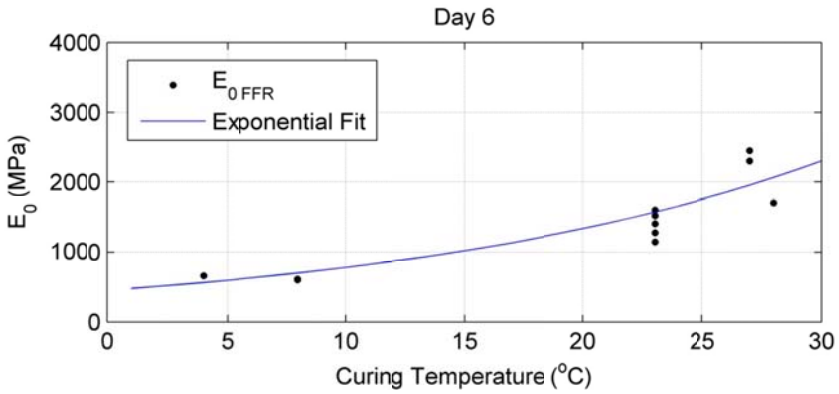

Figure D6: Correlation between E_0 and curing temperature (day 6).

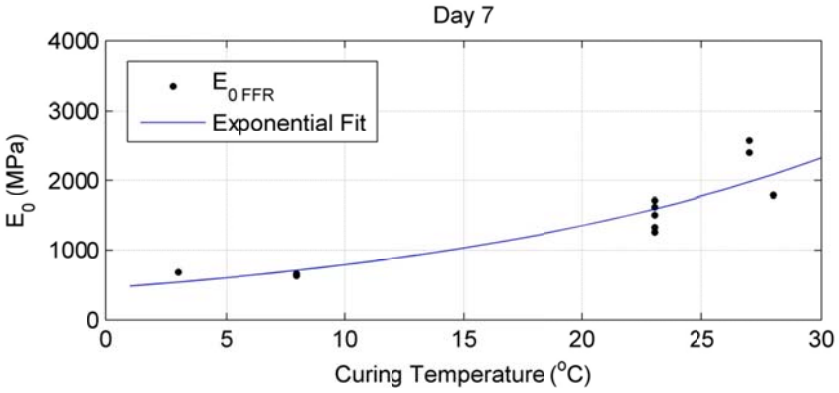

Figure D7: Correlation between E_0 and curing temperature (day 7).

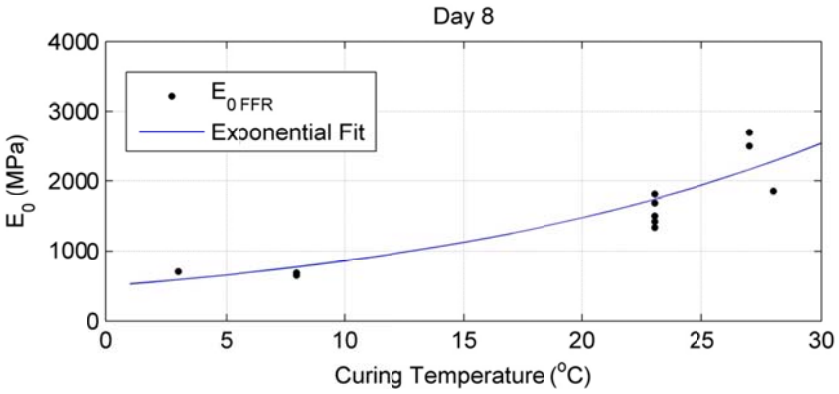

Figure D8: Correlation between E_0 and curing temperature (day 8).

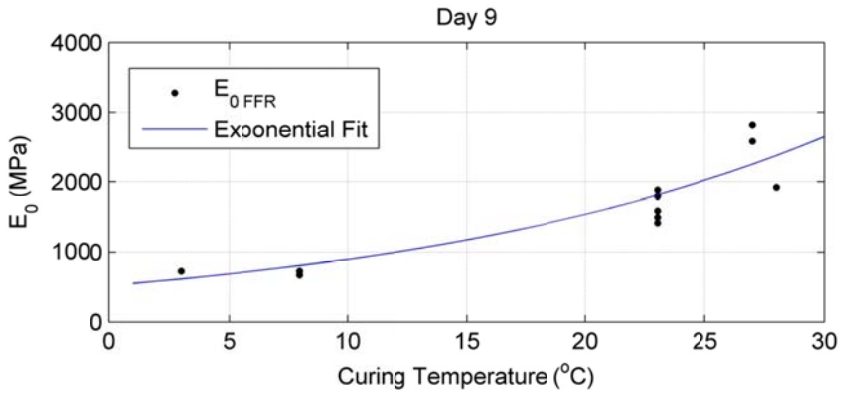

Figure D9: Correlation between E_0 and curing temperature (day 9).

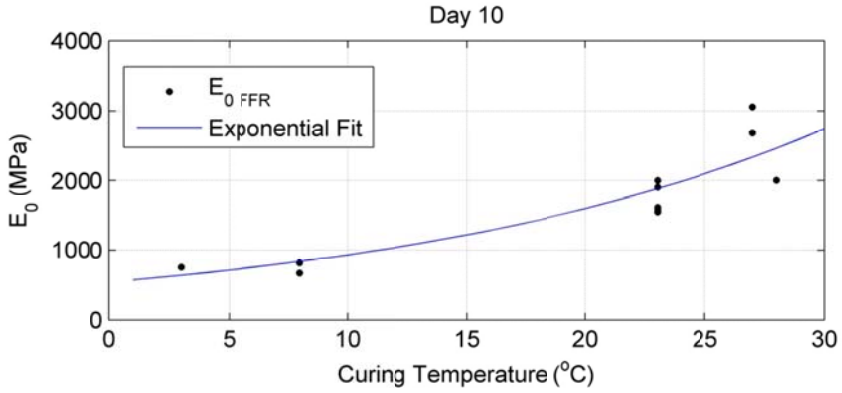

Figure D10: Correlation between E_0 and curing temperature (day 10).

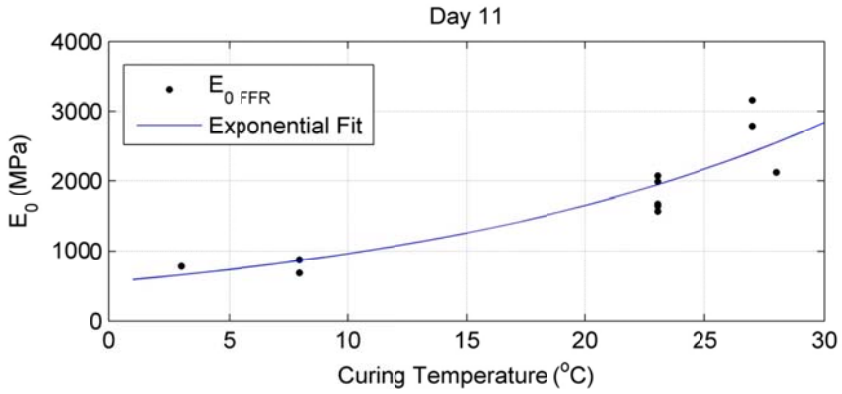

Figure D11: Correlation between E_0 and curing temperature (day 11).

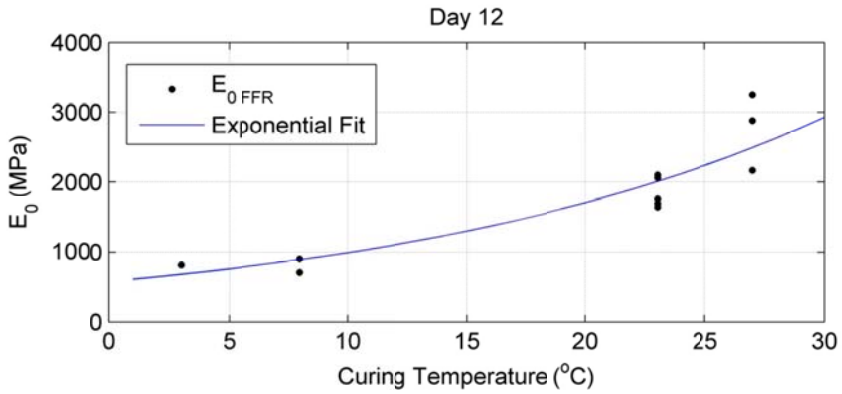

Figure D12: Correlation between E_0 and curing temperature (day 12).

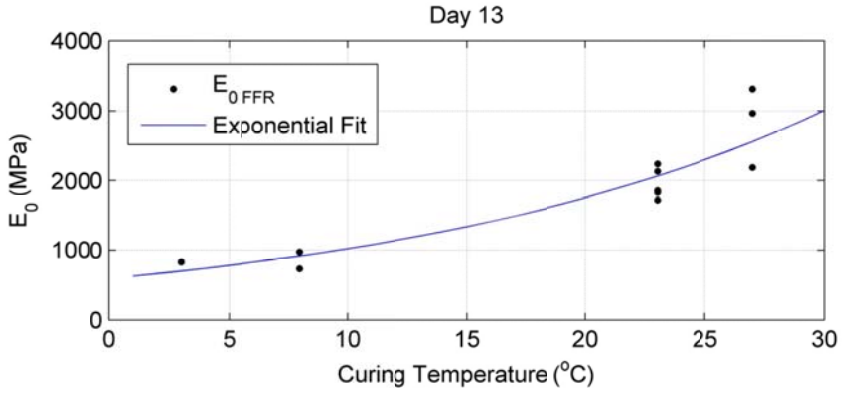

Figure D13: Correlation between E_0 and curing temperature (day 13).

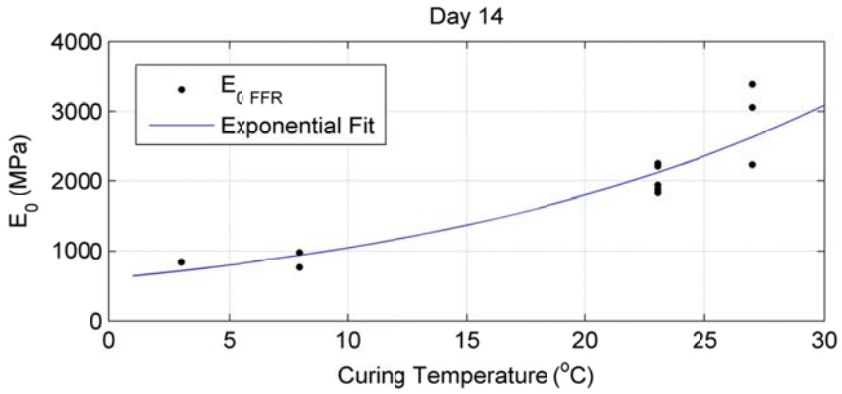

Figure D14: Correlation between E_0 and curing temperature (day 14).

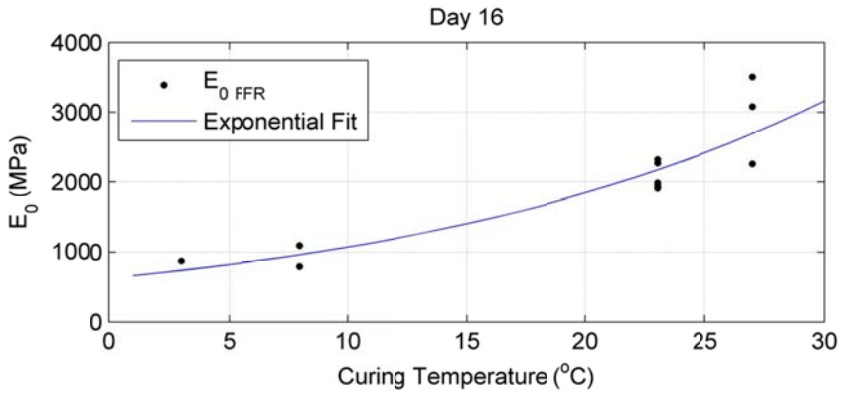

Figure D15: Correlation between E_0 and curing temperature (day 16).

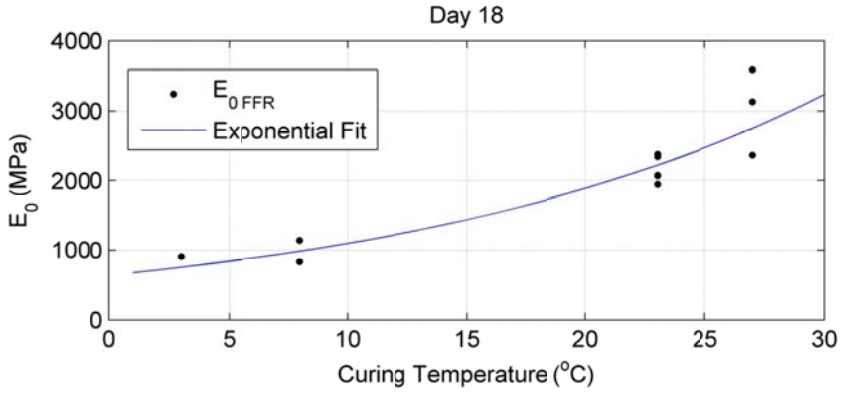

Figure D16: Correlation between E_0 and curing temperature (day 18).

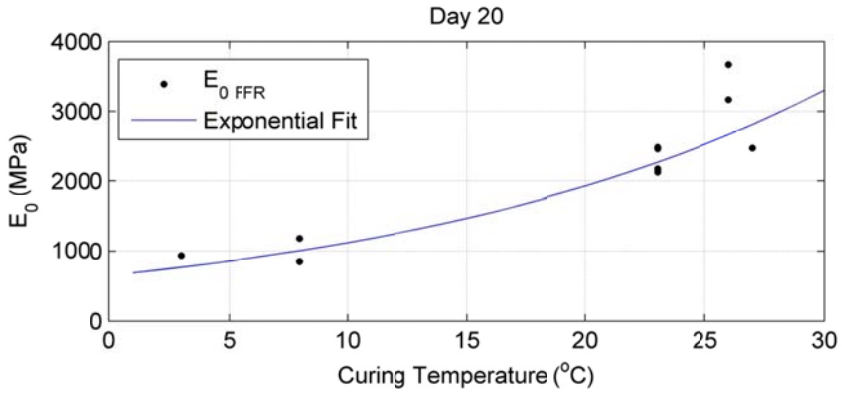

Figure D17: Correlation between E_0 and curing temperature (day 20).

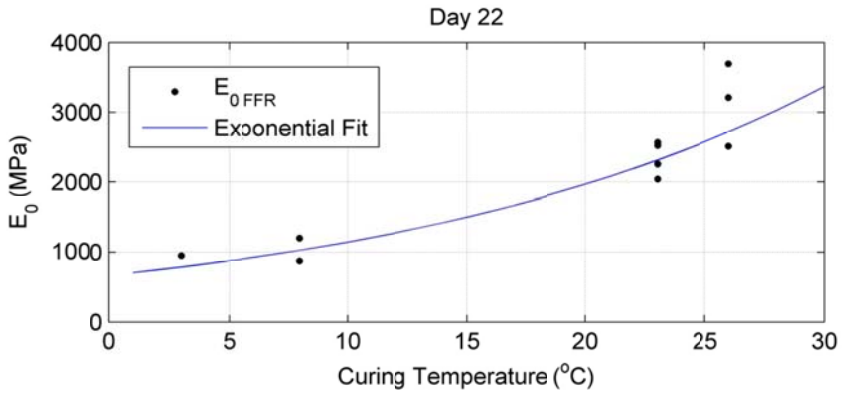

Figure D18: Correlation between E_0 and curing temperature (day 22).

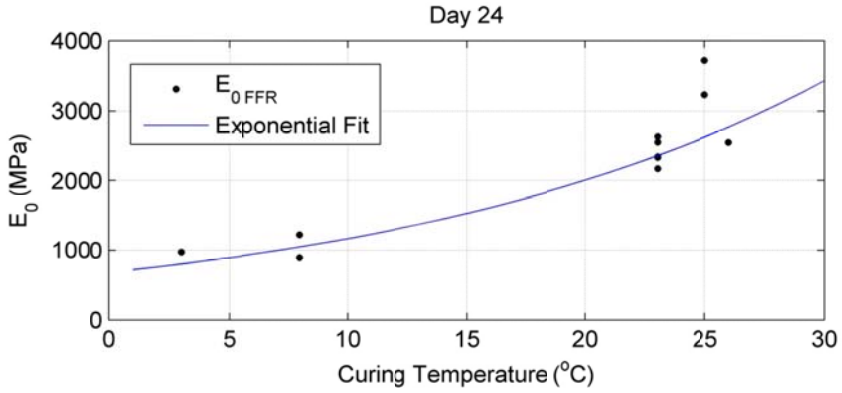

Figure D19: Correlation between E_0 and curing temperature (day 24).

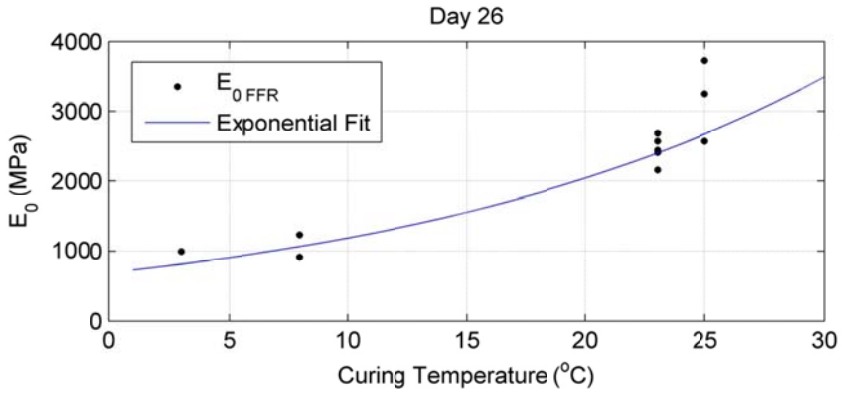

Figure D20: Correlation between E_0 and curing temperature (day 26).

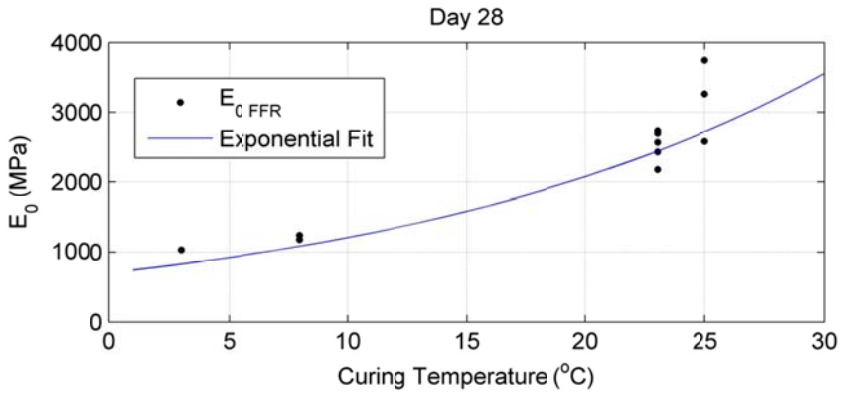

Figure D21: Correlation between E_0 and curing temperature (day 28).

APPENDIX E – TEMPERATURE INTERPRETATION

This appendix explains the theory used to estimate average temperature for LSS maturity index implementation. E1 demonstrates the difference between interpretations of temperature and resulting E_{Pred} from the LSS MI. Consider Figure E1a, where $\overline{T}_{t\ Day}$ is the average temperature over each specific 24 hour window. Using each $\overline{T}_{t\ Day}$ value as input for the LSS maturity index, the resulting E_{Pred} (Figure E1) suggests unrealistic behavior for LSS (i.e., significant decrease in modulus from days 15-22) and is therefore not a good choice for temperature interpretation. Using $\overline{T}_{t\ All}$ (i.e., the average temperature over days 1-28), the resulting $E_{0\ Pred}$ has a reasonable shape, but implies that testing must be conducted for 28 days to determine the proper temperature average. In the interest of implementing a pilot specification in which QA could be verified at early curing windows (i.e., 3-7 days after compaction), obtaining a 28-day average temperature is unrealistic. The best choice for temperature interpretation is $\overline{T}_{t\ Sum}$ (i.e., the cumulative average of the temperature from day 1-t), defined in Equation E1. This approach helps to account for early variations in temperature but also incorporates the temperature history.

$$\overline{T}_{t\ Sum}(t) = \frac{(\sum_{i=1}^{t} \overline{T}_{t\ Day}(t))}{t} \tag{E1}$$

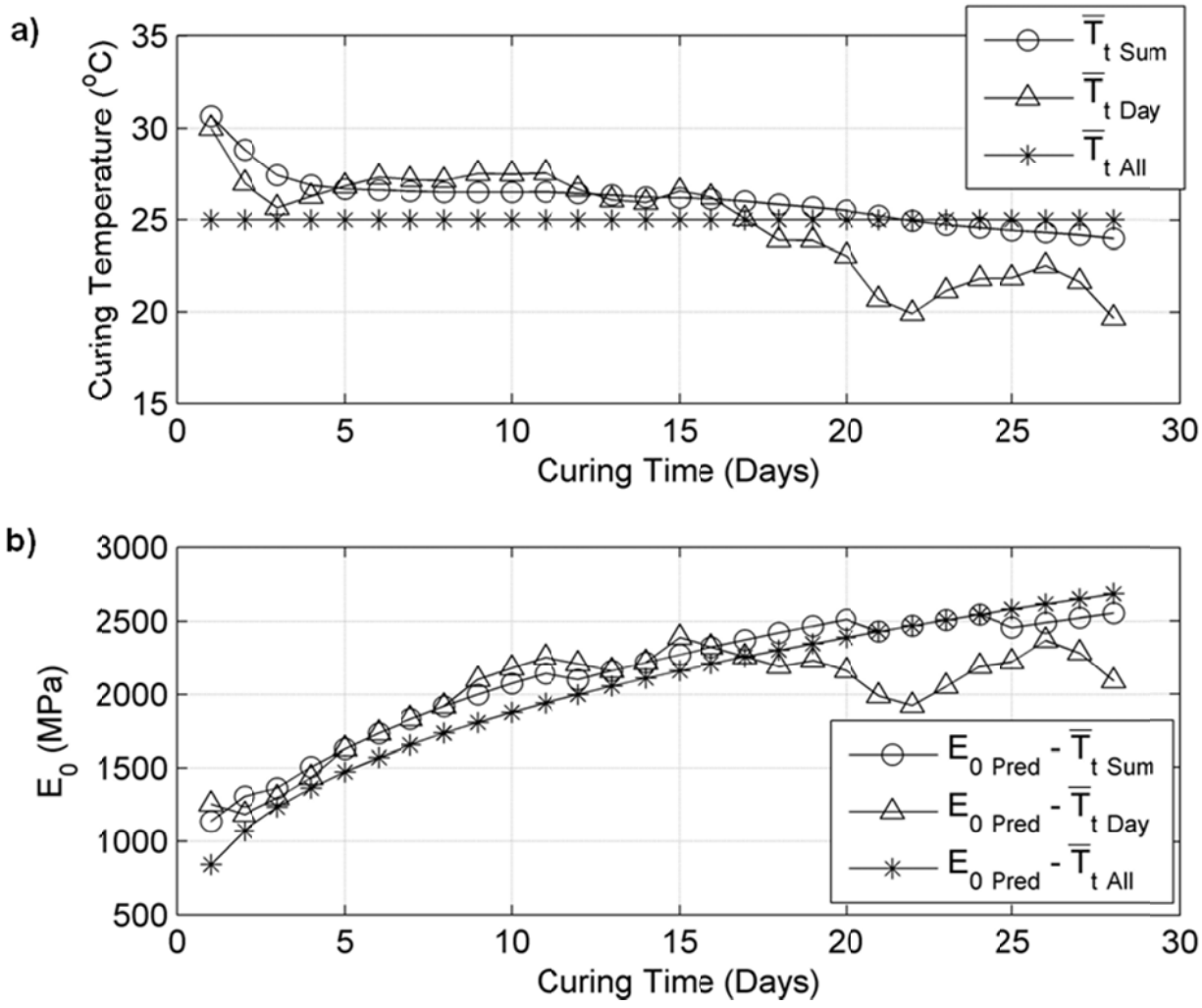

Figure E1: (a) Various interpretations of $\overline{T}_t$ used for experimental data fitting, and (b) resulting E_{Pred} from $\overline{T}_t$ (t) in part a.